Integrated Sensing and Communications in Time-Varying Channels

by **Yang Sun**

Thesis submitted in fulfilment of the requirements for the degree of

Doctor of Philosophy

under the supervision of Andrew Zhang, Renping Liu, Kai Wu, Ming Ding

School of Electrical and Data Engineering

Faculty of Engineering and IT

University of Technology Sydney

April 15, 2024

Certificate of Authorship / Originality

I, Yang Sun, declare that this thesis is submitted in fulfilment of the requirements for the award of Doctor of Philosophy, in the School of Electrical and Data Engineering at the University of Technology Sydney.

This thesis is wholly my own work unless otherwise referenced or acknowledged. In addition, I certify that all information sources and literature used are indicated in the thesis.

This document has not been submitted for qualifications at any other academic institution.

This research is supported by the Australian Government Research Training Program.

Signature: Production Note: Signature removed prior to publication.

Date: April 15, 2024

Abstract

In the era of 5G beyond wireless communication systems, a significant advancement lies in the integration of sensing capabilities, a function traditionally associated with radar systems. This convergence, referred to as integrated sensing and communications (ISAC), empowers the system to detect moving vehicles, human activities, and environmental changes by leveraging received communication signals. However, the presence of time-varying channels, usually caused by fast-moving objects, poses significant challenges for both communication and sensing. One of the promising approaches to address time-varying scenarios is the orthogonal time frequency space (OTFS) modulation system, which remains in its early stage.

Several critical issues need attention within the context of integrated sensing and communication in time-varying channels:

Flexible Data Allocation in OTFS: In OTFS systems, the allocation of different user data to the same delay-Doppler grid in one OTFS frame lacks flexibility and adaptability to different varying channel conditions.

Mitigating Large Doppler Frequencies: The presence of large Doppler frequencies in integrated sensing and communication scenarios has not been considered, potentially leading to significant intercarrier interference.

Sensing Performance Bound: The sensing performance bounds for ISAC in

time-varying channels remains unknown.

Addressing these challenges, in this thesis, I propose the following solutions:

1. Mixed-stage OTFS System: To address the first issue, I first show that channel parameters play a role in determining the optimal choice of delay-Doppler grid in OTFS systems. Consequently, I propose a mixed-stage OTFS system capable of accommodating users with different channel conditions in one OTFS frame.

2. Frequency-Domain Sensing Framework: To address the second issue, I propose a frequency-domain sensing framework for OFDM ISAC systems. I first derive a frequency-domain closed-form expression of the received signals, to characterise the delay and Doppler frequency impact. I then propose a sensing framework, taking advantages of both intra-block and inter-block sensing methods. The framework is further completed with exemplified pilot design and periodogram sensing algorithm.

3. Sensing Performance Bound Establishment: To address the third issue, I aim to establish the sensing performance bound for ISAC in time-varying channels. Firstly, I establish input-output relationships in such channels. Then, I derive the delay and Doppler Cramér-Rao lower bound (CRLB) in time-varying channels. Finally, I optimize preambles via CRLB minimization.

Dedication

For my mom, Li Zhu, who wishes to see me be a PhD.

Acknowledgements

I would like to thank my family for supporting me emotionally and financially. Without your patience and understanding, I can not finish this thesis. I would like to give thanks to my supervisor, Andrew Zhang, your supervision and guidance helps me to go through the difficulties in the research. I specially need to thank Ming Ding, my external supervisor. You accompanied and stayed with me in my most difficult time. I will remember this forever. Finally, I would like to thank anyone who care about me: some of them are my labmates, and some come from UTS HELPS, and some are just even acquaintances.

Yang Sun

April 15, 2024

Sydney, Australia

Contents

1 Introduction **2**

1.1 Background 2

1.2 Research Objectives 5

1.3 Contributions 6

1.4 Thesis Organization 8

1.5 List of Publications 10

2 Literature Review **11**

2.1 Time-varying Channels 11

2.1.1 Challenges from Time-varying Channels 12

2.1.2 Channel Estimation Algorithms 19

2.1.3 Channel Estimation in Time-varying Channels 22

2.2 ISAC in Time-varying Channels 27

2.2.1 Communication System in Time-varying Channels 27

2.2.2 Sensing in Time-varying Channels 31

2.2.3 Sensing Bounds 34

3 Signal and Channel Models **37**

3.1 Introduction 37

3.2 Time-varying Channel Models in Different Domains and Their Relationships . . . 37
3.2.1 Detailed Continuous Channel Models . . . 38
3.2.2 Detailed Discrete Channel Models . . . 40
3.3 Data Symbols Modulated in Delay-Doppler Domain . . . 42
3.4 Data Symbols Modulated in Frequency Domain . . . 44
3.5 Linear Equalization in Different Domains . . . 45
3.5.1 Relationship Between Delay-Doppler Domain and Frequency Domain Channels for OTFS System . . . 46
3.5.2 Comparison of Delay-Doppler Domain Equalization and Frequency Domain Equalization for OTFS System . . . 47
3.6 Conclusions . . . 54

4 Mixed-stage OTFS Systems **56**
4.1 Introduction . . . 56
4.2 OTFS Performance Difference under Different Delay-Doppler Grid Size 57
4.3 Concept of Mixed-stage OTFS . . . 61
4.4 Mixed-stage OTFS Signal Models . . . 62
4.5 Multi-user Data Symbols Allocation . . . 66
4.6 Simulation Results . . . 67
4.7 Conclusions . . . 70

5 Frequency-Domain Sensing in Time-Varying Channels **72**
5.1 Introduction . . . 73
5.2 System and Signal Models . . . 75
5.3 Proposed Sensing Scheme . . . 77
5.3.1 Intra-block Sensing with a Single OFDM Block . . . 78
5.3.2 Inter-block Sensing with Multiple OFDM Blocks . . . 79

5.3.3 Exemplified Pilot Design for Estimating $\mathbf{H}_{fd}$ 81
5.3.4 Overall Algorithm 82
5.4 Simulation Results 83
5.5 Conclusions 93

6 Performance Bounds of ISAC in Time-Varying Channels 94
6.1 Introduction 95
6.2 System and Signal Models 96
6.3 Sensing Performance Bound in Time-varying channels 98
6.4 CRLBs for Channels with a Line-of-sight Path 101
6.4.1 Delay CRLB with Known Channel Doppler 102
6.4.2 Doppler CRLB with Known Channel Delay 102
6.4.3 Delay and Doppler CRLBs with Unkown Channel Doppler and Delay 103
6.4.4 Analysis on LoS Path CRLB 105
6.5 CRLB Minimization via Signal Optimization 105
6.6 Simulation Results 109
6.6.1 LoS Path Channels 109
6.6.2 Multipath Channels 112
6.7 Conclusions 113

7 Conclusions and Future Work 114
7.1 Concluding Remarks 114
7.2 Future Work 115

8 Appendix 118
8.1 Proof of Theorem 1 in Chapter 6 118
8.2 Proof of Theorem 2 in Chapter 6 120

List of Figures

1.1 ISAC system diagram. 3
1.2 Chapters Relationship. 10

3.1 Comparison between delay-Doppler domain and frequency domain ZF equalization. 51
3.2 Comparison between delay-Doppler domain and frequency domain MMSE equalization. 52
3.3 ZF equalization performance in time-varying channels 1. 52
3.4 ZF equalization performance in time-varying channels 2. 53
3.5 MMSE equalization performance in time-varying channels 1. 53
3.6 MMSE equalization performance in time-varying channels 2. 54

4.1 OTFS in time invariant channels. 58
4.2 OTFS in time-varying channels. Doppler ranges from 0 to 1. 59
4.3 OTFS in time-varying channels. Doppler ranges from 0 to 2. 59
4.4 OTFS in time-varying channels. Doppler ranges from 1 to 2. 60
4.5 An example of the mixed-stage OTFS structure 63
4.6 Mixed-stage OTFS. Doppler ranges from 0 to 1/M*N, delay ranges from 0 to 1 68

4.7 Mixed-stage OTFS. Doppler ranges from 10/M*N to 11/M*N, delay ranges from 0 to 4. 68

4.8 Mixed-stage OTFS at different stages. Doppler ranges from 0 to 1/M*N, delay ranges from 0 to 1 69

4.9 Mixed-stage OTFS at different stages. Doppler ranges from 10/M*N to 11/M*N, delay ranges from 0 to 4. 69

5.1 Intra-block estimation Delay-Doppler map 1, where the color scale indicates signal strength as per the color bar. Ground truth of three targets are also highlighted with red circles. 86

5.2 Inter-block estimation Delay-Doppler map 1, where the color scale indicates signal strength as per the color bar. Ground truth of three targets are also highlighted with red circles. 86

5.3 Intra-block estimation Delay-Doppler map 2, where the color scale indicates signal strength as per the color bar. Ground truth of three targets are also highlighted with red circles. 87

5.4 Inter-block estimation Delay-Doppler map 2, where the color scale indicates signal strength as per the color bar. Ground truth of three targets are also highlighted with red circles. 87

5.5 Intra-block estimation Delay-Doppler map 3, where the color scale indicates signal strength as per the color bar. Ground truth of three targets are also highlighted with red circles. 88

5.6 Inter-block estimation Delay-Doppler map 3, where the color scale indicates signal strength as per the color bar. Ground truth of three targets are also highlighted with red circles. 88

5.7 Intra-block estimation Delay-Doppler map 4, where the color scale indicates signal strength as per the color bar. Ground truth of three targets are also highlighted with red circles. 89
5.8 Inter-block estimation Delay-Doppler map 4, where the color scale indicates signal strength as per the color bar. Ground truth of three targets are also highlighted with red circles. 89
5.9 Doppler frequency NRMSE in time-varying channels. 90
5.10 Delay NRMSE in time-varying channels. 90
5.11 Doppler frequency NRMSE in time-varying channels. Only pilots, no data. 91
5.12 Delay NRMSE in time-varying channels. Only pilots,no data. 91

6.1 LoS path CRLB in time-varying channels. 110
6.2 CRLB with different pilot number in time-varying channels,N=32. . . 111
6.3 CRLB with different pilot number in time-varying channels,N=64. . . 111
6.4 CRLB optimization in time-varying channels. 112

List of Tables

2.1 Challenges from Time-varying Channels 13
2.2 Sensing Methods Comparison 33
2.3 Sensing Bounds 34
3.1 Simulation Parameters 51
4.1 Simulation Parameters 67
5.1 Simulation Parameters. 84
6.1 Simulation Parameters 110

Chapter 1

Introduction

1.1 Background

The ongoing evolution of mobile communication technology marks a pivotal shift toward 6G, representing not just an upgrade but a paradigm shift in how we conceive and utilize wireless networks. One part of this progression lies the concept of Integrated Sensing and Communications (ISAC), a transformative integration of communication and sensing capabilities. This convergence stands as a beacon guiding the trajectory of 6G development, fundamentally altering the landscape of mobile networks.

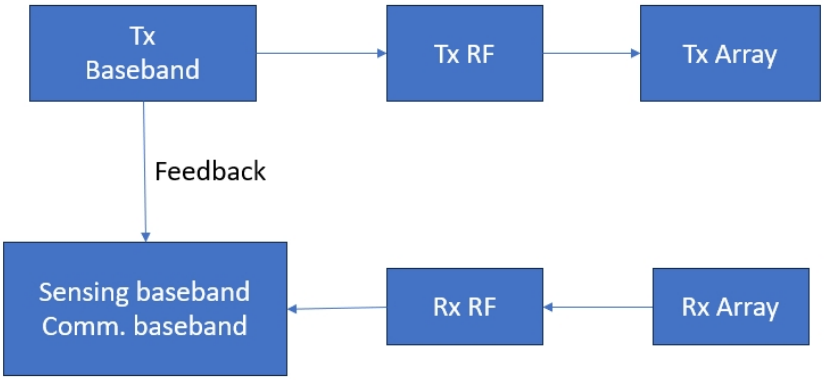

Figure 1.1: ISAC system diagram.

The technological advancements plays a pivotal role in propelling this evolutionary journey. It's not merely about catering to the growing demands for faster data transmission or more reliable connections; it's about catalyzing a qualitative leap towards a multidimensional communication system, that is, not a communication only system, but integrating sensing ability as well. Amidst this burgeoning landscape, ISAC emerges as a transformative force. ISAC's fusion of communication and sensing prowess isn't merely about technical integration; it's about unlocking a plethora of new services and functionalities. These functionalities range from location-based services that redefine how we interact with our environments to the foundational support provided for sectors like autonomous driving and advanced manufacturing.

One of the remarkable promises held by ISAC is its pivotal role in optimizing resource utilization within the spectrum. By harmonizing communication and sensing capabilities, ISAC endeavors to augment spectrum efficiency and make optimal use of the resources. Besides, hardware joint design in ISACs offers numerous advantages, including cost-efficiency and reduced size. Lastly, Communication and sensing can enjoy mutual benefit in ISAC.

However, this transformative potential isn't without its challenges. ISAC systems

encounter intricate hurdles, especially within dynamic, time-varying wireless channels. In the rapid motions within communication environments, the channels become inherently volatile. The resulting time-frequency doubly selective fading, induced by multipath and large Doppler frequency shift, presents a formidable challenge to ISAC systetms. These dynamic time-varying channels demand sophisticated strategies to maintain reliability and efficiency in data transmission and sensing.

Research on ISAC in time-varying channels is still in its infancy. Existing studies are limited in number and have primarily focused on OTFS ISAC systems [1], [2]. In ISAC systems, the Cramér-Rao Lower Bound (CRLB) is widely used as a performance metric. It serves as a lower bound for estimation errors in both radar sensing and communication channel estimation [3], [4]. There is a paucity of research on the sensing CRLB for ISAC systems in time-varying channels. In a study by Gaudio [1], a joint communication and radar sensing system utilizing OTFS modulation was investigated. This system aimed to perform channel parameter estimation at the transmitter and data detection at the receiver. The authors derived the CRLB for a single path and conducted a waterfall analysis. However, this work assumed a time-invariant channel. Although some studies have explored channel estimation, which is similar to the parameter sensing problem [5]–[7], the sensing performance bound of ISAC in time-varying channels has not yet been derived. Furthermore, there is a lack of understanding regarding how channel parameters in time-varying channels can influence the performance bound.

This thesis delves into ISAC system, focusing on its application in dynamic, time-varying channels and addressing the associated challenges.

1.2 Research Objectives

The research aims to advance the ISAC technologies operating in time-varying channel conditions. The primary objectives encompass the development of innovative algorithms and a comprehensive fundamental analysis. The specific research objectives outlined in this thesis are:

- To propose a robust sensing framework designed to extract environmental parameters from mobile signals received in time-varying channel conditions for ISAC system. The complexity arises due to high Doppler and delay parameters, rendering sensing in such environments challenging. Addressing this challenge involves the development of a sensing scheme tailored for time-varying channels. Conventionally, estimating Doppler values in an OFDM system necessitates the accumulation of multiple OFDM symbols. However, adopting a single-OFDM-symbol estimation approach holds potential for achieving a broader estimation range and reducing ambiguity. Hence, this study intends to combine single and multiple OFDM symbols estimation to enhance accuracy and estimation range.

- To leverage the Cram'er-Rao Lower Bound (CRLB) as a metric for evaluating sensing performance bound and derive it within the context of time-varying channel scenarios in ISAC. The aim also involves optimizing pilot design to minimize the CRLB. Previous research focused on sensing performance limits primarily in time-invariant channels, neglecting the impact of Doppler shift within an OFDM block, which becomes significant in scenarios with notable movement. We seek to determine the sensing performance limit in time-varying channels and optimize pilot configurations accordingly.

- To investigate the implementation of a multi-staged Orthogonal Time Fre-

quency Space (OTFS) system. This exploration aims to elevate the OTFS system performance. The study pursues two primary objectives: firstly, to assess the system's behavior by varying the length of the Doppler-Delay grid, enabling a comprehensive understanding of its performance across different grid configurations. Secondly, building upon these evaluations, to propose a multistage OTFS system. This innovative approach aims to individualize OTFS parameters for different users in multi—user systems, thereby enhancing the overall system performance.

1.3 Contributions

This thesis focuses on an in-depth exploration of ISAC system within time-varying channels. The research initially investigates the multi-user OTFS system, subsequently introducing a novel approach termed the mixed-stage multi-user OTFS system. This innovative system accommodates each user with a customized delay-Doppler grid size, enhancing adaptability to varying channel conditions.

Following this investigation, a comprehensive sensing framework tailored for OFDM systems in time-varying channels is proposed. This framework is designed to support an extensive sensing range while simultaneously upholding accuracy.

Finally, the thesis ends with the proposition of a sensing performance bound. This bound serves as a critical metric in evaluating and benchmarking the performance capabilities of the designed systems within the context of time-varying channels.

The detailed contributions of this thesis are delineated as follows:

- First, a novel approach termed the multi-user mixed-stage OTFS system is introduced. In a traditional OTFS system, a single OTFS frame corresponds to a solitary delay-Doppler grid. However, in a multi-user setup, all users are con-

strained to share an identical delay-Doppler grid size. This limitation restricts individual users from adjusting their delay-Doppler grid size based on different channel conditions, consequently impacting communication performance.

The proposed mixed-stage OTFS system addresses this constraint by enabling a single OTFS frame to encompass multiple distinct delay-Doppler grids. This innovative design empowers users with the flexibility to adapt their grid size in accordance with diverse channel conditions, thereby fostering overall system performance.

- We then develop a frequency-domain sensing framework based on the frequency-domain estimated channels for a general OFDM system in time-varying channels. This framework can be used with frequency domain pilots in a traditional OFDM system. First, we expand the frequency-domain input-output signal relationship in [8] to multiple OFDM blocks and adopt practical window functions. We characterise the delay and Doppler frequency in our signal and channel models. Next, we propose inter-block and intra-block sensing algorithms that estimate sensing parameters between multiple blocks and within a single OFDM block, respectively. Furthermore, the sensing framework is completed with an exemplified periodogram sensing algorithm and pilot design strategies. We present simulation results that support the validity of our suggested framework.

- We assess the performance boundaries of ISAC systems in time-varying channel environments. This involves the development of system models specifically to encapsulate the impact of the Doppler effect within a single OFDM block. By integrating the Doppler effect into our models, we derive the Cramér-Rao Lower Bounds (CRLBs) for both Doppler and delay in time-varying channels. Moreover, our pursuit extends to the optimization of preambles with the ob-

jective of minimizing the derived CRLB. The extensive simulations conducted serve a dual purpose: firstly, they provide an in-depth understanding of the implications of parameters on ISAC system design. Secondly, they serve as a validation mechanism for the efficacy and validity of our optimization strategies within these time-varying channel environments.

1.4 Thesis Organization

The structure of this thesis unfolds as follows:

Chapter 2 offers an review focusing on ISAC within time-varying channels. It commences with an encompassing overview of ISAC, providing an introduction to its core concepts, encompassing various performance metrics, and addressing the primary challenges encountered within ISAC. Following this, a detailed exploration of time-varying channels is presented, highlighting the specific challenges posed by these channels. Emphasis is placed on the complexities arising from time-varying channels, followed by channel estimation issues intrinsic to their dynamic nature. The chapter concludes by outlining several research areas related to ISAC in time-varying channels. These encompass communication in time-varying channels, sensing in such channels, and the fundamental sensing bounds within time-varying channel scenarios. These areas closely align with the focus of my research.

Chapter 3 covers the signal and channel models that form the foundation of this thesis. We initially introduce the channel models designed for time-varying channels. Subsequently, considering OTFS system as a potential modulation approach to address the challenges posed by time-varying channels, we outline the signal models specific to OTFS system. Following this, we provide a concise overview of the signal models employed in the OFDM system. Finally, we conduct a comparative analysis

between frequency domain equalization and delay-Doppler domain equalization.

In chapter 4, we introduce a multi-user mixed-stage OTFS system, enabling a single OTFS frame to accommodate multiple delay-Doppler grids without inter-symbol interference across grids. We delve into various aspects: Firstly, we illustrate how the size of delay-Doppler grids influences communication performance. After that, we propose the architecture of the mixed-stage OTFS system and elaborate on the methodology to integrate data symbols of varying delay-Doppler grid sizes into a unified OTFS frame. Finally, the simulation results of the mixed-stage OTFS system are detailed.

In Chapter 5, we establish a frequency-domain sensing framework designed for a OFDM system operating within time-varying channels. The development includes several steps: Initially, we expand the input-output signal relationship in [8], to encompass multiple OFDM blocks. Subsequently, we devise sensing schemes for intra-block and inter-block sensing. The framework is further exemplified with periodogram sensing algorithm and pilot design. Lastly, we provide simulation results that validate the effectiveness and efficiency of our proposed frequency-domain sensing framework.

In chapter 6, the focus is on exploring the performance limits of ISAC system within the time-varying channels. The study first introduces signal and channels models and then derives the Cramér-Rao Lower Bound (CRLB) for both delay and Doppler as a measure of sensing performance bound in such dynamic channels. After that, minimization of the CRLB is undertaken through the optimization of the transmission signal. Finally, the simulation outcomes shed light on the influence of various parameters on the CRLB.

Chapter 7 offers a comprehensive summary of the entire research undertaken. Ad-

ditionally, it explores potential avenues for future research, providing an outlook on prospective areas of study and development within this field.

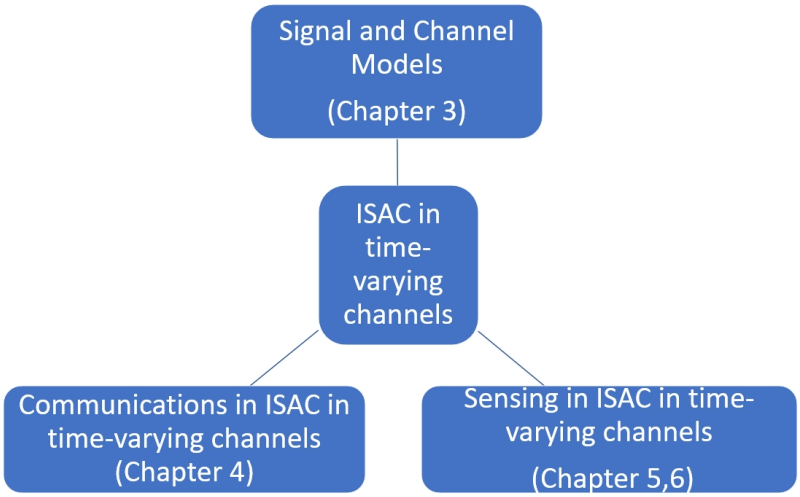

Figure 1.2: Chapters Relationship.

1.5 List of Publications

- **Yang Sun**, J. Andrew Zhang, Kai Wu and Ren ping Liu, "Frequency-Domain Sensing in Time-Varying Channels," in IEEE Wireless Communications Letters, vol. 12, no. 1, pp. 16-20, Jan. 2023, doi: 10.1109/LWC.2022.3214283.
- **Yang Sun** and Zhitong Ni, "Performance Bound of ISAC in Time-Varying Channels," 2023 International Symposium on Communications and Information Technologies, Sydney, Australia, 2023
- **Yang Sun**, J. Andrew Zhang, Kai Wu, Ren ping Liu, and Ming Ding, "Mixed Stage OTFS Systems for Multiuser Communications", under preparation for IEEE Transactions on Vehicular Technologies.

Chapter 2

Literature Review

2.1 Time-varying Channels

The widely held assumption that intercarrier interference (ICI) within one single Orthogonal Frequency Division Multiplexing (OFDM) symbol is negligible no longer holds true in time-varying channels. Additionally, the frequency domain channel matrix is no longer strictly diagonal but becomes stripped. More comprehensive insights into the dynamics of the time-varying channel are available in Section 3.2.

Because of the large velocity of wireless communication user equipment and the dynamic nature of the time-varying channel, the modeling, evaluation, analysis, and design of 6G wireless communication systems face several obstacles. Addressing these challenges typically involves employing advanced signal processing, adaptive algorithms, and adaptive modulation techniques to mitigate the effects of time-varying channels and maintain reliable communication.

2.1.1 Challenges from Time-varying Channels

Time-varying channels present several challenges:

1. Doppler Effect and Intercarrier Interference

The paper [9] focuses on OFDM systems and their challenges of computational complexity in time-varying channels like high-speed mobile scenarios or underwater acoustics, where channels change rapidly. These shifts introduce ICI, impacting system performance. The paper introduces a low-complexity ICI mitigation scheme for MIMO system in time-varying channels. This approach decouples symbols and ICIs on individual subcarriers, demonstrating superior performance compared to conventional equalizers under high mobility scenarios. The methodology centers on dividing the equalization process based on ICI contributions structure in time-varying channels, and allowing independent symbol demodulation on each subcarrier.

[10] conducts analysis under the fast-fading channel. This paper explores Spatial Modulation (SM) in MIMO systems, addressing issues like high RF chains and interference. While pivotal for 5G, most research on SM focuses on time invariant channels, overlooking high-mobility scenarios. They propose a study modeling channel changes within data blocks, offering simplified expressions for error probabilities in both time invariant and time-varying channels. This work aims to quantify SM's error performance in time-varying channels.

Current mobile networks often rely on OFDM systems. However, in time-varying channels, significant intercarrier interference due to large Doppler frequencies within OFDM Joint Communications and Sensing (JCAS) has been overlooked in the context of sensing. [11] introduces a frequency-domain sensing framework tailored for OFDM JCAS systems. Initially, the researchers establish a frequency-domain closed-form expression for received signals, enabling us to understand the impact of delay

and Doppler frequency across and within OFDM blocks. Subsequently, we design intra-block and inter-block sensing algorithms using this expression. To enhance the framework, they give examples of the pilot design and sensing algorithms. Simulations affirm the efficiency and effectiveness of the proposed framework.

Table 2.1: Challenges from Time-varying Channels

Challenges	Related Research
Doppler Effect and Intercarrier Interference	[9],[10],[11]
Channel Estimation	[12],[13], [14], [15], [16], [17], [18], [19], [20], [21], [22], [23], [24], [25]
Adaptive Techniques	[26],[27]
Complexity	[28],[29],[30],[31]
Resource Allocation	[32], [33],[34],[35],[36],[37],[38]

2. Channel Estimation

It becomes difficult to accurately estimate the state of the channel at any given time due to its variability. Constantly estimating and adapting to the changing channel conditions is crucial for maintaining optimal communication performance.

For example, in [12], the paper discusses channel estimation challenges in shallow-water surface scattered acoustic channels for coherent demodulation in broadband transmissions. These channels exhibit sparse structures and rapid fluctuations because of dynamic interaction with surface gravity wave, making accurate estimation difficult. However, exploiting the sparse structure can improve algorithm performance by reducing computational complexity and memory requirements. A novel sparse channel estimation approach utilizing delay-Doppler-spread function representation is proposed, capable of tracking first-order channel dynamics, critical for

highly dynamic channels caused by significant waves. This approach addresses time variations and sparse structures simultaneously. The method aims to enhance coherent demodulation in challenging dynamic underwater acoustic environments.

3. Adaptive Techniques

To cope with time-varying channels, adaptive modulation and coding techniques are necessary, adjusting parameters like modulation scheme and error correction codes in real-time to match the current channel conditions and maximize data throughput.

The paper [26] addresses adaptive cognitive radio technique for spectrum sharing in fast-fading channels. The spectrum scarcity issue, despite ample licensed spectrum being underutilized, is addressed by cognitive radio (CR) enabling secondary users (SUs) to opportunistically access licensed bands. For seamless coexistence, SUs need to sense the band within a timeframe and transmit only when no primary user (PU) activity is detected. An optimization between sensing accuracy and SU throughput is crucial, dictating an optimal sensing duration for shared access while protecting PUs. Prior research focused on this trade-off, assuming full channel knowledge, impractical in dynamic scenarios. Recent studies introduced estimation-sensing-throughput tradeoffs for imperfect link knowledge and explored multi-antenna systems to improve sensing-throughput tradeoffs over fading channels. However, they solely relied on statistical probability. This work emphasizes time-varying fading channels' impact, proposing an adaptive sensing schedule based on real-time channel estimation. It introduces a dynamic state-space model, formulates a dynamic optimization problem, and designs an adaptive schedule driven by joint spectrum sensing and real-time channel data, optimizing sensing duration considering the nature of fading channels.

The article [27] explores the potential of full-duplex (FD) operation in underwater

acoustic (UWA) systems, aiming to enhance data capacity and sonar capabilities. FD's implementation in UWA systems is limited due to self-interference (SI) challenges arising from near-end transmission. The study extends a digital cancellation scheme to counter delay sensitivity and investigates adaptive filters' performance in FD UWA systems with time-varying SI channels. It highlights challenges posed by time-varying surface reflections and proposes the SIC factor (SICF) as a novel metric for evaluating SI cancellation performance. Additionally, it introduces a new adaptive algorithm, SRLS-P, and compares its performance with classical RLS adaptive algorithms through simulations and lake experiments, aiming to enhance FD UWA systems in time-varying channels.

4. Complexity

Dealing with time-varying channels often requires sophisticated signal processing techniques and algorithms, increasing the complexity of communication systems.

Single-input multiple-output in time-varying channel is the subject of the paper [28]. These channels are time- and frequency-selective because of mobility as well as high data rate. The channel is modelled using a complex exponential basis expansion model (CE-BEM). They examine a block transmission system in which the maximal diversity possible for a CE-BEM channel is enabled on the transmitter side by use of a precoder. The resultant channel, upon block and symbol level direct decoding on the receiver side, is similar to a finite-impulse-response filter. As a result, they propose an equaliser with a structure similar to the effective channels.

The paper [29] examines OTFS modulation for high-mobility scenarios. The study introduces a precoded message passing algorithm with Doppler compensation, reducing receiver complexity. Additionally, it presents an enhanced approximate message passing algorithm with better performance and similar complexity compared

to conventional methods.

The paper [30] focuses on the uplink of a wireless MIMO communication system, employing multicarrier code-division multiple access for high-speed vehicular users. This study introduces a low-complexity receiver based on the Krylov subspace method, known for its efficient solutions with a tradeoff between accuracy and computational efficiency. Existing methods lack optimization for iterative interference cancellation, limiting their computational complexity reduction. The paper proposes an efficient iterative receiver in fast-fading channel for MU MIMO system. It employs parallel interference cancellation and joint channel estimation through soft-symbol-based techniques. The study explores PIC configurations in chip and user space, optimizing computational complexity while maintaining multiuser detection efficiency. Additionally, the paper presents reduced-rank channel estimation and efficient joint antenna detection methods for multicarrier code-division multiple access MIMO, aiming to significantly reduce computational load without compromising performance.

The paper [31] explores mmWave systems for high-data-rate communication, highlighting challenges with path and penetration loss. The paper proposes a novel hybrid precoding and combining algorithm, leveraging singular value decomposition to design analog precoders/combiners and reducing complexity by eliminating iterative processes. The adaptive algorithm updates singular vectors for improved performance without increased complexity, promising better efficiency in single-user systems.

5. Resource Allocation

Efficiently allocating resources, such as power and bandwidth, to adapt to changing channel conditions is a challenge in time-varying channels to ensure optimal

performance without wasting resources.

The research work [32] discusses resource allocation problems in multiuser OFDM systems in time-varying channels, highlighting the complexities in joint subcarrier and power allocation. It proposes an adaptive allocation scheme aiming to minimize transmit power while satisfying user data rate and BER constraints. The proposed algorithm utilizes a function designed via Lagrangian technique, selecting user-subcarrier pairs efficiently based on channel gain, data rate, and assigned subcarriers. This function aids in adjusting allocations across consecutive time frames. The computational complexity is reduced with fewer iterations. The scheme is considered state-of-the-art due to its effectiveness in solving the allocation problem with minimal complexity.

The paper in [33] addresses the surge in wireless data traffic due to video streaming and explores how OFDMA networks cater to this demand. It outlines challenges in on-demand streaming due to time-varying channels and proposes a resource management scheme. It introduces adaptive streaming and its role in providing multi-quality videos based on channel conditions. It proposes a dynamic resource management scheme integrating rate control and resource allocation for personalized on-demand streaming, aiming to maximize long-term quality satisfaction without prior channel statistics. The contributions include a user-quality satisfaction model, a joint resource allocation algorithm, and optimal low-complexity solutions for subcarrier assignment and power allocation. This scheme achieves competitive quality satisfaction levels compared to algorithms with complete channel knowledge.

The paper [34] focuses on optimizing resource allocation algorithms with QoS in time-varying channels. It discusses the challenges in meeting QoS requirements due to unpredictable channels and proposes an algorithm to adapt error protection to channel status and QoS needs. It evaluates this algorithm's efficiency in a time-

varying UWB channel under different receiver speeds.

The paper [35] examines Orthogonal Frequency Division Multiple Access (OFDMA) scheduling strategies. While typical approaches focus on instantaneous throughput, assuming infinite user data, this work considers realistic packet arrivals with finite rates. It prioritizes long-term average performance rather than instant optimization, highlighting the impact of queue backlog state information (QSI). The study also emphasizes the importance of QSI over CSI in practical scenarios.

In [36], the researchers state that the emergence of the Internet of Vehicles (IoV) in the Internet of Things (IoT) landscape has enabled intelligent traffic management and new user services. However, computational demands exceed the resources available in vehicles, prompting the rise of Vehicular Edge Computing (VEC). This system extends cloud services to the radio network's edge, optimizing resource utilization and reducing end-to-end delays. Challenges arise in dynamic resource allocation due to the mismatch between channel fading and task offloading time scales. Paper [36] addresses the impact of time-varying channels on resource allocation strategies in VEC systems, formulating utility maximization problems while considering task delay requirements. To solve these problems, novel algorithms are proposed, aiding in effective bandwidth allocation. Simulation results demonstrate these algorithms' efficacy in achieving high utility and meeting task delay requirements in the presence of time-varying channels, with a marginal utility gap compared to the upper bound.

The paper [37] explores power allocation in a satellite system transmitting data to multiple ground locations over time-varying downlink channels. They establish the capacity region, ensuring system stability under power-allocation policy. With unknown arrival rates and channel probabilities, the authors propose a policy which stabilizes the system within the capacity region, maintaining queue occupancy within limits. The study extends to joint routing and power-allocation problems.

The author also address interference issues due to bandwidth limitations and employing a Lyapunov function for analysis. It emphasizes its contribution in formulating a multibeam satellites power-control problem and developing algorithms which maximize the throughput. The method's applicability can extend to other wireless networking problems.

The paper [38] examines D2D networks coexisting with cellular networks, exploring their gains and interference challenges. It discusses resource allocation strategies (centralized vs. distributed), highlighting limitations in acquiring global network information. A novel distributed scheme using uncoupled Stochastic Learning Algorithm (SLA) is introduced. However, ensuring Cellular User Equipment (CUE) QoS remains a challenge. The paper's key contributions are: 1) Introducing an SLA-based distributed learning algorithm for D2D pairs without information exchange, addressing interference issues. 2) Formulating a Stackelberg game with pricing to maintain CUE QoS, dictating a price for D2D resource reuse. 3) Comparative analysis with existing schemes like hybrid and centralized exhaustive search methods. The proposed scheme focuses on reducing computational load and signaling overhead while balancing interference concerns and CUE QoS.

2.1.2 Channel Estimation Algorithms

Commonly used channel estimaiton algorithms includes least squares estimator, linear minimum mean squared error estimator and recursive least-squares(LS) estimator.

In [39], the author construct a windowed LS estimator for double-selective channels, and apply a straightforward windowing and dewindowing approach to enhance an existing BEM accuracy. Additionally, they create the ideal pilot pattern for the windowed least-squares estimator estimator.

In [40], the authors provide a channel estimator based on LS FFT. In the context of noninteger multipath delay profiles, the impact of intrinsic model misalignment error in the proposed estimator is examined, along with a performance study. An investigation is conducted into the best criteria for determining the ideal number of significant taps, after the relationship between the number of selected taps and the MSE is made clear.

[41] analyses the best possible system architecture for wireless communication networks in time-varying channels with incomplete CSI in order to maximise spectral efficiency. The proportion of pilot in the data block being transmitted has a significant impact on the performance; larger pilot percentages result in more overhead but also more accurate channel estimations. Using asymptotic analysis, the channel estimate MSE is obtained as the system parameters' closed-form expression. The MSE is used to quantify the impacts of pilot percentage.

In [42], researchers explore transmission over the double selective channel using cyclic-prefixed blocks, under the assumption that the channel obeys a complex-exponential basis expansion model. Firstly, a lower limit of channel estimation MSE is obtained. And then necessary constraints on the pilot pattern which accomplishes this limit are defined. Based on these, the author proposed a new MMSE methods, and lower and upper limit on their ergodic attainable rates are obtained. Additionally, a power allocation method between data and pilots is created. The analysis suggests that consideration should be given to the spreading parameters of the channel while selecting among affine proposed MMSE schemes. In particular, researchers prove that when the channel's Doppler-spread is far less than its delay-spread, the multicarrier scheme outperforms the single-carrier scheme, and vice versa.

The key factor contributing to the challenge of LMMSE estimation is the channel

covariance matrix's inverse. This is often considerable for time-varying channels. To minimise the number of estimating parameters, one method is to apply linear minimum mean squared error estimator with BEM. Channel coefficients in the frequency domain can also be utilised with the BEM. In this case, the highest Doppler shift determines the bandwidth. In [17], a BEM is utilised to approximate the channels, which are supposed to be fast-fading. The resultant frequency domain channel matrix is roughly banded instead of diagonal due to the time-variation. Researchers suggest new LMMSE and LS channel estimators to tackle out-of-band interference and noise. Furthermore, the receiver window's impact on the estimate of the channel is examined.

In [43], researchers study data detection and channel estimation for OFDM systems across doubly-selective channels. They develop the statistical features of an oversampling BEM for doubly-selective channels. With the help of the BEM, the temporal variety in the ICI caused by Doppler spread and its connection to the ICI caused by carrier frequency offset are demonstrated. Using the BEM, researchers construct two LMMSE channel estimators with low complexity. To equalise the ICI channel, modifications are made to the sphere decoder. Furthermore, an iterative low-complexity equaliser without matrix inversion is suggested. The low-complexity iterative equaliser also achieves performance that is comparable to sphere decoder.

In [44], using training symbols that are regularly sent and time-multiplexed, the researchers provide a tracking technique for the coefficients of BEM. They examine RLS techniques for BEM coefficient tracking, which do not require any model for the BEM coefficients.

In [45], the authors present an adaptive channel estimation method for OFDM systems. When parameters are selected appropriately, the proposed method can reach a steady state in a matter of a few OFDM symbols. The proposed method

is particularly effective and suited for a wide variety of channel circumstances, as shown by the authors' simulation results. Furthermore, this method may be used to MIMO OFDM systems with appropriate training sequence designs on transmitter antennas.

2.1.3 Channel Estimation in Time-varying Channels

In wireless communication systems, the accurate estimation of channel characteristics is paramount for reliable data transmission in time-varying channels. Channel estimation is crucial for decoding the transmitted signals accurately. Time-varying channels pose a significant challenge due to their dynamic nature, resulting in varying signal strengths and multipath effects. Robust and efficient channel estimation techniques are essential to adaptively track these changes, ensuring optimal signal reception and minimizing errors in data recovery.

Single Carrier System

The paper [14] discusses challenges in wireless digital communication systems like GSM due to Doppler spread, multipath delay spread and signal fading. It emphasizes the necessity of equalizers and diversity combining to mitigate intersymbol interference (ISI) and low signal-to-noise ratio (SNR). While slow fading can be managed with equalizers and diversity combining, fast frequency-selective fading poses receiver design challenges. The study explores effective methods for tracking fast-changing channels, focusing on a block adaptive decision feedback equalizer (DFE) with feedforward channel estimation. It introduces a novel channel estimation technique resilient to fast fading, and this can reduce training sequence length. A new DFE coefficient computation algorithm is proposed to handle rapid fadings.

The quasi-synchronous code-division multiple access (QS-CDMA) system employs

quasi-synchronous operation via GPS receivers. In QS-CDMA, the code acquisition complexity is reduced. However, mobile channel fluctuations impact performance. Prior joint estimation/detection efforts include expectation maximization algorithms and least-mean-square/recursive least-squares (RLS) approaches but struggle with rapid fading. The extended Kalman filter (EKF) method, handling time-varying channels as nonlinear parameters, is proposed. Unlike RLS, the EKF avoids over-parameterization by modeling delays as nonlinear variables. [13] introduces a joint channel estimation and multiuser detection method, using one EKF with the QR decomposition combined with the M-algorithm (QRD-M) algorithm, significantly enhancing QS-CDMA system performance over conventional detectors.

Deep learning (DL) has emerged as a promising tool, applied in diverse areas including network resource allocation, beamforming, speech processing, and channel estimation. [15] proposes a DL-based channel estimator for time-varying channels, training DNNs offline and fine-tuning them incrementally with pilot symbols. Simulation results showcase DNNs' capability to track channel variations, setting a path for future exploration in doubly-selective channels.

Multi Carrier System

While most OFDM systems rely on coherent detection, obtaining accurate channel state information poses challenges in time-varying channels, often achieved through training data-based channel estimation methods. However, these methods can lead to outdated information, reducing system performance and impeding techniques like adaptive modulation. The proposed novel schemes in [16] for decision-directed MMSE and adaptive channel prediction in OFDM systems offer updated, accurate channel information without additional delays, reduce complexity with efficient FFT implementations, and enable techniques improving system capacity and reliability.

These adaptive predictors don't require prior statistical knowledge and can track nonstationary channel and noise statistics. These advancements have potential applications in fading channel prediction in non-OFDM contexts as previously explored in the literature.

[17] focus on OFDM system in time-varying channels. The paper investigates frequency domain clustered pilot scheme, treating the frequency-domain channel matrix as approximately banded, concentrating most power around the main diagonal. The challenge lies in defining the bandwidth of this matrix. By intelligently considering this interference in traditional estimator designs like LMMSE and best linear unbiased estimator (BLUE), the paper shows enhanced estimation accuracy, contrasting the LS estimator's need for minimal interference. It proposes criteria to select optimal interference levels for different estimators.

[18] delves into channel estimation (CE) methods for coherent OFDM communication in time-varying channels characterized by wide Doppler and multipath delay spreads. Pilot-symbol-based CE methods, especially those employing comb-type pilot patterns, are highlighted for their effectiveness in tracking rapidly changing channel coefficients. This paper emphasizes techniques suitable for time-varying channels to analyze CE performance. It addresses CE issues related to residual timing errors in OFDM systems and proposes an LS CE method leveraging linearly frequency-modulated (LFM) or sliding partial-period pseudorandom (SPPPR) pilot symbols for effective interference reduction. The paper offers a novel approach for CE in OFDM systems with better resistance against timing errors, avoiding model mismatch, and extra phase rotation problems. Extensive simulations and statistical analyses validate the proposed technique.

The paper [19] discusses the challenges in channel estimation due to sparse multipath propagation in fast-fading channels. The paper introduces a dynamic para-

metric model allowing delays and path number to change with time. The proposed method suggests a low-complexity approach for time-varying OFDM channels, employing adaptive delay grids and an algorithm to track delay variation, followed by estimating the path gain with polynomial BEM. This method aims to offer efficient channel estimation and tracking while mitigating complexity issues in time-varying environments.

The paper [20] discusses time-domain synchronous orthogonal frequency division multiplexing (TDS-OFDM) systems, employed in digital terrestrial multimedia broadcasting standard. Unlike cyclic prefix-based OFDM, TDS-OFDM uses pseudo-noise sequences for synchronization and channel estimation, enhancing spectrum use and mitigating inter-block interference. Numerous studies have tackled time-varying multipath channels, employing compressive sensing, Bayesian methods, and adaptive estimation approaches. However, conventional methods neglect rapid channel changes, crucial in highly mobile scenarios. This study proposes a novel approach using a basis expansion model to estimate highly mobile channels in TDS-OFDM systems. To address rapid variations, a partitioned TDS-OFDM framework is introduced, enhancing channel estimation and symbol detection performance.

The paper [21] discusses channel estimation in OFDM systems for macrocellular uplink transmissions, which is critical for coherent detection. Existing methods tackle channel estimation in quasi-static channels but struggle with rapidly changing mobile scenarios where channel responses vary within an OFDM symbol. The paper introduces a new approach focusing on macrocellular OFDM uplink transmissions, aiming to estimate channel parameters by exploiting the orthogonality of training symbols. This method decouples channel parameters and proposes an order-recursive algorithm to handle nonlinear effects caused by Doppler shifts. Unlike prior works that assumed smaller Doppler shifts, this approach allows for larger Doppler

shifts, offering a refined channel estimation technique for time-varying channels in macrocellular OFDM systems.

MIMO System

In the applications like high-speed railways and vehicle-to-everything (V2X) communications, the complexity of fast-changing channels in MIMO-OFDM systems presents a significant challenge for efficient channel estimation algorithms.

The paper [22] outlines a novel sparse channel estimation method for massive MIMO-OFDM systems operating over time-varying channels. It emphasizes the need for accurate downlink channel state information and addresses challenges posed by the complexity of estimating numerous channel parameters, particularly in time-varying channels. The paper introduces a generalized spatial basis expansion model to capture spatial correlation and a quasi-block simultaneous orthogonal matching pursuit (SOMP) algorithm for channel recovery, addressing both delay domain sparsity and spatial correlation effectively. The simulation results validate the effectiveness of the proposed algorithms in achieving higher accuracy in channel estimation for massive MIMO-OFDM systems over time-varying channels.

The paper [23] details spatial modulation in MIMO systems, highlighting its benefits over conventional methods by utilizing antenna indices for information transmission. It presents challenges in dealing with fast time-varying channel. The paper proposes a novel channel estimation technique based on curve fitting. It addresses the challenges posed by SM-MIMO systems in rapidly changing channels, aiming for efficient estimation while minimizing overhead. Simulations validate the proposed algorithm's performance, showcasing its superiority compared to conventional methods and providing an analytical Bayesian MSE lower bound for benchmarking purposes.

Millimeter Wave System

In the realm of millimeter-wave (mmWave) communication in time-varying channels, channel estimation plays an even more critical role due to the huge propagation loss of these high-frequency bands. Accurate channel estimation techniques tailored for mmWave systems become pivotal, facilitating reliable and high-throughput data transmission. Robust algorithms capable of swiftly tracking the channel's changes in real-time while mitigating the effects of fading and multipath propagation are essential to harness the immense potential of mmWave technology in time-varying channels.

It is extremely difficult to estimate the channel for mmWave MU-MIMO downlink communications across a time-varying channel. This is because the enormous number of channel coefficients that need to be estimated as well as the significant mmWave transmission propagation loss. [25] proposes an efficient channel estimate approach for time-varying mmWave channels to address this issue. After finding that the variations in AoAs/AoDs change much more slowly than the variations in path gain, they come up with one structure of the transmission frame in which the channel estimation is divided into two distinct stages: the first stage involves estimating AoAs/AoDs, and the second stage involves estimating path gains.

2.2 ISAC in Time-varying Channels

2.2.1 Communication System in Time-varying Channels

In a time-varying channel, the channel conditions change rapidly over time due to factors such as movement of objects, multipath effects, and environmental changes. This poses significant challenges for communication systems, as the channel may vary within a single transmission or reception period. To combat the effects of fast

fading, communication systems employ techniques such as diversity and equalization. Current research mainly focus on OTFS system. As current 5G and 4G are both based on OFDM system, OFDM also needs attention in tackcling the challenges in ISAC in time-varying channels. Communication systems in time-varying channels require sophisticated signal processing techniques to ensure reliable communication in the presence of rapidly changing channel conditions.

OFDM in Time-varying Channels

Studies of communications in time-varying channels date back to the early 2000s. Time-varying channels are often handled using short packets and channel tracking based on frequent pilots. This method's primary advantage is its ease of use. It is not possible to replicate this technique in time-varying channels, though. A shorter OFDM symbol length results in worse spectral efficiency, which is unacceptable. Large Doppler frequency interference may also be eliminated from OFDM systems by using equalisers that can handle intercarrier interference (ICI) [46]. Nevertheless, until the recent release of [8], no closed-form equations have been given for frequency-domain signal models in time-varying channels. The frequency-domain relationship between the the received signal, transmitted signal and the channel is revealed in the work of [8]. It has been investigated to use a variety of signal preprocessing techniques to remove the ICI effects, but the majority of these cannot be applied to OFDM systems.

ICI Cancellation in OFDM

ICI cancellation can be reduced by taking use of frequency domain channel matrix's banded structure. The matrix inversion is one of the primary reasons of complexity. An easy way to solve this issue is to use the zero-forcing (ZF) equalizer. In the paper [47], the author presents a low-complex ZF approach to address the issue in SISO

OFDM systems. The fundamental concept is using Newton's iteration to inverse the matrix and investigate the unique structure present in the ICI matrix. The concept allows the complexity to be reduced from $O(N^3)$ to $O(Nlog2N)$ by using FFTs.

A novel theory of mobility adaptation is put out in [48] for high mobility OFDM systems. This theory allows for the dynamic optimisation and adjustment of some system parameters, which include the number of subcarriers, transmission power, and data rate, in response to movement speeds. Mobility adaptation's primary concept is to modify different system parameters for the purpose of keeping a balance between the effects of ICI and performance benefits. According to [48], based on the Doppler spread, the number of subcarriers is constantly changed so that systems with a larger Doppler spread require fewer subcarriers. Cutting down the subcarrier number will lower the ICI power at a given subcarrier bandwidth, but at cost of a larger proportion of CP.

OTFS

To cope with the large Doppler shifts in time-varying channels, OTFS systems [49] are also proposed recently. To deal with fast time-varying channels, in OTFS, the modulated signals at the transmitter are placed at the delay-Doppler domain. It is shown that OTFS can be regarded as a precoded OFDM system [8], with the capability of exploiting the channel diversity gain over time and frequency. OTFS has been hotly discussed in recent years. Though many aspects still remain unknown, some researchers place their hope on this modulation scheme. Research on integrated sensing and communication in fast-fading channels is still in its early stage.

Signal model of OTFS

At the transmission side, the symbols are initially placed at delay-Doppler domain. Then OTFS system maps symbols to time-frequency domain [50]

$$\mathbf{x}_{tf}[n,m] = \frac{1}{\sqrt{NM}} \sum_{o=0}^{N-1} \sum_{l=0}^{M-1} \mathbf{x}_{dd}[o,l] e^{j2\pi(\frac{no}{N} - \frac{ml}{M})} \tag{2.1}$$

for $m = 0, ..., M-1, n = 0, ..., N-1$, where $\mathbf{x}_{dd}$ represents the delay-Doppler domain signals , $\mathbf{x}_{tf}$ represents the time-frequency domain signals and M and N represent delay-Doppler grid size .

Then OTFS system modulates time-frequency domain samples to time domain using a rectangular transmit waveform g_{tx} as

$$x_t(t) = \sum_{m=0}^{M-1} \sum_{n=0}^{N-1} e^{j2\pi(t-nT)m\triangle f} g_{tx}(t-nT)\mathbf{x}_{tf}[n,m], \tag{2.2}$$

where x_t is the continuous time domain signals, T is sampling rate and $\triangle f$ is the subcarrier width.

At the receiver, the continues time-frequency domain signal is

$$y_{tf}(t,f) = \int e^{j2\pi f(t-s)} y_t(s) g^*_{rx}(s-t) ds \tag{2.3}$$

Then by sampling $y_{tf}(t,f)$ with different grid size, we obtain discrete time-frequency domain signal

$$\mathbf{y}_{tf}[n,m] = y_{tf}(t,f)|_{t=nT, f=m\triangle f} \tag{2.4}$$

for $n = 0, ..., N-1$ and $m = 0, ..., M-1$.

Next, the delay-Doppler domain signal is obtained by applying SFFT to the discrete time-frequency signal $\mathbf{y}_{tf}[n,m]$

$$\mathbf{y}_{dd}[o,l] = \frac{1}{\sqrt{MN}} \sum_{o=0}^{N-1} \sum_{l=0}^{M-1} \mathbf{y}_{tf}[n,m] e^{-j2\pi(\frac{no}{N} - \frac{ml}{M})} \tag{2.5}$$

2.2.2 Sensing in Time-varying Channels

Sensing in time-varying channels refers to the process of detecting and estimating parameters of interest (such as target location, velocity, or characteristics) using signals that experience rapid variations in the channel. In such channels, the received signal can be severely distorted due to multipath effects, Doppler shifts, and other phenomena.

To address the challenges of sensing in time-varying channels, various techniques can be employed. These include adaptive signal processing algorithms to track and estimate the changing channel conditions, as well as advanced modulation and coding schemes to improve the reliability of the transmitted signals. Additionally, beamforming and other spatial processing techniques can be used to enhance the signal-to-noise ratio and reduce the impact of fading.

Sensing Methods

DFT: It is also called periodogram. This method is widely used for estimating the signal parameters in various applications, including communication systems, signal analysis, and more [51]. The periodogram is calculated using the Fast Fourier Transform (FFT) algorithm, which efficiently computes the Discrete Fourier Transform (DFT). However, the basic periodogram might suffer from resolution issues, especially with limited data or noisy signals. Windowing techniques are often applied before computing the FFT to mitigate these issues and obtain a more accurate estimation of the spectral content. The 2D DFT extends the concept of the DFT to two-dimensional data, like images or spatial information. It's a powerful tool used in image processing, where spatial data is transformed into the frequency domain. Applications of 2D DFT include image compression, filtering, and feature extraction in image processing tasks. Understanding the frequency content in two dimensions

aids in various analytical and processing tasks related to spatial data.

Subspace Based Spectrum Analysis Techniques: Classical methods like Estimation of Signal Parameters via Rotational Invariance Techniques (ESPRIT) and the Multiple Signal Classification (MUSIC) algorithm belong to subspace-based spectrum analysis.

The MUSIC algorithm, introduced by Schmidt in 1986 [52], leverages matrix eigenspace decomposition. Operating in signal processing spaces divided into signal and noise subspaces—orthogonal to each other—the MUSIC algorithm capitalizes on their orthogonality. This approach constructs spectral functions and conducts peak searching to estimate signal parameters. Beyond Angle of Arrival (AOA) and Direction of Arrival (DOA) estimation, MUSIC finds applications in diverse fields like imaging [53], [54], acoustics [55], and even power transformer location [56]. Recent research explores novel domains, such as combining MUSIC with deep learning frameworks [57], extending the algorithm to 2D and 3D scenarios [54], [58].

ESPRIT, a variant of MUSIC, directly estimates parameters without peak searching, offering advantages for continuous parameters. Variants of ESPRIT like TLS-ESPRIT, Unitary-ESPRIT [59], EB-ESPRIT [60], SRI-ESPRIT [61], and QR TLS-ESPRIT [62] further enhance its adaptability.

Compressive Sensing Algorithms: Compressed sensing compresses signals during sampling and can achieve comparable performance to full sampling using fewer points. This technique finds applications in radar, communications, imaging, and audio signals. The concept, introduced by Candes and Donoho in 2004, reconstructs sparse signals with sampling rates far below the Nyquist bandwidth. Successful implementation hinges on sparsity and incoherence, requiring non-periodic sampling to avoid incoherent interferences resembling noise caused by original signal leakage.

Table 2.2: Sensing Methods Comparison

Methods	Advantages	Disadvantages
DFT	simple	low resolution, on-grid only
Subspace Based Spectrum Analysis Techniques	use fewer samples, off-grid	MUSIC requires peak search, which is inefficient
Compressive Sensing	use fewer samples, off-grid	

Sensing Domain

Time Domain: Studies exploring channel estimation in the time domain, such as the work by Suvra Sekhar Das [63], propose that the time-domain channel exhibits more sparsity than the delay-doppler domain. Their findings suggest a potential strategy: utilizing delay-Doppler domain pilots to estimate coefficients in the time-domain channel [63].

Frequency Domain:Research by [46] investigates pilot design, optimal estimation algorithms, and guard intervals in the frequency domain for time-varying channels. OFDM's prevalence in commercial wireless systems positions the frequency domain as a promising arena for channel estimation. However, design choices involving guard symbols to prevent intra-block interference pose challenges in balancing estimation simplicity and spectral efficiency.

Delay-Doppler Domain:A promising approach for addressing time-varying channels is the Orthogonal Time Frequency Space (OTFS) Modulation, first introduced by Hadani Ronny and Rakib Shlomo [64]. OTFS capitalizes on the delay-doppler domain, exploiting channel diversity across time and frequency. While OTFS garners significant attention and discussion in recent literature [65], [66], its efficacy in sensing applications remains uncertain. Sensing algorithms tailored for conventional systems like OFDM are yet to be studied. Most studies on OTFS focus on channel estimation in the delay-doppler domain, often utilizing guard symbols [5], [6]. For instance, [5] presents a pilot design scheme and a corresponding channel

estimation algorithm, ensuring interference-free estimation by incorporating guard intervals. Similarly, [6] extends guard symbols to 3-D and proposes a channel estimation algorithm for massive MIMO, leveraging channel sparsity across multiple dimensions.

While OTFS offers benefits like unified signal optimization for communication and sensing, complexities arise in signal processing and algorithmic design. The design's drawback becomes evident in time or frequency selective channels, where large delay or doppler may necessitate numerous guard symbols, severely impacting spectral efficiency.

2.2.3 Sensing Bounds

The Cramer-Rao lower bound (CRLB) is a commonly used performance constraint in ISAC systems. The lowest bound of estimate errors for communication channel estimation and radar sensing may be measured using the CRLB metric [3], [4]. Mutual Information(MI) is also a useful tool for measuring communication and radar performance.

Table 2.3: Sensing Bounds

Metrics	Meaning	Papers
MI	mutual dependence between the two variables	[67],[68],[69]
CRLB	lower bound of estimation error	[70],[1]

MI

As a waveform optimisation criteria, the mutual information between received signals and channels may be utilised for communications, while sensing can utilize the

mutual information between channel and signals [67], [69]. For example, in [67], the issue of designing radar waveforms for target identification and classification is discussed. The scattering properties of the extended target are modelled by a random target impulse response, and two problems related to designing radar waveforms have been examined. One is to use the knowledge of transmitted waveforms to construct waveforms that maximise the mutual information between the reflected waveforms and the random target impulse response. The second is to identify transmitted waveforms that minimises the MSE of impulse response of target. Research shows that these two problems bring about the same result that specifies the crucial component of the ideal waveform design when the overall power restriction is the same. Water-filling is used in the solution to distribute the limited power in the right places.

Mutual information is applied in enhancement for the functionality of coexisting communication radar system. For example, the performance of ISAC is derived in [68]. First, the authors determine the MI between the received signal and the target for ISAC sensing application. They calculate the maximum communication data rate that ISAC is capable of achieving. The MI for ISAC is then calculated.

CRLB

The Cramér-Rao Lower Bound (CRLB) is a fundamental concept in estimation theory, particularly in the context of parameter estimation. It provides a lower bound on the variance of any unbiased estimator for a given parameter. In simpler terms, it quantifies the best achievable precision or accuracy that any unbiased estimator can attain when estimating a parameter.

The CRLB is derived from the Fisher Information Matrix(FIM). The inverse of the Fisher Information matrix provides the lower bound on the covariance matrix of any

unbiased estimator for the parameters.

In various fields such as signal processing, communications, and radar, the CRLB is used extensively to evaluate the performance of estimators. It serves as a benchmark for assessing the quality of estimators, indicating the theoretical best performance one can achieve when estimating unknown parameters. If an estimator achieves a variance close to the CRLB, it suggests that the estimator is efficient and close to the best possible accuracy attainable in that scenario.

The CRLB is a powerful theoretical tool in understanding the fundamental limits of parameter estimation and plays a crucial role in designing and evaluating estimation algorithms in a wide array of scientific and engineering applications

CRLB in Time-varying Channels for ISAC

There is a lack of research on the sensing of CRLB in time-varying channels for ISAC systems. Since its closed-form formulations are normally difficult to acquire, numerical results are usually the only option when using the metric in signal optimisation [70]. The authors of [1] studied a cooperative radar sensing and communication system that uses OTFS modulation for data detection at the receiver and channel parameter estimation at the transmitter. They performed a waterfall analysis and calculated the CRLB for a single path. On the other hand, time-invariance of the channel is assumed in this work. Channel estimation is related to the parameter sensing problem [5]–[7] and has been studied in other works. There is currently no derivation of the sensing performance bound of ISAC in time-varying channels, and lack of knowledge of how the channel parameters in time-varying channels can affect the performance bound.

Chapter 3

Signal and Channel Models

3.1 Introduction

We first present the channel models in the time-varying channel in this chapter. Then, as OTFS system merges as a promising modulation scheme to tackle large Doppler, we present the signal models for OTFS system. After this, we brief the signal models for the OFDM system. Finally, we compare the frequency domain equalization to delay-Doppler domain equalization.

3.2 Time-varying Channel Models in Different Domains and Their Relationships

Consider the general time-varying channels in such an OFDM system, which can include time-invariant channel as a special case. Though we consider OFDM system here, the channel model can be applied to other system like OTFS as well. We assume the channel parameters such as channel amplitude, delay, and Doppler fre-

quency stay consistent throughout the interested period, and the channel variation is caused by the varying phases of the multipath due to Doppler frequencies.

Let $x(t)$ and $X(f)$ be the time- and frequency-domain representations of the transmitted signals, and $y(t)$ and $Y(f)$ be the corresponding received ones. We consider one block of OFDM signals of length $T = (N + N_{cp})T_0$, where T_0 is the sampling period when digitization, N is the number of samples of the OFDM symbol, and N_{cp} is the CP length. With the use of CP, $x(t) = x(t + NT_0)$ for $t \in [-N_{cp}T_0, 0]$. The total signal bandwidth is $B = 1/T_0$, and $f_0 = B/N$ is subcarrier width.

3.2.1 Detailed Continuous Channel Models

We consider a channel coherent processing interval (CPI) when the values of all the multipath parameters including amplitude, delay and Doppler frequency are almost unchanged. We first provide the basic channel models without considering the impact of CP.

During the k-th OFDM block, the delay-Doppler channel is

$$h_v(\tau, v) = \sum_{\ell=1}^{L} h'_\ell e^{j2\pi v_\ell kT} g_1(\tau - \tau_\ell) g_2(v - v_\ell), \tag{3.1}$$

where τ_ℓ, v_ℓ, and h'_ℓ are the delay, Doppler frequency, and amplitude of the ℓ-th path, $e^{j2\pi v_\ell kT}$ is the accumulated phase shift across OFDM blocks due to he Doppler frequencies, and $g_1(\cdot)$ and $g_2(\cdot)$ are Fourier transforms of the two windowing functions $G_1(f)$ and $G_2(t)$, respectively.

Without loss of generality, we consider the signal and channel in the duration of $[0, T)$, and the difference of channel and signal models between different OFDM blocks will be implicitly reflected via $h_\ell = h'_\ell e^{j2\pi v_\ell kT}$. The two windowing functions can have any shape. In the ideal case, $g_1(x) = g_2(x) = \delta(x)$ is an impulsive function. However, due to the limited spanning period, they are actually not. Without using

an explicit windowing function, the frequency-domain windowing function $G_1(f)$ is implicitly a rectangular function of width B with non-zero span from $-B/2$ to $B/2$, and the time-domain windowing function $G_2(t)$ is also a rectangular function with width corresponding to the signal period used for Doppler estimation. In the scenario considered here, $G_2(t)$ has a span of $NT_0 = N/B$ with $t \in [0, NT_0)$, as CP is discarded at the receiver. So implicitly, both $g_1(\cdot)$ and $g_2(\cdot)$ are sinc functions, multiplied with phase shifting terms if the central is not at 0. That is,

$$g_2(f) = \frac{\sin(\pi N T_0 f)}{(\pi N T_0 f)} \exp(-j\pi f N T_0). \tag{3.2}$$

The continuous delay-time domain channel over $t \in [0, T)$ can be represented as

$$h(\tau, t) = \int_{-\infty}^{+\infty} h_v(\tau, v) e^{j2\pi v t}\, dv = G_2(t) \sum_{\ell=1}^{L} h_\ell g_1(\tau - \tau_\ell) e^{j2\pi v_\ell t}. \tag{3.3}$$

The corresponding frequency-Doppler channel is

$$H_{fd}(f, v) = \int_{-\infty}^{+\infty} h_v(\tau, v) e^{-j2\pi f \tau} d\tau = G_1(f) \sum_{\ell=1}^{L} h_\ell g_2(v - v_\ell) e^{-j2\pi f \tau_\ell}. \tag{3.4}$$

The corresponding frequency-time channel can be represented as

$$H_{ft}(f, t) = \int_{-\infty}^{+\infty} H_{fd}(f, v) e^{j2\pi t v} dv = G_1(f) G_2(t) \sum_{\ell=1}^{L} h_\ell e^{j2\pi v_\ell t} e^{-j2\pi f \tau_\ell}. \tag{3.5}$$

Considering one block of the transmitted signal $x(t), t \in [0, T)$, with the use of CP such that $x(t) = x(t + T)$ for $t \in [-T_{CP}, 0)$. The corresponding received signal, after discarding the CP, is converted to the frequency domain. Without considering noise, the frequency-domain signal can be represented as

$$\begin{aligned} Y(f) &= \int_{-\infty}^{+\infty} y(t) e^{-j2\pi f t} dt \\ &= \int_{-\infty}^{+\infty} \left(\int_{-\infty}^{+\infty} H_{ft}(f', t) X(f') e^{j2\pi f' t} df' \right) e^{-j2\pi f t} dt \qquad (3.6) \\ &= \int_{-\infty}^{+\infty} H_{fd}(f', f - f') X(f') df', \qquad (3.7) \end{aligned}$$

where we have exploited the relationships of

$$y(t) = \int_{-\infty}^{+\infty} H(f', t)X(f')e^{j2\pi f' t}df', \ t \in [0, NT_0);$$
$$H_{fd}(f, v) = \int_{-\infty}^{+\infty} H_{ft}(f, t)e^{-j2\pi vt}dt. \tag{3.8}$$

3.2.2 Detailed Discrete Channel Models

We now derive the discrete channel and signal models, by considering the effect of CP and the sampling frequency in both the delay and Doppler domains. Let the discrete Fourier transform matrix be $\mathbf{F}$. Let $\mathbf{x}_f$ and $\mathbf{x}_t = \mathbf{F}\mathbf{x}_f$ be the frequency- and time-domain transmitted signal vectors of size $N \times 1$, corresponding to the continuous version signal of $x(t)$. Assume that CP of sufficient length is appended to $\mathbf{x}_t$.

Let $\mathbf{H}_t$ denote the general time-varying delay-time domain (i.e., time domain) discrete channel matrix in such an OFDM system, which can include time-invariant channel as a special case. For discrete signals, the time-domain received baseband signal for one OFDM block can be represented as

$$\mathbf{y}_t = \mathbf{H}_t\mathbf{x}_t. \tag{3.9}$$

When time-varying, $\mathbf{H}_t$ is not a circulant matrix. Instead, it may have correlated but different elements over different rows.

The freq-domain received signal can be represented as

$$\mathbf{y}_f = \mathbf{F}\mathbf{y}_t = \mathbf{F}\mathbf{H}_t\mathbf{x}_t = \mathbf{H}_{ft}\mathbf{x}_t = (\mathbf{F}\mathbf{H}_t\mathbf{F}^H)\mathbf{F}\mathbf{x}_t = \mathbf{H}_{fd}\mathbf{x}_f, \tag{3.10}$$

where $\mathbf{x}_f = \mathbf{F}\mathbf{x}_t$. In the equation, $\mathbf{H}_{fd}$ and $\mathbf{H}_{ft}$ denote the corresponding freq-doppler and freq-time channel matrices, respectively. We have the following relationships:

- $\mathbf{H}_{fd} = \mathbf{F}\mathbf{H}_t\mathbf{F}^H = \mathbf{H}_{ft}\mathbf{F}^H$. $\mathbf{H}_{fd}$ is a diagonal matrix for time-invariant channels, but not for time-varying channels;
- $\mathbf{H}_{ft} = \mathbf{H}_{fd}\mathbf{F} = \mathbf{F}\mathbf{H}_t$.

Following the time-varying convolution process, the elements of the matrix $\mathbf{H}_t$ are given by

$$\mathbf{H}_t = \begin{pmatrix} h(0,0) & h(N-1,0) & \dots & h(1,0) \\ h(1,1) & h(0,1) & \dots & h(2,1) \\ \vdots & \vdots & \ddots & \vdots \\ h(N-1,N-1) & h(N-2,N-1) & & h(0,N-1) \end{pmatrix}. \tag{3.11}$$

Therefore, the (n,m)-th element of $\mathbf{H}_t$, $(\mathbf{H}_t)_{n,m}$, $n = 0, \cdots, N-1, m = 0, \cdots, N-1$, is

$$(\mathbf{H}_t)_{n,m} = h((n-m)_N, n), \tag{3.12}$$

where $(n)_N$ is the modular operation $\mod(n, N)$, and

$$h(n,m) \triangleq h(nT_0, mT_0) = G_2(mT_0) \sum_{\ell=1}^{L} h_\ell \, g_1((nT_0 - \tau_\ell)_{NT_0}) \, e^{j2\pi v_\ell m T_0}, \tag{3.13}$$

where the modular operation is similarly due to the use of CP.

Referring to (3.7), we can get the (n,m)-th element of $\mathbf{H}_{fd}$, $(\mathbf{H}_{fd})_{n,m}$ as

$$(\mathbf{H}_{fd})_{n,m} = H_{fd}(mf_0, (n-m)_N f_0) = G_1(mf_0) \sum_{\ell=1}^{L} h_\ell \, g_2(((n-m)f_0 - v_\ell)_{Nf_0}) \, e^{-j2\pi m f_0 \tau_\ell}. \tag{3.14}$$

Note that the digitized $H_{fd}(f,v)$ exhibits periodicity of period B in Doppler domain, corresponding to time-domain sampling period $1/B$. Therefore, $(\mathbf{H}_{fd})_{n,m}$ corresponds to the frequency-Doppler domain sample with digital frequency mf_0 and Doppler frequency $(n-m)f_0$. Note that elements in each column of $\mathbf{H}_{fd}$ correspond to the same frequency, but with different Doppler frequencies. Also note

that the discrete functions $g_1(\cdot)$ and $g_2(\cdot)$ will not have the exact forms with their continuous versions because sampling causes spectrum overlapping, so each of them could be the sum of the basic function and its shifted versions at the sampling rate, respectively. When aliasing is small, however, they approximately resemble the continuous versions. According to the DFT relationship, we can also obtain

$$g_1(\tau) = \frac{(1 - \exp(j2\pi\tau))}{N(1 - \exp(j2\pi\tau/N))}, \tag{3.15}$$

and

$$g_2(f) = \frac{(1 - \exp(-j2\pi f))}{N(1 - \exp(-j2\pi f/N))}, \tag{3.16}$$

which can be shown to match the shifted sinc functions well. Taking note of the fact that $g_1(\tau)$ and $g_2(f)$ both exhibit periodic behaviour with a period of T_0N and f_0N, respectively. For simplicity of notation, we will omit the modular operation in them hereafter.

3.3 Data Symbols Modulated in Delay-Doppler Domain

The data processing at both transmitter and receiver are illustrated as follow.

At transmission side, symbols are initially positioned at delay-Doppler domain. Then OTFS system maps symbols to time-frequency domain

$$\mathbf{X}_{tf}[n, m] = \frac{1}{\sqrt{NM}} \sum_{o=0}^{N-1} \sum_{l=0}^{M-1} \mathbf{X}_{dd}[o, l] e^{j2\pi(\frac{no}{N} - \frac{ml}{M})}, \tag{3.17}$$

for $n = 0, ..., N-1, m = 0, ..., M-1$, where $\mathbf{X}_{dd}$ represents the delay-Doppler domain signals , $\mathbf{X}_{tf}$ represents the time-frequency domain signals and M and N represent delay-Doppler grid size .

Then OTFS system modulates time-frequency domain samples to time domain using a rectangular transmit waveform g_{tx} as

$$x_t(t) = \sum_{m=0}^{M-1} \sum_{n=0}^{N-1} e^{j2\pi(t-nT)m\triangle f} g_{tx}(t - nT)\mathbf{X}_{tf}[n, m], \tag{3.18}$$

where x_t is the continuous time domain signals, T is sampling rate and $\triangle f$ is the subcarrier width .

The transmitted signal $x_t(t)$ propagates over time-varying channel. The received signal $y_t(t)$ is given by

$$y_t(t) = \iint h(\tau, \nu)x_t(t - \tau)e^{j2\pi\nu(t-\tau)}d\tau d\nu. \tag{3.19}$$

Because only a few reflectors associated with Doppler and delays, only a few of parameters exist in channel model. The expression for $h(\tau, \nu)$ is

$$h(\tau, \nu) = \sum_{i=1}^{P} h_i g_1(\tau - \tau_i)g_2(\nu - \nu_i). \tag{3.20}$$

where τ_i, ν_i and h_i represent the delay, Doppler and subpath gain associated with i-th subpath, respectively; P is subpaths number. Moreover, $g_1(\cdot)$ and $g_2(\cdot)$ are the Fourier transforms of window functions $G_1(f)$ and $G_2(t)$. The two windowing functions can have any shape. In the ideal case, $g_1(x) = g_2(x) = \delta(x)$ is an impulsive function. However, due to the limited spanning period, they are actually not. Without using an explicit windowing function, the frequency-domain windowing function $G_1(f)$ is implicitly a rectangle of width B with non-zero span from $-B/2$ to $B/2$, and the time-domain windowing function $G_2(t)$ is also a rectangle with width corresponding to the signal period used for Doppler estimation. In the

scenario considered here, $G_2(t)$ has a span of $NT_0 = N/B$, as CP is discarded at the receiver. So implicitly, both $g_1(\cdot)$ and $g_2(\cdot)$ are sinc functions, multiplied with phase shifting terms if the center of $G_1(f)$ or $G_2(t)$ is not at 0.

At the receiving side, the continues time-frequency signals are

$$y_{tf}(t,f) = \int e^{j2\pi f(t-s)} y_t(s) g_{rx}^*(s-t) ds. \tag{3.21}$$

Then by sampling $y_{tf}(t,f)$ with different grid size, we obtain discrete time-frequency domain signal

$$\mathbf{Y}_{tf}[n,m] = y_{tf}(t,f)|_{t=nT, f=m\triangle f}, \tag{3.22}$$

for $m = 0, ..., M-1$ and $n = 0, ..., N-1$.

Next, we get delay-Doppler domain signal by applying SFFT to $\mathbf{Y}_{tf}[n,m]$

$$\mathbf{Y}_{dd}[o,l] = \frac{1}{\sqrt{MN}} \sum_{o=0}^{N-1} \sum_{l=0}^{M-1} \mathbf{Y}_{tf}[n,m] e^{-j2\pi(\frac{no}{N} - \frac{ml}{M})}. \tag{3.23}$$

3.4 Data Symbols Modulated in Frequency Domain

The received continuous signal in the frequency domain can be represented as [8]

$$Y(f) = \int_{-\infty}^{+\infty} H_{fd}(f', f-f') X(f') df', \tag{3.24}$$

where $X(f')$ is the transmission signal in the frequency domain.

By sampling and digitalization, we obtain discrete frequency signals and channel models:

$$\mathbf{y}_f = \mathbf{H}_{fd}\mathbf{x}_f, \tag{3.25}$$

where $\mathbf{x}_f$ denotes the transmitted signal in frequency domain and $\mathbf{y}_f$ denotes the received signal in frequency domain. $\mathbf{H}_{fd}$ is the frequency-Doppler channel matrix.

3.5 Linear Equalization in Different Domains

OTFS stands out for its potential to harness both frequency diversity and time diversity, rendering it a promising modulation scheme adept at addressing challenges posed by time-varying channels [64], [71]. While symbols in OTFS reside within the delay-Doppler domain, the choice of domain for equalization isn't confined solely to the delay-Doppler space. Alternatively, received data symbols can be transformed into the frequency domain for equalization, mirroring the process seen in OFDM. This prompts inquiries regarding the performance discrepancies between equalization in the frequency domain and equalization in the delay-Doppler domain.

This section aims to conduct a theoretical comparison between delay-Doppler domain equalization and frequency domain equalization within OTFS system. The endeavor begins by elucidating the relationship between the delay-Doppler domain channel and its counterpart in the frequency domain. Subsequently, a comparative performance analysis of delay-Doppler domain equalization versus frequency domain equalization is conducted. The illustration encompasses both MMSE equalization and Zero-Forcing (ZF) equalizer techniques. Theoretical proofs substantiate these comparisons, followed by validation through simulation results.

3.5.1 Relationship Between Delay-Doppler Domain and Frequency Domain Channels for OTFS System

As showed in section3.4, OTFS can be regarded as a precoded OFDM system. The formulate is below

$$\mathbf{y}_f = \mathbf{H}_{fd}[\mathbf{F}_{MN}(\mathbf{F}_N^H \otimes \mathbf{I}_M)]vec(\mathbf{X}_{dd}) + \mathbf{w}. \tag{3.26}$$

To gain the equivalent delay-Doppler domain channel, we turn the frequency domain received signal $\mathbf{y}_f$ into delay-Doppler domain signal

$$\begin{aligned} &vec(\mathbf{Y}_{dd}) = [\mathbf{F}_{MN}(\mathbf{F}_N^H \otimes \mathbf{I}_M)]^H \mathbf{y}_f = \\ &[\mathbf{F}_{MN}(\mathbf{F}_N^H \otimes \mathbf{I}_M)]^H \mathbf{H}_{fd}[\mathbf{F}_{MN}(\mathbf{F}_N^H \otimes \mathbf{I}_M)]vec(\mathbf{X}_{dd}) + \\ &[\mathbf{F}_{MN}(\mathbf{F}_N^H \otimes \mathbf{I}_M)]^H \mathbf{w}. \end{aligned} \tag{3.27}$$

So the relationship of delay-Doppler domain channel matrix $\mathbf{H}_{dd}$ and the frequency domain channel matrix $\mathbf{H}_{fd}$ is

$$\mathbf{H}_{dd} = [\mathbf{F}_{MN}(\mathbf{F}_N^H \otimes \mathbf{I}_M)]^H \mathbf{H}_{fd}[\mathbf{F}_{MN}(\mathbf{F}_N^H \otimes \mathbf{I}_M)]. \tag{3.28}$$

3.5.2 Comparison of Delay-Doppler Domain Equalization and Frequency Domain Equalization for OTFS System

We first illustrate using ZF equalizer. Then we extend our results to MMSE equalizer. The ZF equalizer in delay-Doppler domain is

$$vec(\hat{\mathbf{X}}_{dd}) = \mathbf{H}_{dd}^H(\mathbf{H}_{dd}\mathbf{H}_{dd}^H)^{-1}vec(\mathbf{Y}_{dd}). \tag{3.29}$$

And the frequency domain ZF equalizer is

$$\dot{\mathbf{x}}_f = \mathbf{H}_{fd}^H(\mathbf{H}_{fd}\mathbf{H}_{fd}^H)^{-1}\mathbf{y}_f. \tag{3.30}$$

Next, we show that delay-Doppler domain equalization equals to that in frequency domain. We show this in the following derivaiton

As

$$\mathbf{H}_{dd} = [\mathbf{F}_{MN}(\mathbf{F}_N^H \otimes \mathbf{I}_M)]^H\mathbf{H}_{fd}[\mathbf{F}_{MN}(\mathbf{F}_N^H \otimes \mathbf{I}_M)], \tag{3.31}$$

and

$$vec(\hat{\mathbf{X}}_{dd}) = [\mathbf{F}_{MN}(\mathbf{F}_N^H \otimes \mathbf{I}_M)]^H\hat{\mathbf{x}}_f, \tag{3.32}$$

$$vec(\mathbf{Y}_{dd}) = [\mathbf{F}_{MN}(\mathbf{F}_N^H \otimes \mathbf{I}_M)]^H\mathbf{y}_f \tag{3.33}$$

,

equation (3.29) becomes

$$[\mathbf{F}_{MN}(\mathbf{F}_N^H \otimes \mathbf{I}_M)]^H \hat{\mathbf{x}}_f = [[\mathbf{F}_{MN}(\mathbf{F}_N^H \otimes \mathbf{I}_M)]^H \mathbf{H}_{fd}^H [\mathbf{F}_{MN}(\mathbf{F}_N^H \otimes \mathbf{I}_M)]] \tag{3.34}$$
$$([\mathbf{F}_{MN}(\mathbf{F}_N^H \otimes \mathbf{I}_M)]^H \mathbf{H}_{fd} [\mathbf{F}_{MN}(\mathbf{F}_N^H \otimes \mathbf{I}_M)][\mathbf{F}_{MN}(\mathbf{F}_N^H \otimes \mathbf{I}_M)]^H \mathbf{H}_{fd}^H [\mathbf{F}_{MN}(\mathbf{F}_N^H \otimes \mathbf{I}_M)])^{-1}$$
$$[\mathbf{F}_{MN}(\mathbf{F}_N^H \otimes \mathbf{I}_M)]^H \mathbf{y}_f.$$

As

$$[\mathbf{F}_{MN}(\mathbf{F}_N^H \otimes \mathbf{I}_M)]^H = [\mathbf{F}_{MN}(\mathbf{F}_N^H \otimes \mathbf{I}_M)]^{-1}, \tag{3.35}$$

we simplify the equation above and the result is

$$\begin{aligned}
&\hat{\mathbf{x}}_f = \mathbf{H}_{fd}^H [\mathbf{F}_{MN}(\mathbf{F}_N^H \otimes \mathbf{I}_M)]([\mathbf{F}_{MN}(\mathbf{F}_N^H \otimes \mathbf{I}_M)]^H \qquad (3.36)\\
&\mathbf{H}_{fd} \mathbf{H}_{fd}^H [\mathbf{F}_{MN}(\mathbf{F}_N^H \otimes \mathbf{I}_M)])^{-1} [\mathbf{F}_{MN}(\mathbf{F}_N^H \otimes \mathbf{I}_M)]^H \mathbf{y}_f\\
&= \mathbf{H}_{fd}^H [\mathbf{F}_{MN}(\mathbf{F}_N^H \otimes \mathbf{I}_M)][\mathbf{F}_{MN}(\mathbf{F}_N^H \otimes \mathbf{I}_M)]^H (\mathbf{H}_{fd} \mathbf{H}_{fd}^H)^{-1} [\mathbf{F}_{MN}(\mathbf{F}_N^H \otimes \mathbf{I}_M)]\\
&[\mathbf{F}_{MN}(\mathbf{F}_N^H \otimes \mathbf{I}_M)]^H \mathbf{y}_f\\
&= \mathbf{H}_{fd}^H (\mathbf{H}_{fd} \mathbf{H}_{fd}^H)^{-1} \mathbf{y}_f.
\end{aligned}$$

Compare the result above to equation (3.30), we can see that $\hat{\mathbf{x}}_f$ is identical to $\dot{\mathbf{x}}_f$, which indicates that the delay-Doppler domain ZF equalization in OTFS is identical to the frequency domain ZF equalization.

We now illustrate using MMSE equalizer. The MMSE equalizer in delay-Doppler domain is

$$vec(\hat{\mathbf{X}}_{dd}) = \mathbf{H}_{dd}^H (\mathbf{H}_{dd} \mathbf{H}_{dd}^H + \sigma^2 \mathbf{I})^{-1} vec(\mathbf{Y}_{dd}). \tag{3.37}$$

And the frequency domain MMSE equalizer is

$$\dot{\mathbf{x}}_f = \mathbf{H}_{fd}^H(\mathbf{H}_{fd}\mathbf{H}_{fd}^H + \sigma^2\mathbf{I})^{-1}\mathbf{y}_f. \tag{3.38}$$

Next, we show that delay-Doppler domain equalization equals to that in frequency domain. We show this in the following derivaiton

As

$$\mathbf{H}_{dd} = [\mathbf{F}_{MN}(\mathbf{F}_N^H \otimes \mathbf{I}_M)]^H \mathbf{H}_{fd}[\mathbf{F}_{MN}(\mathbf{F}_N^H \otimes \mathbf{I}_M)], \tag{3.39}$$

and

$$vec(\hat{\mathbf{X}}_{dd}) = [\mathbf{F}_{MN}(\mathbf{F}_N^H \otimes \mathbf{I}_M)]^H \hat{\mathbf{x}}_f, \tag{3.40}$$

$$vec(\mathbf{Y}_{dd}) = [\mathbf{F}_{MN}(\mathbf{F}_N^H \otimes \mathbf{I}_M)]^H \mathbf{y}_f, \tag{3.41}$$

equation (3.37) becomes

$$\begin{aligned}
&[\mathbf{F}_{MN}(\mathbf{F}_N^H \otimes \mathbf{I}_M)]^H \hat{\mathbf{x}}_f = [[\mathbf{F}_{MN}(\mathbf{F}_N^H \otimes \mathbf{I}_M)]^H \mathbf{H}_{fd}^H[\mathbf{F}_{MN}(\mathbf{F}_N^H \otimes \mathbf{I}_M)]] \\
&([\mathbf{F}_{MN}(\mathbf{F}_N^H \otimes \mathbf{I}_M)]^H \mathbf{H}_{fd}[\mathbf{F}_{MN}(\mathbf{F}_N^H \otimes \mathbf{I}_M)][\mathbf{F}_{MN}(\mathbf{F}_N^H \otimes \mathbf{I}_M)]^H \mathbf{H}_{fd}^H[\mathbf{F}_{MN}(\mathbf{F}_N^H \otimes \mathbf{I}_M)] \\
&+ \sigma^2\mathbf{I})^{-1}[\mathbf{F}_{MN}(\mathbf{F}_N^H \otimes \mathbf{I}_M)]^H \mathbf{y}_f.
\end{aligned} \tag{3.42}$$

As

$$[\mathbf{F}_{MN}(\mathbf{F}_N^H \otimes \mathbf{I}_M)]^H = [\mathbf{F}_{MN}(\mathbf{F}_N^H \otimes \mathbf{I}_M)]^{-1}, \tag{3.43}$$

we simplify the equation above and the result is

$$
\begin{aligned}
\hat{\mathbf{x}}_f &= \mathbf{H}_{fd}^H[\mathbf{F}_{MN}(\mathbf{F}_N^H \otimes \mathbf{I}_M)]([\mathbf{F}_{MN}(\mathbf{F}_N^H \otimes \mathbf{I}_M)]^H \mathbf{H}_{fd}\mathbf{H}_{fd}^H[\mathbf{F}_{MN}(\mathbf{F}_N^H \otimes \mathbf{I}_M)] \\
&+ \sigma^2\mathbf{I})^{-1}[\mathbf{F}_{MN}(\mathbf{F}_N^H \otimes \mathbf{I}_M)]^H \mathbf{y}_f \\
&= \mathbf{H}_{fd}^H[\mathbf{F}_{MN}(\mathbf{F}_N^H \otimes \mathbf{I}_M)]([\mathbf{F}_{MN}(\mathbf{F}_N^H \otimes \mathbf{I}_M)]^H (\mathbf{H}_{fd}\mathbf{H}_{fd}^H)^{-1}[\mathbf{F}_{MN}(\mathbf{F}_N^H \otimes \mathbf{I}_M)] \\
&+ \frac{1}{\sigma^2}\mathbf{I})[\mathbf{F}_{MN}(\mathbf{F}_N^H \otimes \mathbf{I}_M)]^H \mathbf{y}_f \\
&= \mathbf{H}_{fd}^H((\mathbf{H}_{fd}\mathbf{H}_{fd}^H)^{-1} + \frac{1}{\sigma^2}\mathbf{I})\mathbf{y}_f \\
&= \mathbf{H}_{fd}^H(\mathbf{H}_{fd}\mathbf{H}_{fd}^H + \sigma^2\mathbf{I})^{-1}\mathbf{y}_f.
\end{aligned} \tag{3.44}
$$

Compare the equation above to equation 3.38, we can see that $\hat{\mathbf{x}}_f$ is identical to $\dot{\mathbf{x}}_f$, which indicates that the delay-Doppler domain MMSE equalization in OTFS is identical to the frequency domain MMSE equalization.

We next validate our derivation via simulaitons. Unless state otherwise, the simulation parameters are listed below

Figure 3.1 and figure 3.2 compare the BER performance in frequency domain equalization and delay-Doppler domain equalization. Figure 3.1 simulates the ZF equalizaiton method while figure 3.2 simulates the MMSE equalization method. It can be seen from figure 3.1 and figure 3.2 that the delay-Doppler domain equaliazation and frequency domain equalization have the same BER performance, which aligns with our theoretical analysis.

Table 3.1: Simulation Parameters

OTFS frame size	4*16
Bandwidth	1
Sampling period	1
Number of subpath	4
total transmission power	1
Modulation	QPSK
default minimum channel Doppler	0
default maximum channel Doppler	1/MN
default minimum channel delay	0
default maximum channel delay	4

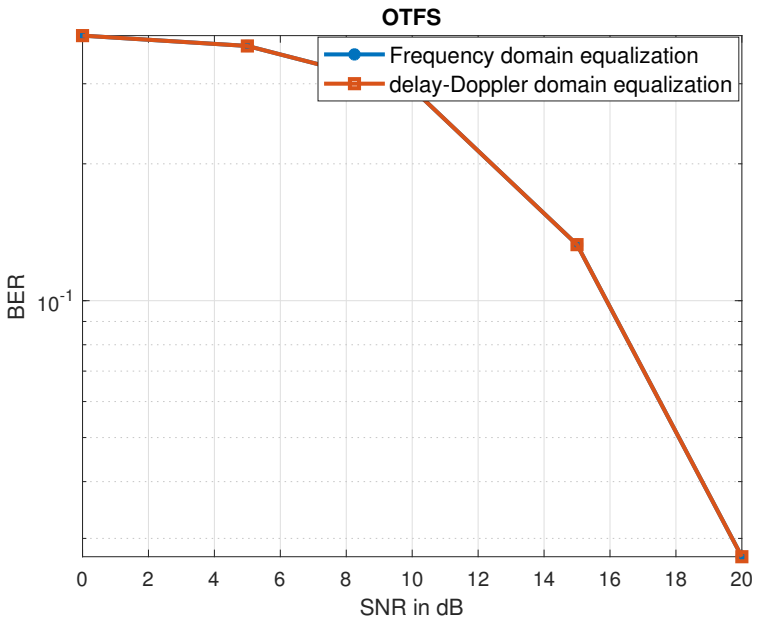

Figure 3.1: Comparison between delay-Doppler domain and frequency domain ZF equalization.

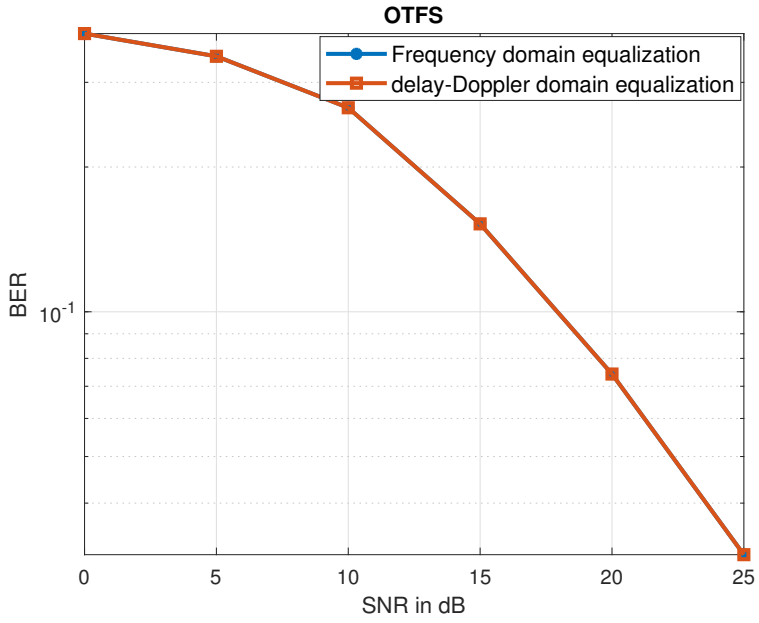

Figure 3.2: Comparison between delay-Doppler domain and frequency domain MMSE equalization.

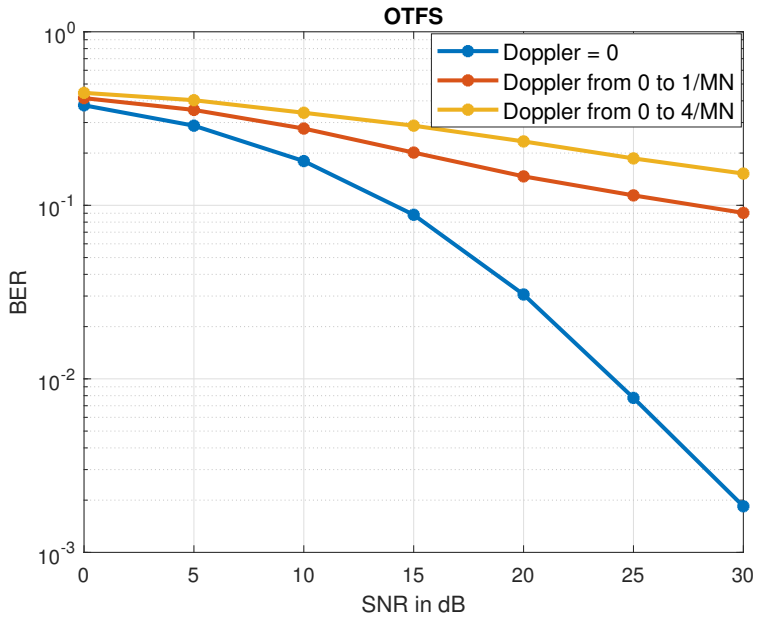

Figure 3.3: ZF equalization performance in time-varying channels 1.

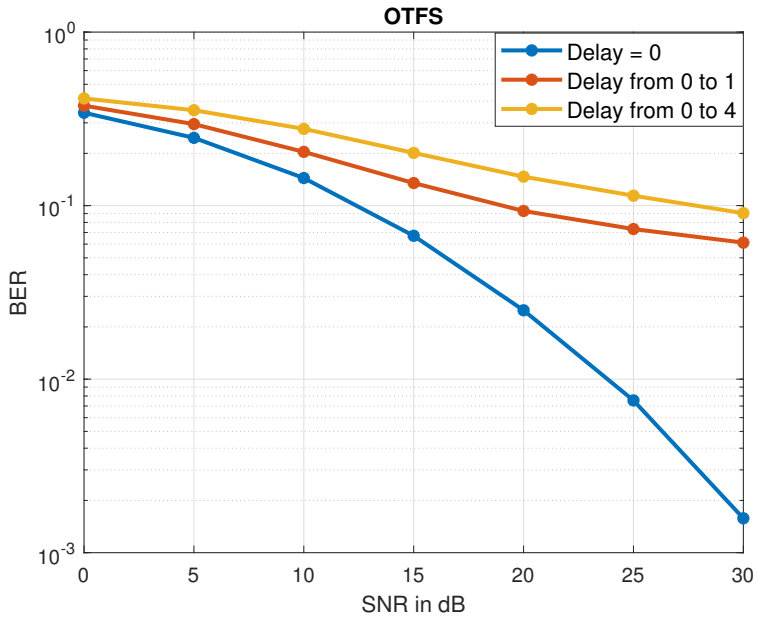

Figure 3.4: ZF equalization performance in time-varying channels 2.

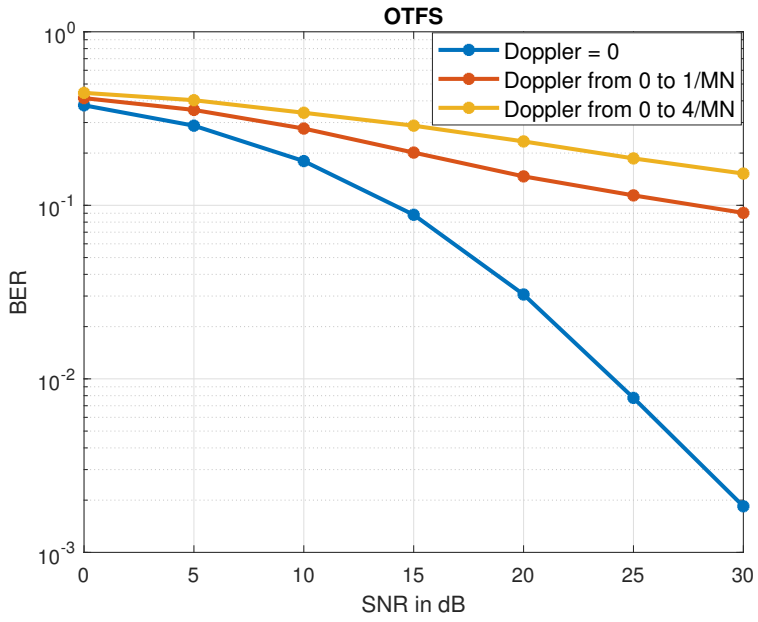

Figure 3.5: MMSE equalization performance in time-varying channels 1.

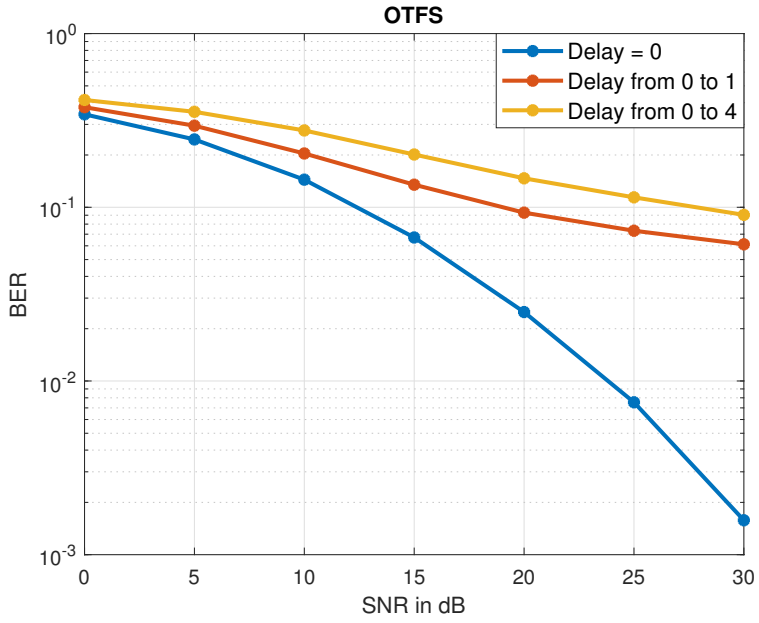

Figure 3.6: MMSE equalization performance in time-varying channels 2.

In the figure 3.3, figure 3.4, figure 3.5 and figure 3.6, we compare the equalization performance with varying Doppler or delay value in the time-varying channels. Figure 3.3 shows the BER performance with various channel Doppler values under ZF equalization. Figure 3.4 shows the BER performance with various channel delay values under ZF equalization. Figure 3.5 shows the BER performance with various channel Doppler values under MMSE equalization. And figure 3.6 shows the BER performance with various channel delay values under MMSE equalization. It can be seen from these figures that the BER performance gets worse with larger channel delay or channel Doppler.

3.6 Conclusions

In this chapter, we begin by introducing the channel model for time-varying channels. Unlike time-invariant channels, these channels exhibit distinct properties: the time

domain channel matrix loses its circular structure, and the frequency domain channel matrix no longer remains diagonal.

Subsequently, we delve into OTFS system, a promising modulation scheme designed to address the challenges posed by time-varying channels. We provide a comprehensive overview of the signal models associated with OTFS system.

Following our exploration of OTFS, we offer a brief examination of the signal model pertaining to the well-established OFDM system.

Lastly, we conduct an analysis, contrasting frequency domain equalization with delay-Doppler domain equalization. It turns out the performances of the two approaches are the same.

Chapter 4

Mixed-stage OTFS Systems

4.1 Introduction

In conventional OTFS system, one OTFS frame corresponds to one delay-Doppler grid. When it comes to multi-user system, all users share the same delay-Doppler grid size. This makes it impossible for individual user to change its delay-Doppler grid size according to the channel condition, thus compromising the communication performance, especially when the channel is highly dynamic.

In this chapter, we propose a multi-user mixed-stage OTFS system, where one OTFS frame can contain multiple delay-Doppler grids. This give the flexibility to the users to adapt their grid size according different channel conditions, thus improving the overall performance.

In the following sections, we first demonstrate in section 4.2 how delay-Doppler grid size can affect communication performance. It turns out that we can achieve better performance by adjust delay-Doppler grid size according to the channel conditions. Then we propose mixed-stage OTFS system in section 4.4. How to put data symbols

of different delay-Doppler grid sizes onto one OTFS frame is also given. Simulation results of mixed-stage OTFS system can be found in section 4.6.

4.2 OTFS Performance Difference under Different Delay-Doppler Grid Size

OTFS modulation system puts symbols onto delay-Doppler grid. However, some fundemental issues have not been addressed so far, for example, how we should choose the grid size. Different channel parameters will affect system performance. Will there be a better grid size for one certain set of channel parameters? In this section, we address these issues via simulation.

Within this section, we present an analysis to the BER performance exhibited by different delay-Doppler grid size OTFS systems. The product of N and M is fixed at 64. When $N = 1$, the system becomes SC-FDE sytem. When $M = 1$, the system becomes OFDM system. We have deliberately excluded system imperfections such as carrier frequency offset and peak-to-average power ratio distortion from the simulation.

The figure depicts the outcomes of our simulations, focusing on uncoded, 16QAM modulated OTFS system with $N = 1(SC - FDE)$ and $M = 1(OFDM)$ systems as well. The channel model is adopted from [11]. It is important to note that we presume perfect channel estimation for this work.

A) time-invariant channels

In time-invarint scenarios, Doppler values are set to zeros. It can be seen from the Figure 4.1 that smaller N results in lower BER in high SNR region, and smaller M results in lower BER in low SNR region. The precise SNR level at which the two

systems exhibit equivalent performance depends on the specific parameters of the channel. Consequently, this distinction in performance between OTFS, OFDM and SC-FDE ssytems becomes evident. This trend above is because $N = 1(SC - FDE)$ system has frequency diversity, but suffers from noise enhancement problems due to the extra IFFT operation after equalization. So SC-FDE outperforms others when SNR is high, and perform relatively poor when SNR is low. When N increases and M decreases, the system frequency diversity decreases but suffers from less noise enhancement at the same time. Therefore, as the N increases and M decreases, the system does better in low SNR but perform worse in high SNR.

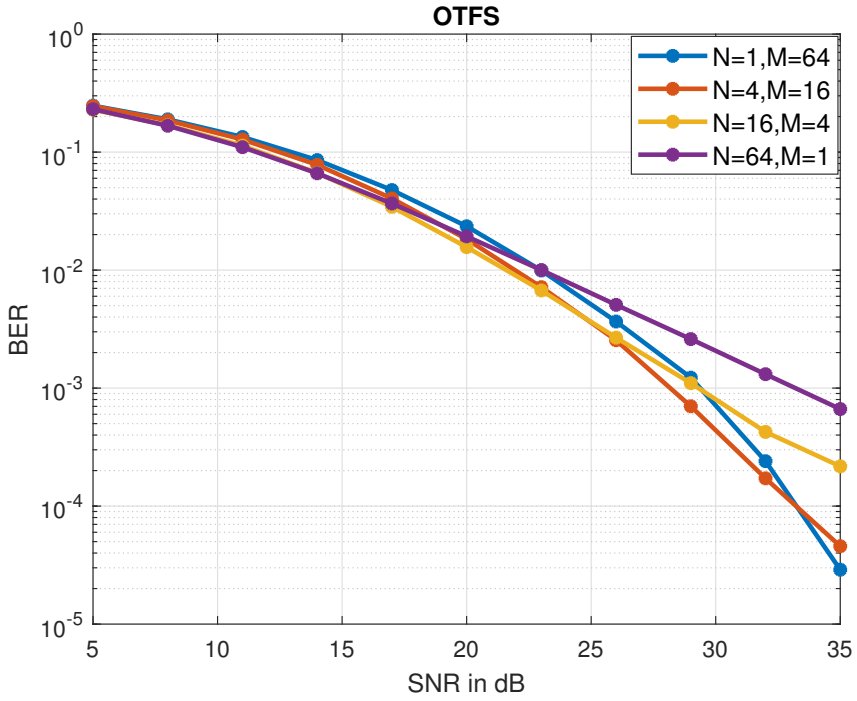

Figure 4.1: OTFS in time invariant channels.

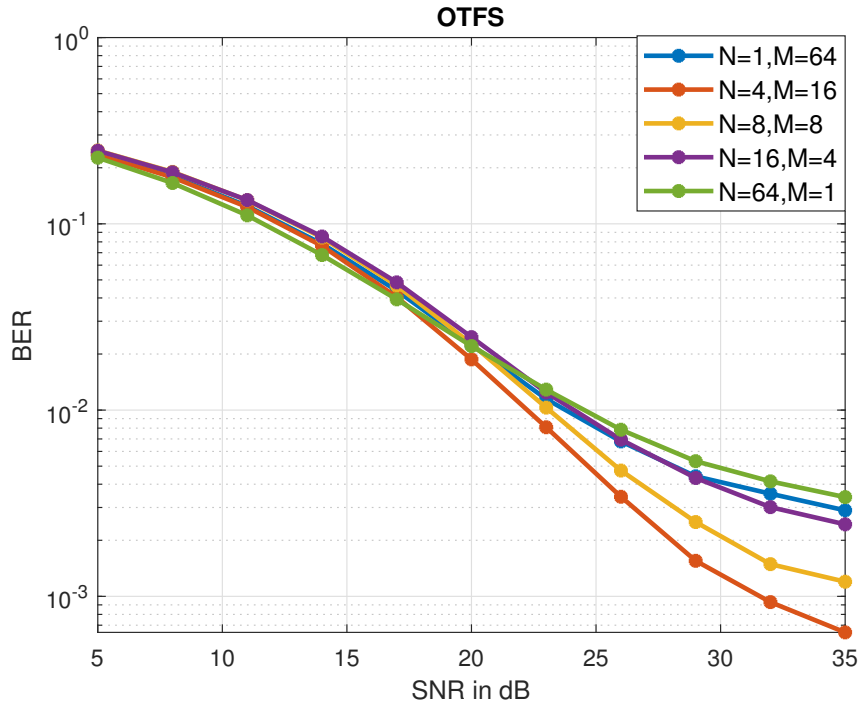

Figure 4.2: OTFS in time-varying channels. Doppler ranges from 0 to 1.

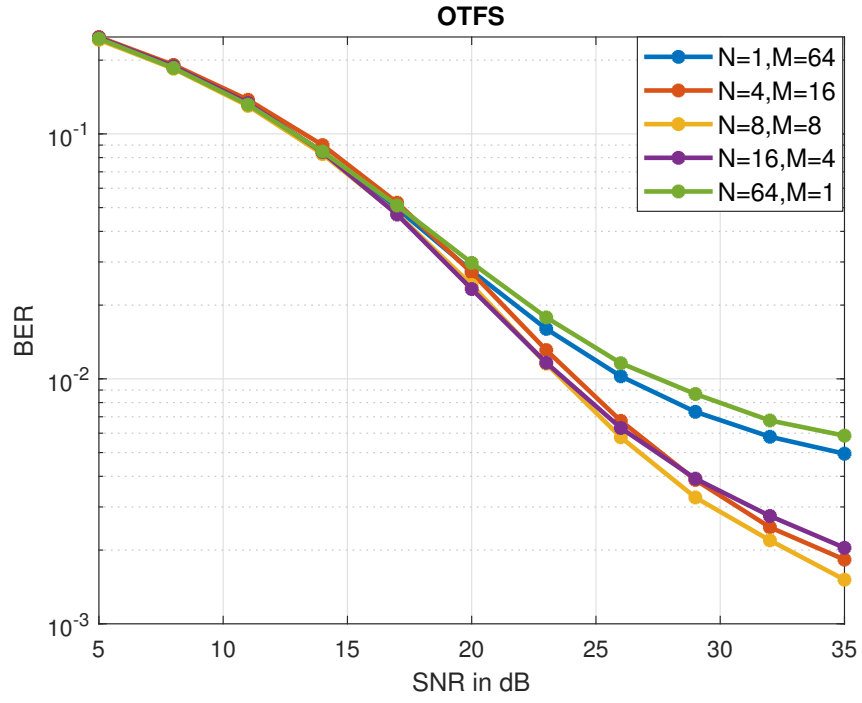

Figure 4.3: OTFS in time-varying channels. Doppler ranges from 0 to 2.

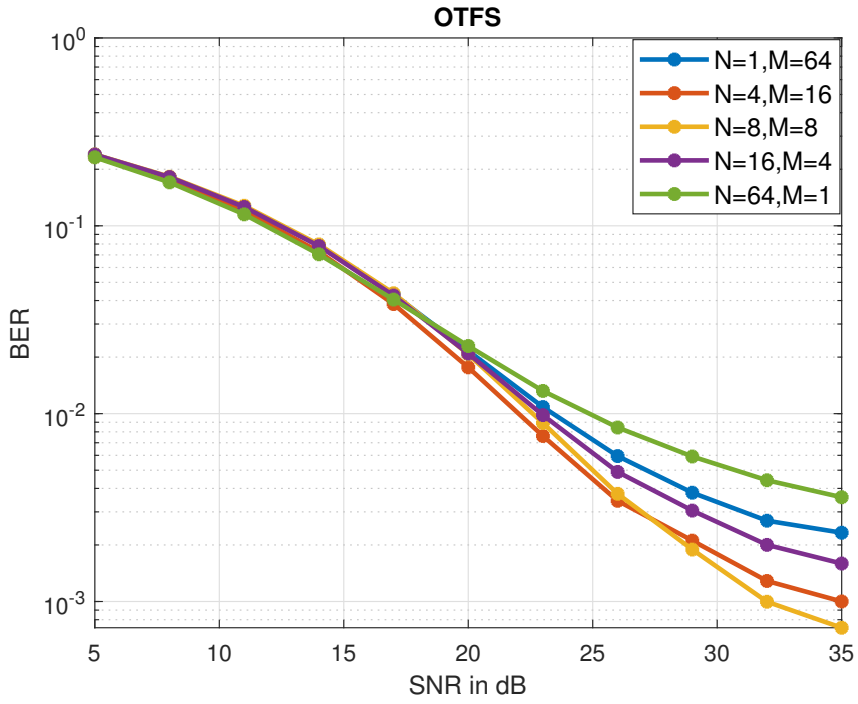

Figure 4.4: OTFS in time-varying channels. Doppler ranges from 1 to 2.

B) time-varying channels

We set channel Doppler to different values and plot figures accordingly. It can be seen from the Figures 4.2, Figures 4.3 and Figures 4.4 that, for $N = 1(SC - FDE)$, as it only has frequency diversity, hence at higher SNRs, its performance is always slightly better than N=64 (OFDM), but worse than the others. For time-varying channels, it seems that better performance is achieved when both N and M are large. This is due to higher and balanced diversities in both frequency and time domains. When the range of channel Doppler varies, the best values of N and M also vary. We can conclude that the parameter N and M should be carefully chosen to accomodate different channels.

4.3 Concept of Mixed-stage OTFS

In this section, we will first present the classical divide-and-conquer IFFT and then introduce the mixed-stage OTFS system. Please note that the use of divide-and-conquer IFFT here is to better illustrate the mixed-stage OTFS system. The performance gain is because we can adapt different user's delay-Doppler grid size to their channel conditions.

Divide-and-conquer algorithm is classical and famous. A typical divide-and-conquer algorithm addresses a problem through a sequence of three key steps:

1) Divide: In this initial step, the problem is divided into smaller, more manageable sub-problems.

2) Conquer: Each sub-problem is then resolved through recursive calls until a solution is reached.

3) Combine: Finally, the solutions to the sub-problems are integrated or combined to produce the ultimate solution for the entire problem.

The Fast Fourier Transform (FFT) stands as one of the truly remarkable computational advancements of the 20th century. Divide-and-conquer algorithm is one of the famous algorithms to calculate the fast FFT/IFFT. The process of the divide-and-conquer for calculating IFFT is as follows

STEP 1: To arrange the signal data column-wise in an array of $M \times N$

STEP 2: Calculate the $N-$ point IFFT for each row

STEP 3: Multiply each element in the array by a weighting factor $W_{M\times N}^{mn}$, $W_{M\times N}^{mn} = e^{j2\pi mn/(M\times N)}, m = 0, 1, ..., M-1, n = 0, 1, ...N-1$

STEP 4: Calculate the $M-$ point IFFT for each column

STEP 5: Get the array out row-wise.

The signal process of OTFS is similar. Suppose delay-Doppler grid size is $M \times N$. The signal data is first put on the delay-Doppler domain. Then it conducts 2D-FFT to the grid. To get the time-domain signal, $M-$ point IFFT is applied to each column and finally read the array row-wise.

We can see from above that, OTFS signal processing is identical to put signal to STEP 4 in the divide-and-conquer IFFT algorithm.

We can also know that the divided-and-conquer algorithm is a recursive algorithm. We can repeatedly use the divided-and-conquer algorithm in STEP 4. By doing so, we obtain the mixed-stage OTFS. An example of this concept is illustrated in figure 4.5. The figure dipict 8 point divided-and-conquer IFFT algorithm. In the figure, besides frequency domain and time domain, there are intermediate domains, like stage 1 and stage 2. These stages are actually on delay-Doppler domains. In fact, the frequency domain and time domain can also be seen as generalized delay-Doppler domain. In the figure, 4 symbols are put in stage 1, 2 symbols are put in stage 2 and 2 symbols are put in stage 3.

4.4 Mixed-stage OTFS Signal Models

In this section, we present the input-output relationship of mixed-stage OTFS system.

Similar to OTFS transmitter, the mixed- K stage OTFS system maps symbols from delay-Doppler domain to time-frequency domain as follows

$$\mathbf{x}_{tf,k}[n,m] = \frac{1}{\sqrt{M_k N_k}} \sum_{o=0}^{N_k-1} \sum_{l=0}^{M_k-1} \mathbf{x}_{dd,k}[o,l] e^{j2\pi(\frac{no}{N_k} - \frac{ml}{M_k})}, \tag{4.1}$$

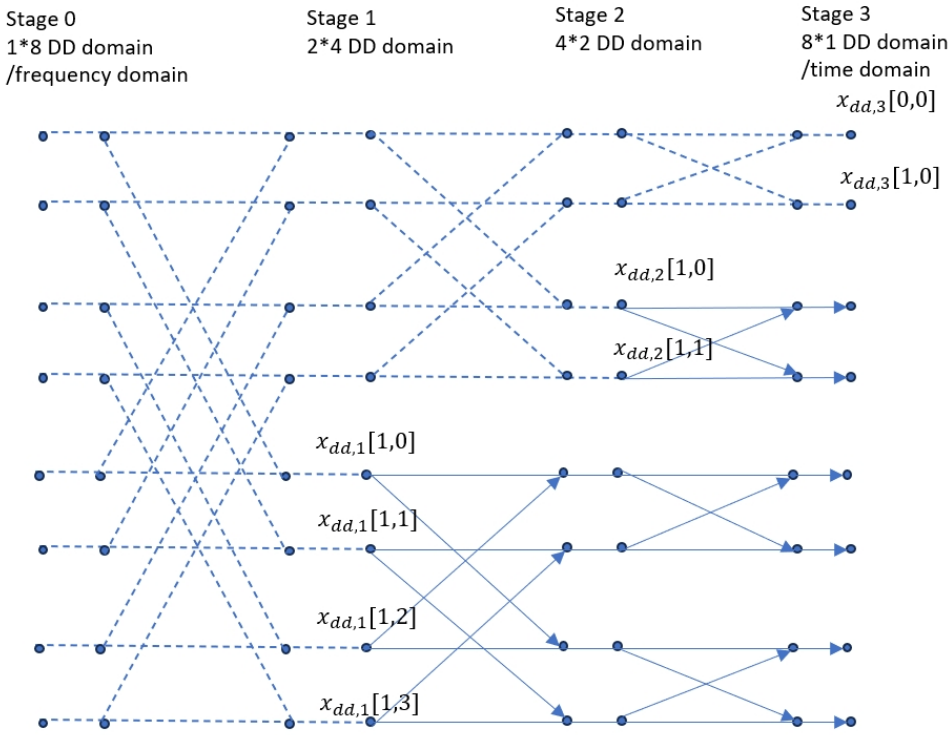

Figure 4.5: An example of the mixed-stage OTFS structure

for $n = 0, ..., N_k - 1, m = 0, ..., M_k - 1, k = 0, ..., K - 1$, where $\mathbf{x}_{dd,k}$ represents the delay-Doppler domain signals in the kth stage, $\mathbf{x}_{tf,k}$ represents the time-frequency domain signals in the kth stage and M_k and N_k represent delay-Doppler grid size in the kth stage.

Then OTFS system modulates time-frequency domain samples to time domain using a rectangular transmit waveform g_{tx} as

$$x_{t,k}(t) = \sum_{m=0}^{M_k-1} \sum_{n=0}^{N_k-1} e^{j2\pi m \triangle f_k (t-nT_k)} g_{tx}(t - nT_k) \mathbf{x}_{tf,k}[n, m], \tag{4.2}$$

where $x_{t,k}$ is the continuous time domain signals in the k stage, T_k is the kth stage sampling rate and $\triangle f_k$ is the subcarrier width in the kth stage.

In the end, the total K-stages signals together form the final transmission signal

$$x_t(t) = \sum_{k=0}^{K-1} x_{t,k}(t). \tag{4.3}$$

The transmitted signal $x_t(t)$ propagates over time-varying channel. The received signal $y_t(t)$ is given by

$$y_t(t) = \iint h(\tau, \nu) x_t(t-\tau) e^{j2\pi\nu(t-\tau)} d\tau d\nu. \tag{4.4}$$

Because only a limited number of reflectors associated with Doppler and delays, only a few parameters exist in the delay-Doppler channel model. The representation of $h(\tau, \nu)$ is

$$h(\tau, \nu) = \sum_{i=1}^{P} h_i g_1(\tau - \tau_i) g_2(\nu - \nu_i), \tag{4.5}$$

where P is the number of subpaths;τ_i, ν_i and h_i represent the delay, Doppler and subpath gain associated with i-th subpath, respectively. Moreover, $g_1(\cdot)$ and $g_2(\cdot)$ are the Fourier transforms of window functions $G_1(f)$ and $G_2(t)$ in the frequency and time domain, respectively. The two windowing functions can have any shape. In the ideal case, $g_1(x) = g_2(x) = \delta(x)$ is an impulsive function. However, due to the limited spanning period, they are actually not. Without using an explicit windowing function, the frequency-domain windowing function $G_1(f)$ is implicitly a rectangle of width B with non-zero span from $-B/2$ to $B/2$, and the time-domain windowing function $G_2(t)$ is also a rectangle with width corresponding to the signal period used for Doppler estimation. In the scenario considered here, $G_2(t)$ has a span of $NT_0 = N/B$, as CP is discarded at the receiver. So implicitly, both $g_1(\cdot)$ and $g_2(\cdot)$ are sinc functions, multiplied with phase shifting terms if the center of $G_1(f)$ or $G_2(t)$ is not at 0.

At the receiver, the continues time-frequency domain signal is

$$y_{tf}(t,f) = \int e^{j2\pi f(t-s)} y_t(s) g_{rx}^*(s-t) ds. \tag{4.6}$$

Then by sampling $y_{tf}(t,f)$ with different grid size, we obtain discrete time-frequency domain signal of the kth stage

$$\mathbf{y}_{tf,k}[n,m] = y_{tf}(t,f)|_{t=nT_k, f=m\triangle f_k}, \tag{4.7}$$

for $k = 0, ..., K-1$, $n = 0, ..., N_k - 1$ and $m = 0, ..., M_k - 1$.

Next, the kth stage delay-Doppler domain siganl is obtained by applying SFFT to the discrete time-frequency signal $\mathbf{y}_{tf,k}[n,m]$

$$\mathbf{y}_{dd,k}[o,l] = \frac{1}{\sqrt{M_k N_k}} \sum_{o=0}^{N_k-1} \sum_{l=0}^{M_k-1} \mathbf{y}_{tf,k}[n,m] e^{-j2\pi(\frac{no}{N_k} - \frac{ml}{M_k})}. \tag{4.8}$$

We can also view the mixed-stage OTFS system as a precoded OFDM system. Consider a K-stages system. As showed earlier, the received frequency-domain signal of a mixed-stage OFDM system is

$$\mathbf{y}_f = \mathbf{H}_{fd} \sum_{k=0}^{K-1} \mathbf{P}_{M_k,N_k} (\mathbf{I}_{N_k} \otimes \mathbf{F}_{M_k}) diag(e^{-j\frac{2\pi}{M_k N_k}(i)_{M_k}\frac{i}{M_k}}) vec(\mathbf{x}_{dd,k}) + \mathbf{w}, \tag{4.9}$$

where $vec(\mathbf{x}_{dd,k})$ is the vectorized delay-Doppler domain signals, and $\mathbf{P}_{M_k,N_k}$ is a permutation matrix. After frequency domain equalization, the frequency domain estimate signal is $\hat{\mathbf{x}_f}$, the vectorized delay-Doppler domain signal is

$$vec(\hat{\mathbf{x}}_{dd,k}) = \mathbf{V}_k^H \mathbf{F}_{M_k N_k}^H \hat{\mathbf{x}_f}, \tag{4.10}$$

where $\mathbf{V}_k = \mathbf{F}_{N_k}^H \otimes \mathbf{I}_{M_k}$

4.5 Multi-user Data Symbols Allocation

Now the question comes to how to generally generate $\mathbf{x}_{dd,k}$. In other words, how to generate a rule to put data symbols in different delay-Doppler grids to form one mixed-stage OTFS symbol. The basis idea is to avoid symbols in one stages cause interference with symbols in another stage. Let the corresponding delay-Doppler grids size be $M_k \times N_k$. Suppose $N_0 > N_1 > ...N_{K-1}$. As all M_k, N_k should be the exponent of 2, let $N_0 = 2^{q_0}N_1, N_1 = 2^{q_1}N_2, ...$, where q_k is a integer greater than 0. As different delay-Doppler grids form one complete OTFS symbol, so each grid consist of rows of zeros and rows of non-zero elements. We first put data symbols in $M_0 \times N_0$ grid, then $M_1 \times N_1$ grid, and then $M_2 \times N_2$ grid... We can put data symbols in arbitrary rows in $M_0 \times N_0$ grid. Let $\mathbb{Q}_0$ and $\mathbb{Z}_0$ be the set of row indexes of non-zero rows and all rows in $M_0 \times N_0$ grid, the set of zeros row for $M_0 \times N_0$ grid is $\mathbb{Z}_0 - \mathbb{Q}_0$. When it comes to $M_1 \times N_1$ grid, to avoid inteference with data symbols in $M_0 \times N_0$ grid, we need to put data symbols according to the $M_0 \times N_0$ grid. After careful investigation, the rows of $\mathbb{Q}_0, \mathbb{Q}_0 + M_0, \mathbb{Q}_0 + 2 * M_0, ..., \mathbb{Q}_0 + (2^{q_0} - 1)M_0$ in $M_1 \times N_1$ grid must be zeros. The rest of the rows in $M_1 \times N_1$ grid could either be zeros or non-zeros rows. Let $\mathbb{Q}_1$ be the set of row indexes of non-zero rows in $M_1 \times N_1$ grid, then similarly, the rows of $\mathbb{Q}_1, \mathbb{Q}_1 + M_1, \mathbb{Q}_1 + 2 * M_1, ..., \mathbb{Q}_1 + (2^{q_1} - 1)M_1$ in $M_2 \times N_2$ grid must be zeros. By iteration, we can put all data symbols onto all the delay-Doppler grids, with no interference with each other.

Now we have generalized the method to put data symbols in different delay-Doppler grids to form one mixed-stage OTFS symbol.

Table 4.1: Simulation Parameters

conventional OTFS frame size	4*32
stage 1 OTFS frame size	4*32
stage 2 OTFS frame size	8*16
Bandwidth	1
Sampling period	1
Number of subpath	4
total transmission power	1
Modulation	QPSK

4.6 Simulation Results

We compare the mixed-stage OTFS system with the conventional OTFS system. We consider the downlink system and the number of users is two. For conventional OTFS system, the same frame size applys to the two users. We let the stage number be two for the mixed-stage system, so one stage for one user. The data amount to transmit to the two users are set equal. We adopt MMSE detector. Unless stated otherwise, the exact parameters can be found in table 4.1.

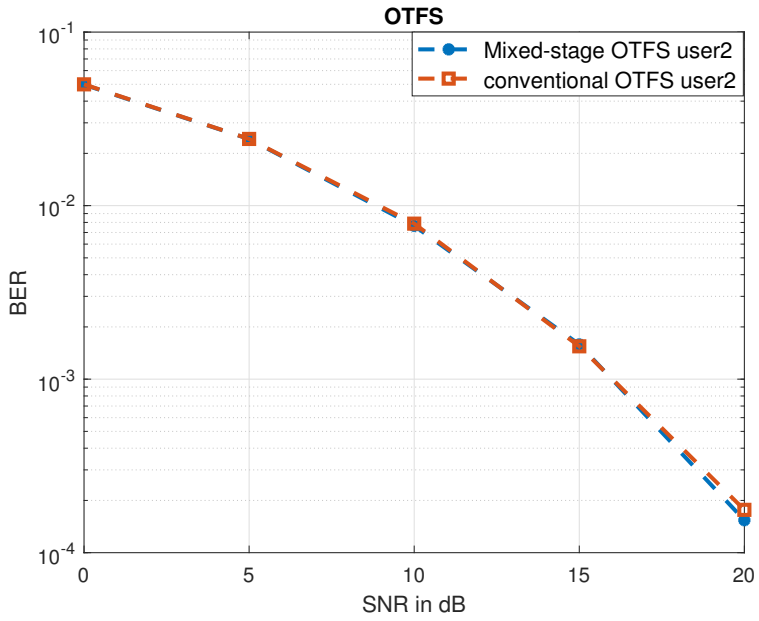

Figure 4.6: Mixed-stage OTFS. Doppler ranges from 0 to 1/M*N, delay ranges from 0 to 1

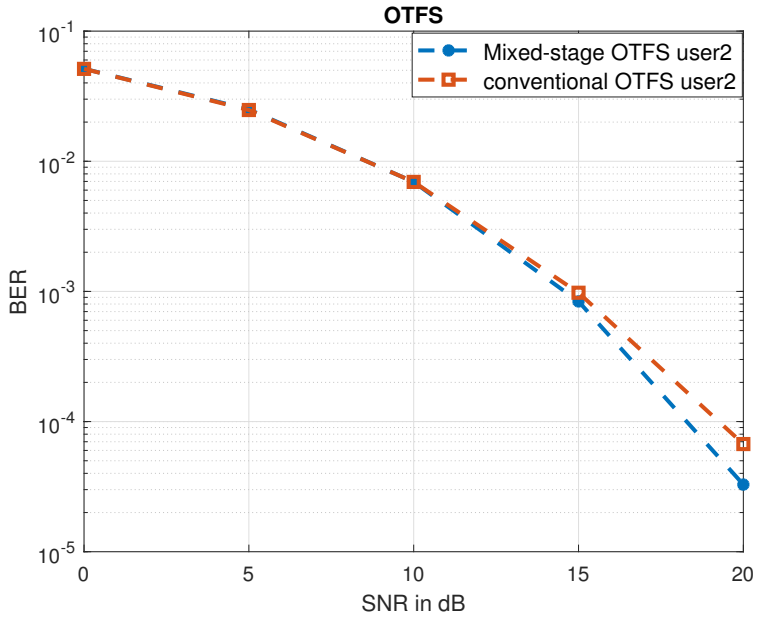

Figure 4.7: Mixed-stage OTFS. Doppler ranges from 10/M*N to 11/M*N, delay ranges from 0 to 4.

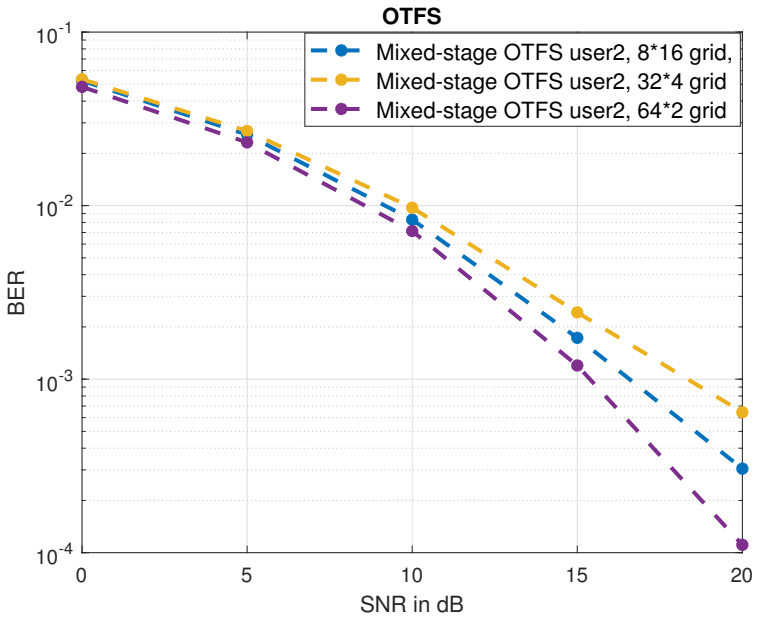

Figure 4.8: Mixed-stage OTFS at different stages. Doppler ranges from 0 to 1/M*N, delay ranges from 0 to 1

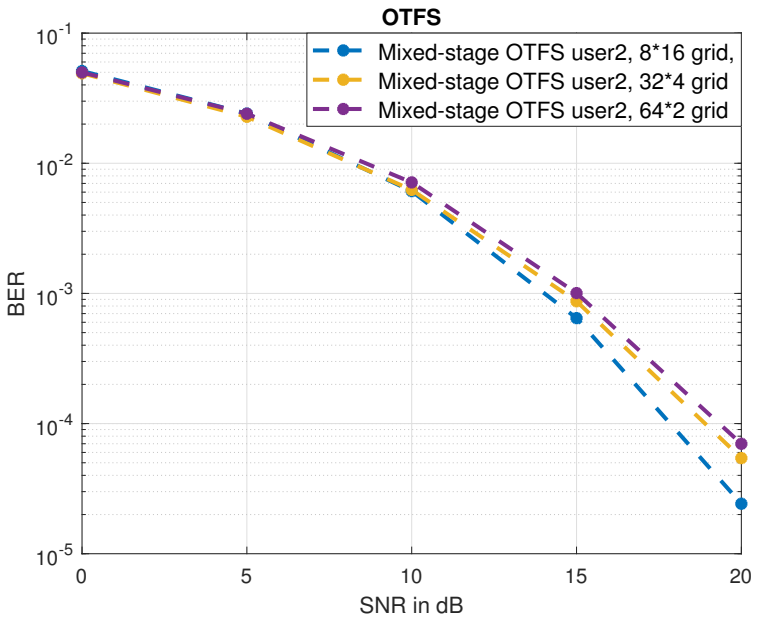

Figure 4.9: Mixed-stage OTFS at different stages. Doppler ranges from 10/M*N to 11/M*N, delay ranges from 0 to 4.

As we can see from figures 4.6, figure 4.7, in our settings, mixed-stage OTFS reaches approximatly the same performance in low SNR and has advantage in high SNR, no matter what the channel Doppler ranges are. In more 'vaying' channels, which means the channel Doppler and delay values are larger, mixed-stage OTFS has more BER advantages. Due to the flexibility of mixed-stage OTFS system, we can always adjust the frame size to suit channel conditions of different users.

Figure 4.8 and figure 4.9 show the mixed-stage OTFS performance at different stages when the channel Doppler is small and large. It can be seen that in different channel parameter settings, the best delay-Doppler grid size is different, which aligns with our previous results. In fast-varying channels, the 'square-like' delay-Doppler grid outperformans the others. This may because it offers good tradeoff in both frequency diversity and time diversity.

4.7 Conclusions

In this chapter, We introduce a novel concept known as the mixed-stage OTFS system, wherein a single OTFS frame accommodates multiple delay-Doppler grids. This innovative approach grants users the flexibility to adapt their grid sizes based on varying channel conditions, ultimately enhancing overall system performance.

First, we illustrate the impact of delay-Doppler grid size on communication performance. Our findings reveal that optimizing the delay-Doppler grid size in alignment with specific channel conditions can improve system performance. Consequently, we present the mixed-stage OTFS system, presenting the mechanisms for integrating data symbols of different delay-Doppler grid sizes into a single OTFS frame.

Our comprehensive simulation results underscore the advantages of the mixed-stage OTFS system over conventional OTFS, chiefly attributable to its inherent flexibil-

ity.

Chapter 5

Frequency-Domain Sensing in Time-Varying Channels

Integrated Sensing and Communications (ISAC) in mobile networks are typically based on Orthogonal Frequency Division Multiplexing (OFDM) systems. For time-varying channels, large Doppler frequencies in OFDM ISAC can cause notable inter-carrier interference, which has not been considered for sensing. In this section, we propose a frequency-domain sensing framework for OFDM ISAC systems. We first derive a frequency-domain closed-form expression of the received signals, to characterise the delay and Doppler frequency impact within and across OFDM blocks. We then develop intra-block and inter-block sensing algorithms, based on the expression. The framework is further completed with exemplified pilot design and periodogram sensing algorithm. Simulation results demonstrate the effectiveness of the proposed framework.

5.1 Introduction

Integrated Sensing and Communications (ISAC) techniques, which integrate radio communication and sensing into one system, have received strong interests from both academia and industry [73]. In particular, perceptive mobile networks with ISAC are able to support large-scale sensing of high-mobility targets, while providing non-compromised communications [70]. In such applications, fast time-varying channels are faced by both communications and sensing, and can cause significant performance degradation if not properly modeled and handled.

Communications in time-varying channels have been studied back to early 2000. Typically, short packets and channel tracking based on frequent pilots are used to cope with time-varying channels. For Orthogonal Frequency Division Multiplexing (OFDM) systems, equalizers capable of dealing with intercarrier interference (ICI) can also be used to remove interference caused by large Doppler frequencies [46]. However, no closed-form expressions had been provided for frequency-domain signal models over time-varying channels, until the recent publication of [8]. The work in [8] discloses the frequency-domain frequency-dependent convolution relationship between the received signal, the channel and the transmitted signal. To deal with fast time-varying channels, orthogonal time-frequency space (OTFS) systems [49] are also proposed recently. In OTFS, the modulated signals at the transmitter are placed at the delay-Doppler domain. It is shown that OTFS can be regarded as a precoded OFDM system [8], with the capability of exploiting the channel diversity gain over time and frequency.

However, the research on ISAC in time-varying channels is still in a very early stage. A limited number of existing studies have mainly been based on OTFS ISAC systems [1], [2]. Channel estimation for OTFS communications, which is

closely related to sensing paramter estimation, has also been studied in, e.g.,[5]–[7]. Although ISAC OTFS offers potential advantages of unified signal design and optimization in the delay-Doppler domain for both communications and sensing, the required signal processing and sensing algorithms are typically complicated due to the two-dimensional convolutional relationship between the signals and channels in the domain. Further considering its general high-complexity signal generation and recovery, OTFS may not be attractive for low-latency and/or low-complexity ISAC applications.

In this section, based on the relationship disclosed in [8], we develop a frequency-domain sensing framework for a general OFDM system in fast time-varying channels, based on the frequency-domain estimated channels. This framework can be applied to a conventional OFDM system with frequency-domain pilots, although an improved pilot design may offer simpler channel estimation. A frequency-domain framework provides better compatibility with existing OFDM systems, and also enables wider selection of sensing algorithms compared to, e.g., a time-domain processing. We first extend the frequency-domain input-output signal relationship in [8] to multiple OFDM blocks and introduce practical windowing functions. The result demonstrates how delay and Doppler frequency can be theoretically characterized. We then develop intra-block and inter-block sensing algorithms, which conduct sensing parameter estimation within one OFDM block and across multiple blocks, respectively. The frequency-domain sensing framework is then completed with exemplified periodogram sensing algorithm, pilot design, and channel estimation. Our proposed framework can be realized at low complexity, with significantly extended estimation ranges for Doppler frequencies, compared to existing schemes without considering the impact of time-varying within an OFDM block. Simulation results are provided and validate our proposed framework.

5.2 System and Signal Models

In this chapter, we consider a general OFDM system, where pilots are placed in the frequency domain and channel estimation can be conducted there. Next, we briefly revisit continuous models and then discrete models for signals over time-varying channels in Section 3.

Assume that an OFDM symbol (or block) has the time duration of $T = (N+N_{cp})T_0$, where T_0 is the sampling interval, N is the number of samples (subcarriers), and N_{cp} is the length of cyclic prefix (CP). The total signal bandwidth is $B = 1/T_0$, and the subcarrier interval is $f_0 = B/N$. We consider a general time-varying channel $h(\tau, t)$, which includes time-invariant channel as a special case. Assume that the sensing parameters, such as path amplitude, delay, and Doppler frequency, remain unchanged during the coherent processing interval (CPI) for sensing.

For the k-th ($k = 0, 1, ...$) OFDM symbol, the continuous delay-Doppler channel can be described as

$$h_v(\tau, v) = \sum_{\ell=1}^{L} h'_\ell e^{j2\pi v_\ell kT} g_1(\tau - \tau_\ell) g_2(v - v_\ell), \tag{5.1}$$

where τ_ℓ, v_ℓ, and h'_ℓ are the delay, Doppler frequency, and amplitude of the ℓ-th path, respectively. Note that $e^{j2\pi v_\ell kT}$ is the accumulated phase of the k-th OFDM symbol caused by v_ℓ. Moreover, $g_1(\cdot)$ and $g_2(\cdot)$ are the Fourier transforms of window functions $G_1(f)$ and $G_2(t)$ in the frequency and time domain, respectively. The two windowing functions can have any shape. In the ideal case, $g_1(x) = g_2(x) = \delta(x)$ is an impulsive function. However, due to the limited spanning period, they are actually not. Without using an explicit windowing function, the frequency-domain windowing function $G_1(f)$ is implicitly a rectangle of width B with non-zero span from $-B/2$ to $B/2$, and the time-domain windowing function $G_2(t)$ is also a rectangle with width corresponding to the signal period used for Doppler estimation.

In the scenario considered here, $G_2(t)$ has a span of $NT_0 = N/B$, as CP is discarded at the receiver. So implicitly, both $g_1(\cdot)$ and $g_2(\cdot)$ are sinc functions, multiplied with phase shifting terms if the center of $G_1(f)$ or $G_2(t)$ is not at 0.

Applying the Fourier transform to (6.1) over τ, we obtain the frequency-Doppler continuous channel as

$$H_{fd}(f, v) = G_1(f) \sum_{\ell=1}^{L} h_\ell g_2(v - v_\ell) e^{-j2\pi f \tau_\ell}. \tag{5.2}$$

Let $y(t)$ and $Y(f)$ denote the received time-domain and frequency-domain continuous signals, respectively. Ignoring noises for brevity, we can represent $Y(f)$ as [8]

$$Y(f) = \int_{-\infty}^{+\infty} H_{fd}(f', f - f') X(f') df', \tag{5.3}$$

which indicates that $Y(f)$ is the frequency-dependent convolution between $H_{fd}(f, v)$ and the frequency-domain transmitted signal $X(f)$.

Sample and digitize the continuous signals in the time domain. The discrete versions of channels and signals in multiple domains can be accordingly derived as follows. The time-domain received signals are given by

$$\mathbf{y}_t = \mathbf{H}_t \mathbf{x}_t, \tag{5.4}$$

where the time-domain channel matrix $\mathbf{H}_t$ is not a circulant matrix anymore in time-varying channels.

Let $\mathbf{F}$ denote the discrete Fourier transform (DFT) matrix. The frequency-domain received signal can be represented as

$$\mathbf{y}_f = \mathbf{F}\mathbf{y}_t = \mathbf{F}\mathbf{H}_t\mathbf{x}_t = (\mathbf{F}\mathbf{H}_t\mathbf{F}^H)\mathbf{F}\mathbf{x}_t = \mathbf{H}_{fd}\mathbf{x}_f, \tag{5.5}$$

where $\mathbf{x}_t$ and $\mathbf{x}_f$ denote the time-domain and frequency-domain transmitted signals, respectively, and $\mathbf{H}_{fd}$ is the frequency-Doppler channel matrix. From (6.2), the (n, m)-th element of $\mathbf{H}_{fd}$ is given by

$$\begin{aligned}(\mathbf{H}_{fd})_{n,m} &= H_{fd}(mf_0, (n-m)_N f_0) \\ &= G_1(mf_0) \sum_{\ell=1}^{L} h_\ell \, g_2(((n-m)f_0 - v_\ell)_{Nf_0}) \, e^{-j2\pi m f_0 \tau_\ell},\end{aligned} \tag{5.6}$$

where $(n)_N$ denotes the modular operation $\mathrm{mod}(n, N)$ as digitization causes spectrum repetition at the period of $B = Nf_0$. The windowing functions may be slightly changed due to spectrum aliasing associated with the digitization operation. At sufficiently high sampling rate, the difference can be ignored. We can see that $\mathbf{H}_{fd}$ is not a diagonal matrix anymore if $v_\ell \neq 0$ for any ℓ.

So far we have uncovered the frequency-domain input-output relationships for signals over time-varying channels, and shown how the delay and Doppler parameters can be theoretically characterized.

5.3 Proposed Sensing Scheme

For sensing, our goal is to estimate τ_i and v_i, via the estimated $\mathbf{H}_{fd}$, $\widehat{\mathbf{H}}_{fd}$. In this section, we first assume that the matrix $\mathbf{H}_{fd}$ is known, and develop intra-block and inter-block sensing parameter estimation methods. We then provide an exemplified pilot design, which is not spectrum-efficient but enables simple estimation of $\mathbf{H}_{fd}$.

From the expression in (6.5), it is interesting to see that the elements along each of the diagonal directions correspond to the same quantized Doppler shift, and elements in the same column correspond to the same frequency/subcarrier. Thus we propose to re-align the entries of $\widehat{\mathbf{H}}_{fd}$ by circularly shifting the m-th column upwards by $(m-1)$ positions. The result of the circular shift is that the elements

corresponding to the same Doppler shift and the same subcarrier will be on the same row and column, respectively. Denote the re-aligned $\widehat{\mathbf{H}}_{fd}$ as $\widetilde{\mathbf{H}}_{fd}$. Its (n, m)-th element becomes

$$\begin{aligned}\widetilde{h}_{fd}(n,m) &= H_{fd}(mf_0, (n)_N f_0) \\ &= G_1(mf_0) \sum_{\ell=1}^{L} h_\ell \, g_2(nf_0 - v_\ell) \, e^{-j2\pi m f_0 \tau_\ell}, \end{aligned} \tag{5.7}$$

where the zero-Doppler elements are in the first row, followed by those corresponding to B/N to $B/2$ and then $-B/2$ to $-B/N$.

Equation (5.7) enables the estimation of both τ_ℓ and v_ℓ, with various techniques ranging from simple periodogram to more complicated compressive sensing and subspace methods [70]. For illustration purpose, we use the simple periodogram method in this section.

The periodogram method, or classical 2D DFT method, is widely utilized in radar applications. This method is employed to make rough estimations of sensing parameters. While a 3D DFT can also be employed, it is often substituted with two or three 2D DFTs due to its intricacy. This method's resolution is somewhat limited because of the extended tail of the inherent sinc function within the DFT.

5.3.1 Intra-block Sensing with a Single OFDM Block

For intra-block sensing, we apply an inverse DFT (IDFT) to the transpose of a single $\widetilde{\mathbf{H}}_{fd}$ and obtain

$$\mathbf{H}_{dd} = \mathbf{F}^H \widetilde{\mathbf{H}}_{fd}^T, \tag{5.8}$$

which shows the delay-doppler channel matrix. From $\mathbf{H}_{dd}$ we can get coarse or quantized estimates for delays and Doppler frequencies, by searching for local peaks from the absolute values or power of the elements in the 2D matrix. Note that

since $g_1(\tau)$ and $g_2(v)$ are practically functions with tails, there are typically leakages from one τ_ℓ and v_ℓ to neigbouring ones when their values are not exactly on the quantized grid (mf_0 or $(n)_N f_0$). Nevertheless, the spectrum of $\mathbf{H}_{dd}$ provides good coarse estimates of delay and Doppler frequencies.

Note that we do not need all elements in $\mathbf{H}_{fd}$ to estimate sensing parameters because of the correlation and redundancy in $\mathbf{H}_{fd}$. Generally, we only need the estimates of $(\mathbf{H}_{fd})_{n,m}$ at N_p subcarriers and M_p Doppler samples, given that $N_p \geq L$ and $M_p \geq N(\max(v_\ell) - \min(v_\ell))/B$. For the periodogram method, the estimates shall be equally spaced across subcarriers and located in a strip along the diagonal elements in $\mathbf{H}_{fd}$, as will be detailed in Section 5.3.3. Working on a smaller channel matrix can save complexities in both computation and peak searching.

For Doppler frequency, intra-block sensing enables the estimation of its values over $(-B/2, B/2]$, with a coarse resolution of B/N. For delay, the resolution is $1/B$, while the estimation range depends on the available estimates of $\mathbf{H}_{fd}$.

5.3.2 Inter-block Sensing with Multiple OFDM Blocks

The signal models above can be extended to multiple OFDM blocks within the CPI.

As was described in (6.1), the channel and signal differences across different OFDM blocks can be reflected by $h_\ell = h'_\ell e^{j2\pi v_\ell kT}$. Thus we can easily extend the previous results for a single OFDM block to multiple ones by explicitly introducing the phase shifts $e^{j2\pi v_\ell kT}$. For example, we can extend (5.7) and collect the estimated and re-aligned channels over K OFDM blocks, and get

$$\widetilde{h}_{fd}(n,m,k) = G_1(mf_0) \sum_{\ell=1}^{L} h'_\ell \, g_2(nf_0 - v_\ell) \cdot e^{-j2\pi m f_0 \tau_\ell} \, e^{j2\pi v_\ell kT}, k = 0, 1, \cdots, K-1. \tag{5.9}$$

For a given n, we see that $g_2(nf_0 - v_\ell)$ only depends on ℓ and hence we can let $a_{\ell,n} = h'_\ell\, g_2(nf_0 - v_\ell)$. Collect the measurements at all used subcarriers and K OFDM blocks for each n and organize them into a matrix $\widetilde{\mathbf{H}}_{fd}(n)$ such that its (m,k)-th element is $\widetilde{h}_{fd}(n,m,k)$. We can represent it as

$$\widetilde{\mathbf{H}}_{fd}(n) = \mathbf{A}_\tau \mathbf{D}_n \mathbf{A}_v^H, \tag{5.10}$$

where $(\mathbf{A}_\tau)_{m,\ell} = e^{-j2\pi m f_0 \tau_\ell}$, $(\mathbf{A}_v^H)_{\ell,k} = e^{-j2\pi v_\ell k T}$, and $\mathbf{D}_n$ is a diagonal matrix with the ℓ-th element $h'_\ell\, g_2(nf_0 - v_\ell)$.

Thus most of the existing sensing parameter estimation techniques as described in [70] can be applied to (5.10) to estimate τ_ℓ and v_ℓ. Since the accumulated phase shifts $e^{-j2\pi v_\ell k T}$ is much larger than those within one OFDM block, we can expect to achieve better estimation performance than using (5.7) in the presence of noise. The resolution is also improved to $B/(N + N_{cp})/K$. The range of Doppler frequencies that can be estimated is $(-B/(N+N_{cp})/2, B/(N+N_{cp})/2]$, due to the requirement of $|v_\ell T| < 1/2$. With the impact of Doppler frequencies on channels fully included in the signal models, better sensing performance can also be expected compared to conventional schemes without considering such an impact.

Once the estimates are obtained for all n's, we may compute the average across all estimates, or determine which estimates to keep based on the range of the estimated Doppler frequencies. This is because $g_2(nf_0 - v_\ell)$ is a function with a narrow main-lobe, and its value is small if $|nf_0 - v_\ell|$ is large. Thus a larger $g_2(nf_0 - v_\ell)$ implies better estimation accuracy.

There are also alternative methods which can better exploit the estimates over all Doppler frequency grids n. For example, we can sum $\widetilde{\mathbf{H}}_{fd}(n)$ over all P grids, and

then apply estimation algorithms to the sum. In this case, we obtain

$$\sum_n \widetilde{\mathbf{H}}_{fd}(n) = \mathbf{A}_\tau(\sum_n \mathbf{D}_n)\mathbf{A}_v^H. \tag{5.11}$$

Since $g_2(\cdot)$ has a narrow mainlobe, $\sum_n g_2(nf_0 - v_\ell)$ for each ℓ will be constructively combined in the sum most of the time.

5.3.3 Exemplified Pilot Design for Estimating $\mathbf{H}_{fd}$

Here, we provide an example of pilot design for the estimation of sufficient elements in $\mathbf{H}_{fd}$ for sensing, by introducing guarding subcarriers with zero values on the two sides of each pilot in conventional OFDM systems. These zero guarding symbols are employed to counterbalance intercarrier interference (ICI) caused by large Doppler frequencies.

Let $\mathbf{s}_f$ denote the frequency-domain data symbols in an OFDM block. We segment $\mathbf{s}_f$ to smaller vectors $\mathbf{s}_{f,m}, m = 0, \cdots, M-1$, which can have identical or different lengths. Let $\mathbf{p} = [p_0, p_1, ..., p_{M-1}]$ and $\mathbf{0}_P$ denote the row vectors of pilots and P zeros, respectively. Thus, we can form a basic sequence of $\mathbf{x}_m^T = [\mathbf{0}_P, p_m, \mathbf{0}_P, \mathbf{s}_{f,m}]$, and construct

$$\mathbf{x}_f = [\mathbf{x}_0^T, \cdots, \mathbf{x}_m^T, \mathbf{0}_P, \mathbf{x}_{m+1}^T, \cdots, \mathbf{x}_{M-1}^T]^T. \tag{5.12}$$

Note that the zero guarding symbols help reduce ICI and hence improve the estimation accuracy of $\mathbf{H}_{fd}$. The value of P is selected according to the maximal Doppler frequencies. In general, $P \geq 2N \max(|v_\ell|)/B$ if negligible ISI is desired.

The number of pilots L_p and the intervals between them can be determined based on the maximum target delay. Generally, the mean interval of these pilot subcarriers shall be smaller than $1/(f_0 \max(\tau_\ell))$ to avoid ambiguity in the delay estimation. Thus a simple method is using interleaved subcarriers at an interval smaller than $1/(f_0 \max(\tau_\ell))$.

With the above pilot design, we can estimate elements in $\mathbf{H}_{fd}$ based on (6.4). Each pilot would allow us to estimate P interference-free channel elements in each column of $\mathbf{H}_{fd}$. More specifically, we can obtain $\widetilde{\mathbf{H}}_{fd}$ with non-zero values at subcarriers in the set of $\mathcal{S}_p$ and Doppler frequencies from $-P/2 \times B/N$ to $P/2 \times B/N$, and zeros elsewhere. Thus we can keep $P+1$ non-zero rows of $\widetilde{\mathbf{H}}_{fd}$ to obtain $\widetilde{\mathbf{H}}_{fd}^{(r_1)}$, and apply an IDFT to the transpose of $\widetilde{\mathbf{H}}_{fd}^{(r_1)}$ to get $\mathbf{H}_{dd}^{(r_1)}$, a reduced size of $\mathbf{H}_{dd}$. Furthermore, if K_2 interleaved subcarriers of equal interval are used, we can further keep only non-zero columns of $\widetilde{\mathbf{H}}_{fd}^{((r_1))}$ and obtain $\widetilde{\mathbf{H}}_{fd}^{(r_2)}$, then apply a reduced-size K_2-point IDFT to its transpose to obtain $\mathbf{H}_{dd}^{(r_2)}$.

Thus for intra-block sensing, we can reduce the channel matrix size from $N \times N$ (e.g., $N = 64$ for WiFi systems) to $(P+1) \times K_2$ (with a typical value of 3×8), and the searching space from $N \times N$ to $K_2 \times K_2$.

5.3.4 Overall Algorithm

The overall parameter estimation scheme based on the periodogram and pilot design can be a combination of intra-block and inter-block sensing, and is summarized below:

S1 Design pilots in the freq-domain by jointly considering communication and sensing requirements;

S2 For each OFDM block, estimate some elements of $\mathbf{H}_{fd}$ using the received signals corresponding to the pilots.

S3 Re-align $\mathbf{H}_{fd}$ to obtain $\widetilde{\mathbf{H}}_{fd}$, or a reduced size version;

S4 Estimate sensing parameters based on $\widetilde{\mathbf{H}}_{fd}$, using $\mathbf{H}_{dd} = \mathbf{W}\widetilde{\mathbf{H}}_{fd}^T$, where $\mathbf{W}$ equals to $\mathbf{F}^H$ or a partial IDFT matrix, depending on the used pilot subcarriers. Then obtain coarse estimation for τ_i and v_i by finding the peaks of $|\mathbf{H}_{dd}|$.

S5 After accumulating K OFDM blocks, apply techniques as described in Section 5.3.2 to obtain fine estimates for Doppler frequencies and delay.

S6 Combine estimates in S4 and S5 by using the Doppler estimates in S4 and S5 to determine their integral and fractional values with respect to f_0, respectively.

5.4 Simulation Results

In this section, we present simulation results to validate the proposed framework, in comparison to the state-of-art OTFS scheme [5] and two conventional OFDM baseline systems. Each OFDM block has the same structure of data subcarriers and embedded pilots. All systems are set to have equal transmission power, the same bandwidth B (normalized to 1), and similar total signal observation period. They also have similar spectrum efficiencies, which are approximately 0.818 for all OFDM schemes and 0.814 for OTFS scheme. Since the exemplified pilot design uses $2P$ zero guarding subcarriers for each pilot, to match the spectrum efficiency, the number of subcarriers is reduced to N_b in Baseline 1 such that $(1-L_p/(N_b+N_{cp}) \approx (1-(2P+1)L_p/(N+N_{cp})$, while the number of pilots in Baseline 2 is increased. For OTFS, we use a single large block as no inter-block sensing techniques are available in the open literature yet. The simulation parameters are provided in Table I, unless stated otherwise. Therefore in Baseline 1 the subcarrier interval and the number of blocks are increased by approximately 3; in Baseline 2 the number of pilots is increased to 40, equally distributed.

We first demonstrate the capabilities of the proposed intra-block and inter-block sensing individually. A channel with 3 paths is simulated. Each path gain follows a complex Gaussian distribution with the zero mean and unit variance. More general channel models may be generated by referring to [74]. Note that non-integer

Table 5.1: Simulation Parameters.

Number of subcarriers, N	256
Number of subcarriers in Baseline 1, N_b	80
Number of blocks, K	16
Number of blocks in Baseline 1, K_b	48
Number of zero guarding symbols, $2P$	4
Number of pilots, L_p	8
CP length, N_{cp}	8
Delay spread	$[0, 5]$
OTFS frame size	256×16
OTFS guarding block size	41×16

delays and Doppler frequencies cause signals to leak to neigbouring samples and subcarriers, due to the practical windowing functions as discussed in Section II. Fig. 5.1 and Fig. 5.2 presents the sensing results for intra-block and inter-block algorithms, where the differences are due to their different sensing ranges and resolution capabilities. From Fig. 5.1 and Fig. 5.2, we can have the following observations: (1) Intra-block sensing resolves these paths without ambiguity, and is capable of estimating Doppler frequencies $|v_\ell| \geq f_0$; (2) Inter-block sensing provides improved resolution, however, there is ambiguity with the Doppler frequency estimates, due to its limited sensing range. Therefore, the final estimation results can be obtained by combining the intra-block and inter-block results. In the presence of multiple paths, the combination requires to associate the estimates first, which may be realized via both the delay and the Doppler values. Detailed combination is beyond the scope of this section.

In demonstrating the enhanced sensing accuracy of inter-block estimation, it be-

comes evident that when the channel Doppler values are in close proximity, distinguishing between these values poses a challenge for intra-block estimation, as depicted in Fig. 5.3. Conversely, inter-block estimation exhibits superior sensing accuracy, enabling it to effectively differentiate between the channel Doppler values, as illustrated in Fig. 5.4.

While inter-block estimation demonstrates enhanced accuracy in distinguishing channel Doppler values when they are in proximity, it's important to note its limitations. When Doppler values differences are excessively small, specially smaller than $1/(N + Ncp)$, both intra-block and inter-block estimations face challenges in distinguishing between these values, as depicted in Fig. 5.5 and Fig. 5.6.

As shown in Fig. 5.7 and Fig. 5.8, if the channel Doppler is not large, say, the channel is slow-fading channel, then the Doppler estimation results of inter-block estimation and intra-block estimation are similar, but the estimation result of inter-block estimaiton is more accurate.

In a slow-fading channel, where the channel Doppler is relatively small. It becomes apparent that both intra-block and inter-block estimations yield comparable Doppler estimation results, as suggested in Fig. 5.7 and Fig. 5.8. However, it's notable that the accuracy of the inter-block estimation is notably higher.

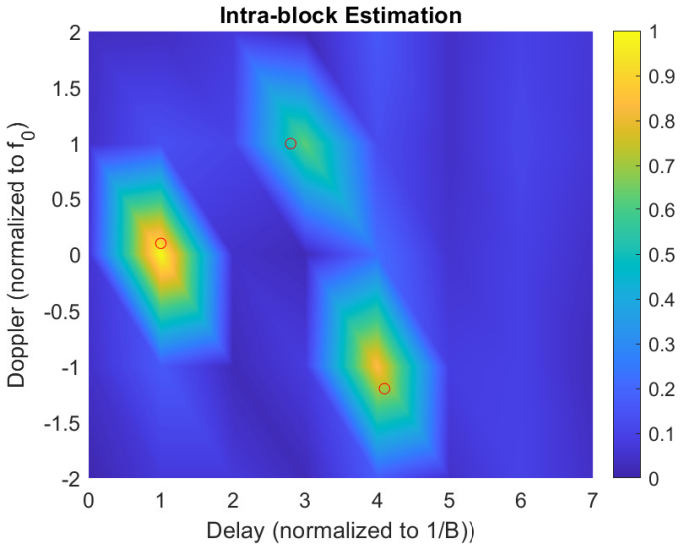

Figure 5.1: Intra-block estimation Delay-Doppler map 1, where the color scale indicates signal strength as per the color bar. Ground truth of three targets are also highlighted with red circles.

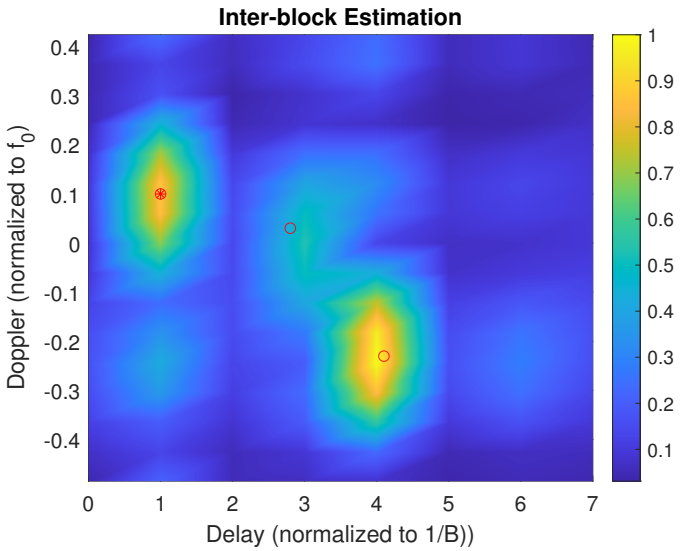

Figure 5.2: Inter-block estimation Delay-Doppler map 1, where the color scale indicates signal strength as per the color bar. Ground truth of three targets are also highlighted with red circles.

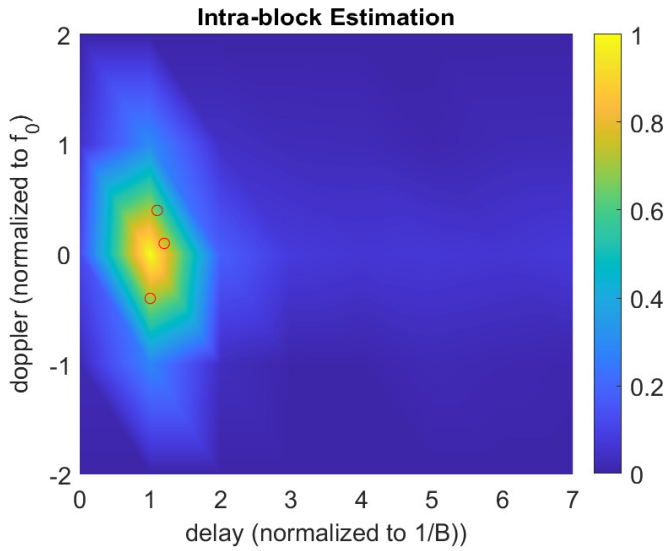

Figure 5.3: Intra-block estimation Delay-Doppler map 2, where the color scale indicates signal strength as per the color bar. Ground truth of three targets are also highlighted with red circles.

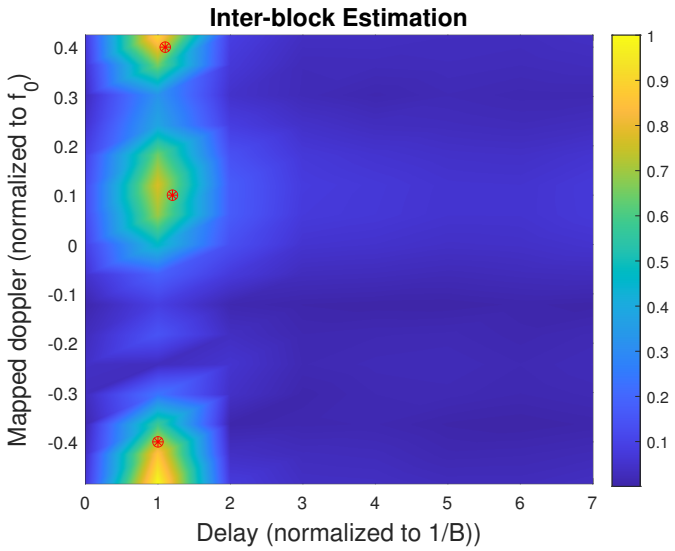

Figure 5.4: Inter-block estimation Delay-Doppler map 2, where the color scale indicates signal strength as per the color bar. Ground truth of three targets are also highlighted with red circles.

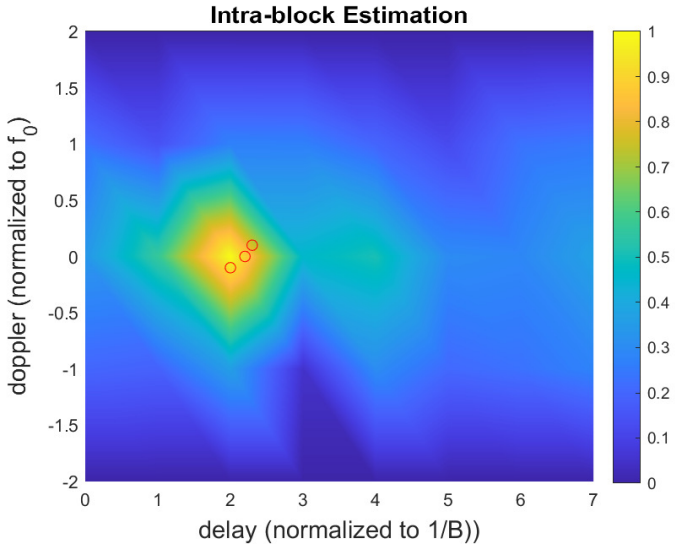

Figure 5.5: Intra-block estimation Delay-Doppler map 3, where the color scale indicates signal strength as per the color bar. Ground truth of three targets are also highlighted with red circles.

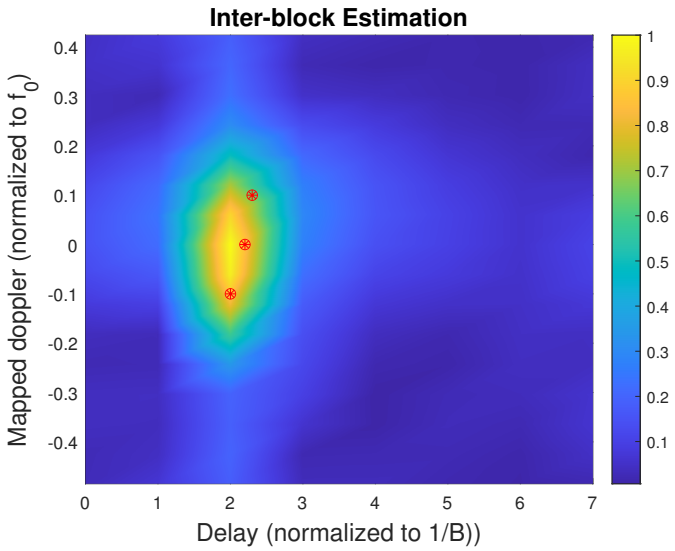

Figure 5.6: Inter-block estimation Delay-Doppler map 3, where the color scale indicates signal strength as per the color bar. Ground truth of three targets are also highlighted with red circles.

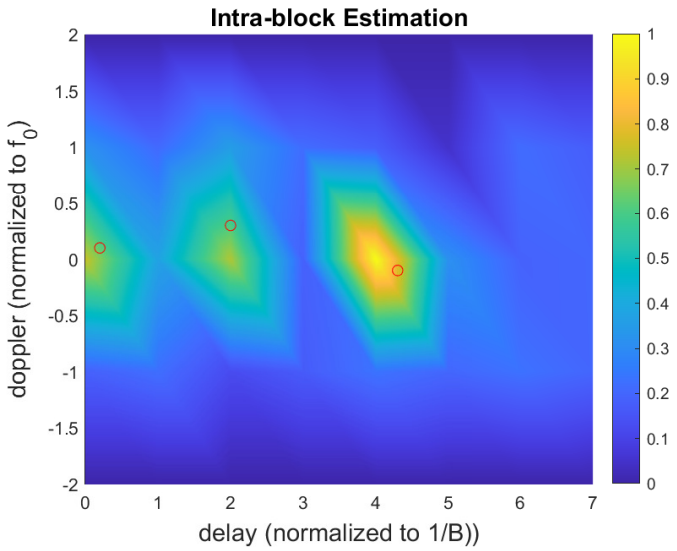

Figure 5.7: Intra-block estimation Delay-Doppler map 4, where the color scale indicates signal strength as per the color bar. Ground truth of three targets are also highlighted with red circles.

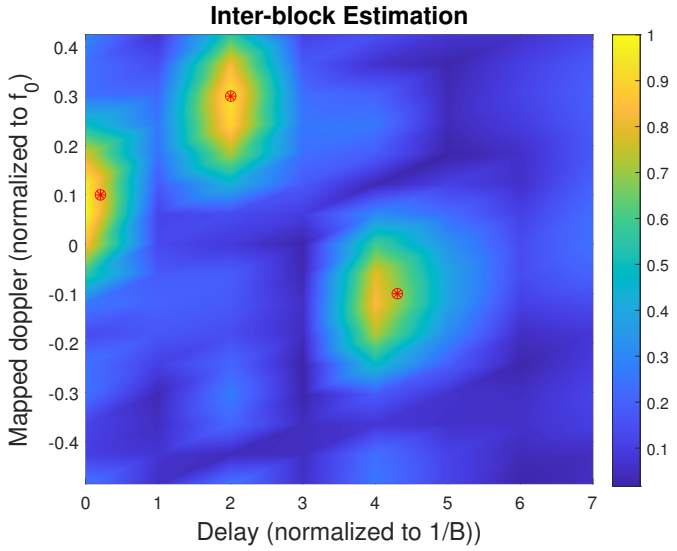

Figure 5.8: Inter-block estimation Delay-Doppler map 4, where the color scale indicates signal strength as per the color bar. Ground truth of three targets are also highlighted with red circles.

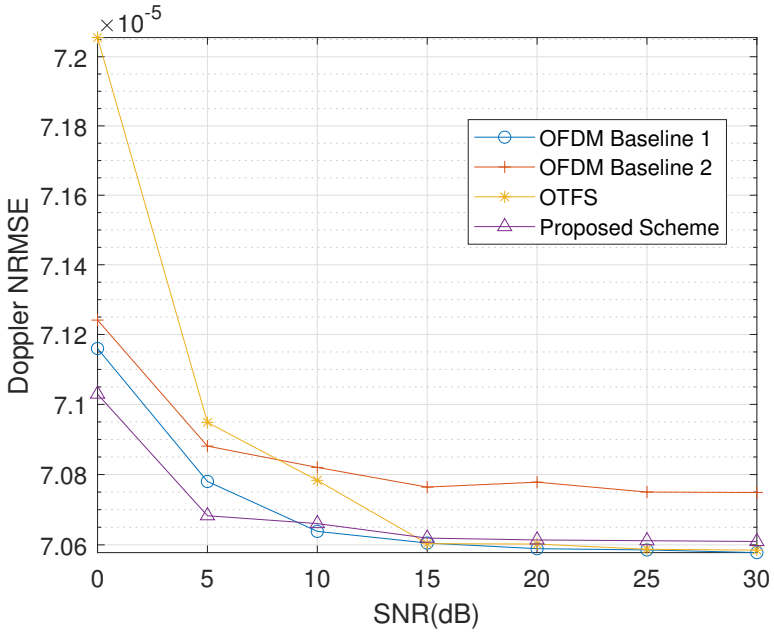

Figure 5.9: Doppler frequency NRMSE in time-varying channels.

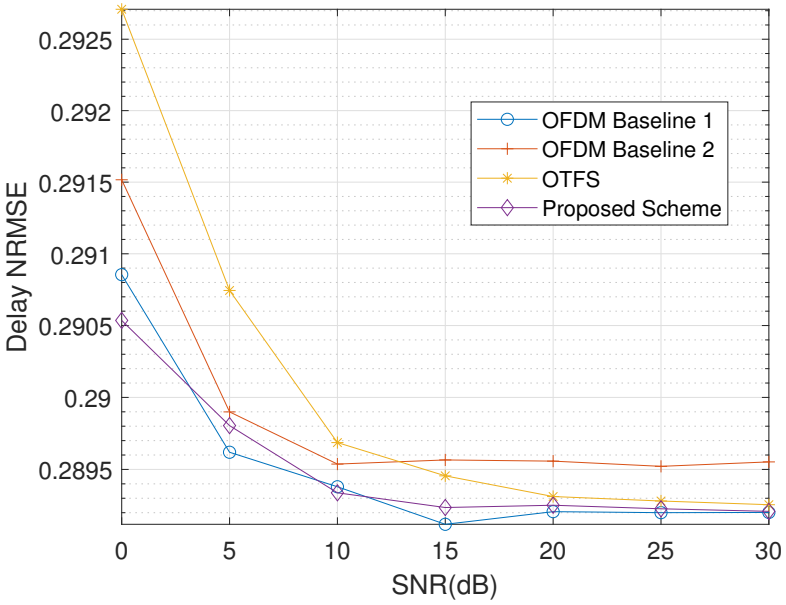

Figure 5.10: Delay NRMSE in time-varying channels.

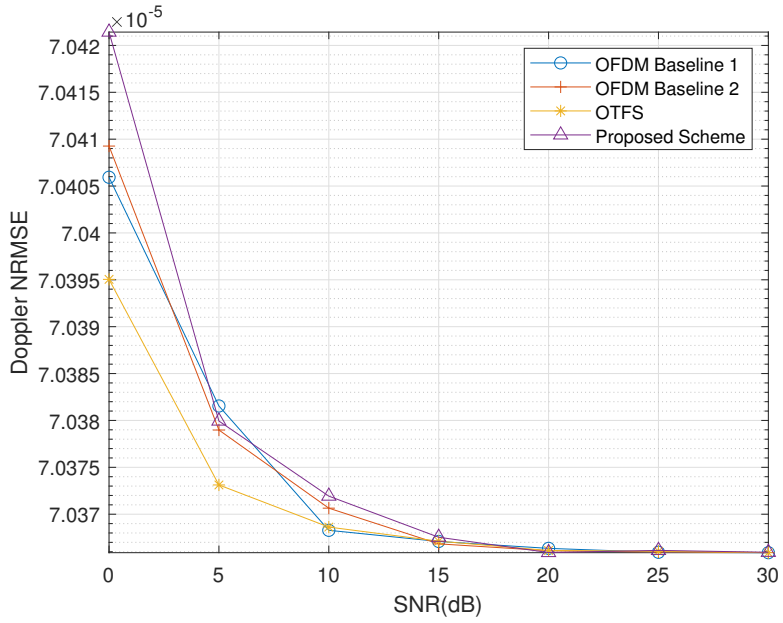

Figure 5.11: Doppler frequency NRMSE in time-varying channels. Only pilots, no data.

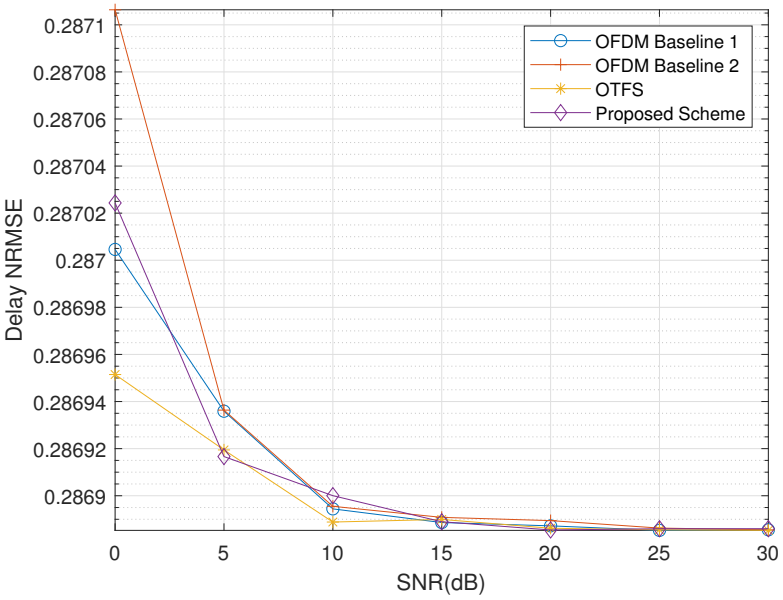

Figure 5.12: Delay NRMSE in time-varying channels. Only pilots,no data.

We then compare the sensing performance under various signal-to-noise power ratios (SNRs). Since conventional OFDM is not able to estimate Doppler frequencies with absolute values larger than half of the subcarrier interval, we let $|v_\ell|$ be uniformly distributed over $[0.3, 0.4]B/N$. Also, to avoid matching the estimates, we simulate only 1 path for all systems. The normalized root mean square errors (NRMSE) are used as performance metrics. The NRMSE is calculated as $\sqrt{\frac{1}{Q}\sum_{q=1}^{Q}(a_q - \hat{a}_q)^2}/b$, where $\hat{a}_q$ and a_q denotes the estimated and true values, respectively, in the q-th out of Q independent trials, b is the normalization factor. For delay and Doppler estimation, b equals to $1/B$ and B respectively.

Figs. 5.9 and 5.10 present the NRMSEs for Doppler frequency and delay estimation, respectively. We can see that the proposed scheme outperforms Baseline 2 over all SNR regions. It performs better than OTFS at lower SNRs, and their performance is similar at higher SNRs. It also performs almost as good as Baseline 1, although it is slightly inferior to the latter at higher SNRs. The results in these two figures seem to suggest that increasing subcarrier interval is more effective in reducing the ICI, compared to using zero guarding symbols, given the simpler implementation in the former. These observations may be specific to the smaller Doppler frequencies used in the simulation; Nevertheless, to fully exploit the potential of the proposed scheme, it would be favorable to develop advanced channel estimation schemes for $\mathbf{H}_{fd}$ based on pilots with reduced zero guarding symbols.

Figures 5.11 and 5.12 depict scenarios where the OFDM and OTFS blocks are solely dedicated to sensing without any involvement of data symbols. In these configurations, our proposed scheme achieve similar performance in high SNR region and exhibits relatively poorer performance compared to the OTFS in low SNR region. So in our simulaiton settings, OTFS is more suitable for sensing only scenario and our propose scheme is more suitable for ISAC scenario.

5.5 Conclusions

In this section, we proposed a frequency-domain sensing framework for a general OFDM ISAC system in time-varying channels, where pilots are placed in the frequency domain. We first provided an improved closed-form expression for the received signals over a time-varying channel. We then developed intra-block and inter-block sensing models, and proposed a sensing scheme with an exemplified periodogram sensing algorithm and pilot design. By combining intra-block and inter-block sensing, the proposed scheme can potentially enable sensing large Doppler frequencies with finer resolution and better performance. Simulation results validate the proposed framework. The proposed framework set a solid foundation for frequency-domain sensing in OFDM ISAC systems. It can also be improved in various aspects, e.g., developing advanced channel estimation scheme with reduced zero guarding symbols so that it can be applied directly to current OFDM systems, and applying advanced techniques for combining intra-block and inter-block sensing.

Chapter 6

Performance Bounds of ISAC in Time-Varying Channels

The current literature on sensing performance bounds for Integrated Sensing and Communications (ISAC) systems is primarily focused on the channels wherein the Doppler shift within one Orthogonal Frequency Division Multiplexing (OFDM) block is neglected. This assumption, however, is not applicable in scenarios involving high mobility. In this section, we aim to establish the sensing performance bound in time-varying channels and optimize preambles. Firstly, we establish input-output relationships in such channels. Then, we derive the delay and Doppler Cramér-Rao lower bound (CRLB) in time-varying channels. Finally, we optimize preambles based on CRLB minimization. Simulation results unfold the impact of parameters on the CRLB and validate our CRLB optimization methods in time-varying channels.

6.1 Introduction

ISAC has recently received significant attention as an innovative approach that integrates sensing and communication [73]. In perceptive mobile networks, ISAC can facilitate sensing of high-mobility targets without compromising communication quality [70]. However, ISAC applications face significant challenges in fast time-varying channels in both sensing and communication systems, and rigorous performance bounds are necessary for theoretical analysis [11].

In ISAC systems, CRLB is one of the most adopted performance bounds. CRLB is a metric that can be used to measure the lower bound of estimation errors for both radar sensing and communication channel estimation [3], [4]. Its closed-form expressions are generally hard to obtain, and the application of the metric in signal optimization typically needs to resort to numerical results [70]. In particular, there is little results on sensing CRLB for ISAC systems in time-varying channels. In [1], the authors investigated a joint communication and radar sensing system that uses OTFS modulation for two functions: channel parameter estimation at the transmitter and data detection at the receiver. They derived the CRLB for a single path and conducted a waterfall analysis. However, this work assumes that the channel is time-invariant. To address time-varying channels, the paper [11] proposes a frequency-domain sensing framework that combines inter-OFDM block sensing and intra- OFDM block sensing for estimating channel parameters. This framework achieves high sensing accuracy while maintaining a large estimation range. Other studies have investigated channel estimation, which is similar to the parameter sensing problem [5]–[7]. To date, the sensing performance bound of ISAC in time-varying channels is yet to be derived, and there are no insights on how channel parameters in time-varying channels can influence the performance bound.

This section presents a study on the performance bound of ISAC systems in time-varying channels. To achieve this, we establish system models which include the Doppler effect within a single OFDM block. Next, the delay and Doppler CRLBs in time-varying channels are derived. Furthermore, we optimize the preambles by minimizing the CRLB. We conduct simulations to unfold implications for the design and optimization of ISAC systems in time-varying channels.

This section is organized as follows: We first describe the system and signal models. Then we describe CRLB bounds for multipath and single-path scenario. After that, we illustrates the CRLB optimization. Simulation results and conclusion can be found at last.

6.2 System and Signal Models

In this section, we briefly revisit the continuous models and discrete model for time-varying channels in Section 3.

We consider a general ISAC OFDM system, where the OFDM symbol duration is T, the sampling time is T_0, and the subcarrier number is N. We use preambles for sensing. The signal bandwidth and the subcarrier interval are $B = 1/T_0$ and $f_0 = B/N$, respectively. The continuous time-varying channel for the k-th ($k = 0, 1, ..., K$) OFDM symbol can be represented as [11]

$$h_v(\tau, v) = \sum_{\ell=1}^{L} h_\ell e^{j2\pi v_\ell kT} g_1(\tau - \tau_\ell) g_2(v - v_\ell), \tag{6.1}$$

where h_ℓ, v_ℓ and τ_ℓ are the ℓ-th path gain, the channel Doppler shift and the channel delay respectively, L is the number of subpaths, $e^{j2\pi v_\ell kT}$ represents the k-th OFDM symbol's Doppler shift, $g_1(\cdot)$ is the inverse Fourier transform of window functions $G_1(f)$ in the frequency domain, and $g_2(\cdot)$ is the Fourier transform of window functions $G_2(t)$ in the time domain. $G_1(f)$ and $G_2(t)$ can have any shape. For analytical

tractability, we adopt the rectangular window for these two windowing functions. Therefore, both $g_1(\cdot)$ and $g_2(\cdot)$ are sinc functions.

The continuous frequency-Doppler channel can be obtained by applying Fourier transform to (6.1). This leads to

$$H_{fd}(f,v) = G_1(f)\sum_{\ell=1}^{L} h_\ell e^{j2\pi v_\ell kT} g_2(v-v_\ell) e^{-j2\pi f\tau_\ell}. \tag{6.2}$$

We ignore noises for brevity, and the received continuous signal in the frequency domain can be represented as [8]

$$Y(f) = \int_{-\infty}^{+\infty} H_{fd}(f', f-f')X(f')df', \tag{6.3}$$

where $X(f')$ is the transmission signal in the frequency domain.

By sampling and digitalization, we obtain discrete frequency signals and channel models:

$$\mathbf{y}_f = \mathbf{H}_{fd}\mathbf{x}_f, \tag{6.4}$$

where $\mathbf{x}_f$ denotes the transmitted signal in frequency domain and $\mathbf{y}_f$ denotes the received signal in frequency domain. $\mathbf{H}_{fd}$ is the frequency-Doppler channel matrix. Referring to [11], the elements in $\mathbf{H}_{fd}$ is

$$\begin{aligned}(\mathbf{H}_{fd})_{n,m} &= H_{fd}(mf_0, (n-m)_N f_0) \\ &= G_1(mf_0)\sum_{\ell=1}^{L} h_\ell e^{j2\pi v_\ell kT} \\ &\quad g_2(((n-m)f_0 - v_\ell)_{Nf_0})\, e^{-j2\pi m f_0 \tau_\ell},\end{aligned} \tag{6.5}$$

where $(n)_N$ denotes the modular operation $\text{mod}(n, N)$. Unlike in the typical time invariant channels, $\mathbf{H}_{fd}$ is not a diagonal matrix anymore in time-varying channels.

We note that (6.4) and (6.5) reveal the signal input-output relationships in time-varying channels, with the impact of delay and Doppler parameters being characterized.

Next, we utilize the discrete channel model to analyze the theoretical ISAC performance limit in time-varying channels.

6.3 Sensing Performance Bound in Time-varying channels

In this section, we focus on the CRLB to derive a theoretical indicator for sensing performance. Following a typical routine for CRLB derivation, we start with deriving the Fisher information matrix (FIM) in time-varying channels.

As derived in (6.4), the system model can be written as follows

$$\mathbf{y}_f = \mathbf{H}_{fd}\mathbf{x}_f + \mathbf{z}, \tag{6.6}$$

where $\mathbf{z}$ represents the noise in the frequency domain.

Consider the case of $k = 0$. Based on (6.4) and (6.5), we can rewrite the received signal in a more convenient form for the CRLB derivation. In particular, we first introduce the following shorthand symbol

$$g_{2l}(n, m) = g_2(((n - m)f_0 - v_l)_{Nf_0}). \tag{6.7}$$

Using $g_{2l}(n, m)$, we can construct the following matrix

$$\mathbf{G}_{v_l} = \begin{bmatrix} g_{2l}(0,0) & g_{2l}(0,1) & ... & g_{2l}(0,N-1) \\ g_{2l}(1,0) & ... & & g_{2l}(1,N-1) \\ \vdots & & & \vdots \\ g_{2l}(N-1,0) & ... & & g_{2l}(N-1,N-1) \end{bmatrix}. \tag{6.8}$$

The matrix $\mathbf{G}_{v_l}$ enables us to obtain the following signal model

$$\mathbf{y}_f = \sum_{l=0}^{L-1} h_l \mathbf{G}_{v_l} \mathbf{D}_{\tau_l} \mathbf{x}_f + \mathbf{z}, \tag{6.9}$$

where $\mathbf{D}$ is a diagonal matrix with diagonal elements being $e^{-j2\pi n f_0 \tau_l}, n = 0, ..., N-1$

Let $\boldsymbol{\eta} = [\boldsymbol{\eta}_0, \boldsymbol{\eta}_1, ..., \boldsymbol{\eta}_{L-1}]$ denote the unknown parameters to be estimated, $\boldsymbol{\eta}_\ell = [\tau_\ell, v_\ell, h_{R,\ell}, h_{I,\ell}]$, where $h_{R,\ell} = \Re\{h_\ell\}$, and $h_{I,\ell} = I\{h_\ell\}$. Let $\boldsymbol{\mu}(\boldsymbol{\eta}) = \sum_{l=0}^{L-1} h_l \mathbf{G}_{v_l} \mathbf{D}_{\tau_l} \mathbf{x}_f$, and the (i,j)th element of FIM is as [75]

$$\boldsymbol{J}_{i,j} = 2\Re\{\frac{\partial \boldsymbol{\mu}^H}{\partial \eta_i} \mathbf{R}^{-1} \frac{\partial \boldsymbol{\mu}}{\partial \eta_j}\}, \tag{6.10}$$

where

$$\mathbf{R}^{-1} = \frac{1}{\sigma^2} \boldsymbol{I}. \tag{6.11}$$

The σ^2 is the power of noise.

Let $l_1, l_2 \in [1, L]$ be two arbitrary subpaths. The elements of FIM are gevin by:

$$\mathbf{J}_{\tau_{l1},\tau_{l2}} = \frac{2}{\sigma^2} \mathbb{R}\{h_{l1}^H \mathbf{x}_f^H \mathbf{D}_{\tau_{l1}}^{'H} \mathbf{G}_{v_{l1}}^H h_{l2} \mathbf{G}_{v_{l2}} \mathbf{D}_{\tau_{l2}}^{'} \mathbf{x}_f\},$$

$$\mathbf{J}_{\tau_{l1},v_{l2}} = \frac{2}{\sigma^2} \mathbb{R}\{h_{l1}^H \mathbf{x}_f^H \mathbf{D}_{\tau_{l1}}^{'H} \mathbf{G}_{v_{l1}}^H h_{l2} \mathbf{G}_{v_{l2}}^{'} \mathbf{D}_{\tau_{l2}} \mathbf{x}_f\},$$

$$\mathbf{J}_{\tau_{l1},h_{R_{l2}}} = \frac{2}{\sigma^2}\mathbb{R}\{h_{l1}^H \mathbf{x}_f^H \mathbf{D}_{\tau_{l1}}^{'H} \mathbf{G}_{v_{l1}}^H \mathbf{G}_{v_{l2}} \mathbf{D}_{\tau_{l2}} \mathbf{x}_f\},$$

$$\mathbf{J}_{\tau_{l1},h_{I_{l2}}} = \frac{2}{\sigma^2}\mathbb{R}\{h_{l1}^H \mathbf{x}_f^H \mathbf{D}_{\tau_{l1}}^{'H} \mathbf{G}_{v_{l1}}^H j\mathbf{G}_{v_{l2}} \mathbf{D}_{\tau_{l2}} \mathbf{x}_f\},$$

$$\mathbf{J}_{v_{l1},\tau_{l2}} = \frac{2}{\sigma^2}\mathbb{R}\{h_{l2}^H \mathbf{x}_f^H \mathbf{D}_{\tau_{l2}}^{'H} \mathbf{G}_{v_{l2}}^H h_{l1} \mathbf{G}_{v_{l1}}^{'} \mathbf{D}_{\tau_{l1}} \mathbf{x}_f\},$$

$$\mathbf{J}_{v_{l1},v_{l2}} = \frac{2}{\sigma^2}\mathbb{R}\{h_{l1}^H \mathbf{x}_f^H \mathbf{D}_{\tau_{l1}}^{H} \mathbf{G}_{v_{l1}}^{'H} h_{l2} \mathbf{G}_{v_{l2}}^{'} \mathbf{D}_{\tau_{l2}} \mathbf{x}_f\},$$

$$\mathbf{J}_{v_{l1},h_{R_{l2}}} = \frac{2}{\sigma^2}\mathbb{R}\{h_{l1}^H \mathbf{x}_f^H \mathbf{D}_{\tau_{l1}}^{H} \mathbf{G}_{v_{l1}}^{'H} \mathbf{G}_{v_{l2}} \mathbf{D}_{\tau_{l2}} \mathbf{x}_f\},$$

$$\mathbf{J}_{v_{l1},h_{I_{l2}}} = \frac{2}{\sigma^2}\mathbb{R}\{h_{l1}^H \mathbf{x}_f^H \mathbf{D}_{\tau_{l1}}^{H} \mathbf{G}_{v_{l1}}^{'H} j\mathbf{G}_{v_{l2}} \mathbf{D}_{\tau_{l2}} \mathbf{x}_f\},$$

$$\mathbf{J}_{h_{R_{l1}},h_{R_{l2}}} = \frac{2}{\sigma^2}\mathbb{R}\{\mathbf{x}_f^H \mathbf{D}_{\tau_{l1}}^{H} \mathbf{G}_{v_{l1}}^{H} \mathbf{G}_{v_{l2}} \mathbf{D}_{\tau_{l2}} \mathbf{x}_f\},$$

$$\mathbf{J}_{h_{R_{l1}},h_{I_{l2}}} = \frac{2}{\sigma^2}\mathbb{R}\{\mathbf{x}_f^H \mathbf{D}_{\tau_{l1}}^{H} \mathbf{G}_{v_{l1}}^{H} j\mathbf{G}_{v_{l2}} \mathbf{D}_{\tau_{l2}} \mathbf{x}_f\},$$

$$\mathbf{J}_{h_{I_{l1}},h_{I_{l2}}} = \frac{2}{\sigma^2}\mathbb{R}\{\mathbf{x}_f^H \mathbf{D}_{\tau_{l1}}^{H} \mathbf{G}_{v_{l1}}^{H} \mathbf{G}_{v_{l2}} \mathbf{D}_{\tau_{l2}} \mathbf{x}_f\}.$$

$$\mathbf{J}_{\tau_{l2},\tau_{l1}} = \frac{2}{\sigma^2}\mathbb{R}\{h_{l1}^H \mathbf{x}_f^H \mathbf{D}_{\tau_{l1}}^{'H} \mathbf{G}_{v_{l1}}^H h_{l2} \mathbf{G}_{v_{l2}} \mathbf{D}_{\tau_{l2}}^{'} \mathbf{x}_f\},$$

$$\mathbf{J}_{v_{l2},\tau_{l1}} = \frac{2}{\sigma^2}\mathbb{R}\{h_{l1}^H \mathbf{x}_f^H \mathbf{D}_{\tau_{l1}}^{'H} \mathbf{G}_{v_{l1}}^H h_{l2} \mathbf{G}_{v_{l2}}^{'} \mathbf{D}_{\tau_{l2}} \mathbf{x}_f\},$$

$$\mathbf{J}_{h_{R_{l2}},\tau_{l1}} = \frac{2}{\sigma^2}\mathbb{R}\{h_{l1}^H \mathbf{x}_f^H \mathbf{D}_{\tau_{l1}}^{'H} \mathbf{G}_{v_{l1}}^H \mathbf{G}_{v_{l2}} \mathbf{D}_{\tau_{l2}} \mathbf{x}_f\},$$

$$\mathbf{J}_{h_{I_{l2}},\tau_{l1}} = \frac{2}{\sigma^2}\mathbb{R}\{h_{l1}^H \mathbf{x}_f^H \mathbf{D}_{\tau_{l1}}^{'H} \mathbf{G}_{v_{l1}}^H j\mathbf{G}_{v_{l2}} \mathbf{D}_{\tau_{l2}} \mathbf{x}_f\},$$

$$\mathbf{J}_{\tau_{l2},\,v_{l1}} = \frac{2}{\sigma^2}\mathbb{R}\{h_{l2}^H \mathbf{x}_f^H \mathbf{D}_{\tau_{l2}}^{'H} \mathbf{G}_{v_{l2}}^H h_{l1} \mathbf{G}_{v_{l1}}^{'} \mathbf{D}_{\tau_{l1}} \mathbf{x}_f\},$$

$$\mathbf{J}_{v_{l2},\,v_{l1}} = \frac{2}{\sigma^2}\mathbb{R}\{h_{l1}^H \mathbf{x}_f^H \mathbf{D}_{\tau_{l1}}^H \mathbf{G}_{v_{l1}}^{'H} h_{l2} \mathbf{G}_{v_{l2}}^{'} \mathbf{D}_{\tau_{l2}} \mathbf{x}_f\},$$

$$\mathbf{J}_{h_{R_{l2}},v_{l1}} = \frac{2}{\sigma^2}\mathbb{R}\{h_{l1}^H \mathbf{x}_f^H \mathbf{D}_{\tau_{l1}}^H \mathbf{G}_{v_{l1}}^{'H} \mathbf{G}_{v_{l2}} \mathbf{D}_{\tau_{l2}} \mathbf{x}_f\},$$

$$\mathbf{J}_{h_{I_{l2}},v_{l1}} = \frac{2}{\sigma^2}\mathbb{R}\{h_{l1}^H \mathbf{x}_f^H \mathbf{D}_{\tau_{l1}}^H \mathbf{G}_{v_{l1}}^{'H} j\mathbf{G}_{v_{l2}} \mathbf{D}_{\tau_{l2}} \mathbf{x}_f\},$$

$$\mathbf{J}_{h_{R_{l2}},h_{R_{l1}}} = \frac{2}{\sigma^2}\mathbb{R}\{\mathbf{x}_f^H \mathbf{D}_{\tau_{l1}}^H \mathbf{G}_{v_{l1}}^H \mathbf{G}_{v_{l2}} \mathbf{D}_{\tau_{l2}} \mathbf{x}_f\},$$

$$\mathbf{J}_{h_{I_{l2}},h_{R_{l1}}} = \frac{2}{\sigma^2}\mathbb{R}\{\mathbf{x}_f^H \mathbf{D}_{\tau_{l1}}^H \mathbf{G}_{v_{l1}}^H j\mathbf{G}_{v_{l2}} \mathbf{D}_{\tau_{l2}} \mathbf{x}_f\},$$

$$\mathbf{J}_{h_{I_{l2}},h_{I_{l1}}} = \frac{2}{\sigma^2}\mathbb{R}\{\mathbf{x}_f^H \mathbf{D}_{\tau_{l1}}^H \mathbf{G}_{v_{l1}}^H \mathbf{G}_{v_{l2}} \mathbf{D}_{\tau_{l2}} \mathbf{x}_f\}.$$

The CRLBs for the parameters of a given path are the corresponding elements in $\boldsymbol{J}^{-1}$. Now we have derived the CRLB. This is beneficial to understand the theoretical sensing performance limit.

The CRLB involves the inverse of the FIM matrix and as is typical [76], [77], it is hard to get the explicit CRLB expressions. However, when some special, yet practical scenarios are considered, we can apply certain conditions to the above partial derivatives and obtain closed-form CRLB expressions. This is illustrated next.

6.4 CRLBs for Channels with a Line-of-sight Path

When there is only a single path, we can simplify and obtain closed-form CRLB expressions. This case may include the channels with a dominating line-of-sight (LoS) path, which are practical in both sensing and communications [78]. In this section, we first derive LoS CRLB as the special case and then conduct analysis on it.

6.4.1 Delay CRLB with Known Channel Doppler

In this case, $\boldsymbol{\eta} = [\tau, h_R, h_I]$. To keep concise, we define vector $\mathbf{u}$ and $\mathbf{w}$ and let their nth entries be, respectively

$$u(n) = \sum_{i=0}^{N-1} g_{2\ell}(n,i) e^{-j2\pi i f_0 \tau} x_i, \tag{6.12}$$

$$w(n) = \sum_{i=0}^{N-1} i g_{2\ell}(n,i) e^{-j2\pi i f_0 \tau} x_i. \tag{6.13}$$

Theorem 1 *According to the definition of FIM, we can obtain the closed-form CRLB for τ as*

$$\begin{aligned} CRLB_\tau &= \left[\mathbf{O}^{-1}\right]_{0,0} \\ &= \frac{1}{\frac{2}{\sigma^2}(2\pi f_0 h^H)(2\pi f_0 h)} \frac{\mathbf{u}^H\mathbf{u}}{\mathbf{w}^H\mathbf{w}\mathbf{u}^H\mathbf{u} - \mathbf{w}^H\mathbf{u}\mathbf{u}^H\mathbf{w}}. \end{aligned} \tag{6.14}$$

See proof in Appendix.

As $\mathbf{u}$ and $\mathbf{w}$ are functions of delay τ, the delay CRLB, $CRLB_\tau$ is also a function of τ, and hence is dependent of τ.

6.4.2 Doppler CRLB with Known Channel Delay

In this case, $\boldsymbol{\eta} = [v, h_R, h_I]$. To keep concise, we define the vector $\mathbf{q}$. Let its n-th entries be

$$q(n) = \sum_{i=0}^{N-1} g'_{2\ell}(n,i) e^{-j2\pi i f_0 \tau} x_i. \tag{6.15}$$

Theorem 2 *The Doppler CRLB with known channel delay is*

$$CRLB_v = \frac{2}{\sigma^2} h h^H \frac{\boldsymbol{q}^H\boldsymbol{q}\mathbf{u}^H\mathbf{u} - \boldsymbol{q}^H\boldsymbol{u}\boldsymbol{u}^H\boldsymbol{q}}{\mathbf{u}^H\mathbf{u}}. \tag{6.16}$$

See proof in the Appendix.

6.4.3 Delay and Doppler CRLBs with Unkown Channel Doppler and Delay

In this case, $\boldsymbol{\eta} = [\tau, v, h_R, h_I]$. Based on the results in section III, the FIM matrix is

$$\mathbf{S} = \begin{bmatrix} \mathbf{S}_A & \mathbf{S}_B \\ \mathbf{S}_B^T & \mathbf{S}_C \end{bmatrix}, \tag{6.17}$$

with

$$\mathbf{S}_A = \begin{bmatrix} \mathbf{S}_{\tau,\tau} & \mathbf{S}_{\tau,v} \\ \mathbf{S}_{v,\tau} & \mathbf{S}_{v,v} \end{bmatrix}, \mathbf{S}_B = \begin{bmatrix} \mathbf{S}_{\tau,h_R} & \mathbf{S}_{\tau,h_I} \\ \mathbf{S}_{v,h_R} & \mathbf{S}_{v,h_I} \end{bmatrix}, \tag{6.18}$$

$$\mathbf{S}_C = \begin{bmatrix} \mathbf{S}_{h_R,h_R} & \mathbf{S}_{h_R,h_I} \\ \mathbf{S}_{h_I,h_R} & \mathbf{S}_{h_I,h_I} \end{bmatrix} \tag{6.19}$$

According to (S18) in the supplement material of [75], we can calculate the inter-media matrix $\mathbf{H}$ as follows

$$\begin{aligned} \mathbf{H} &\triangleq \mathbf{S}_A - \mathbf{S}_B \mathbf{S}_C^{-1} \mathbf{S}_B^T \\ &= \mathbf{S}_A - \frac{1}{\mathbf{S}_{h_R,h_R}} \mathbf{S}_B \mathbf{S}_B^T \\ &= \begin{bmatrix} \mathbf{S}_{\tau,\tau} & \mathbf{S}_{\tau,v} \\ \mathbf{S}_{v,\tau} & \mathbf{S}_{v,v} \end{bmatrix} - \frac{1}{\mathbf{S}_{h_R,h_R}} \\ &\begin{bmatrix} \mathbf{S}_{\tau,h_R}\mathbf{S}_{h_R,\tau} + \mathbf{S}_{\tau,h_I}\mathbf{S}_{h_I,\tau}, \mathbf{S}_{\tau,h_R}\mathbf{S}_{h_R,v} + \mathbf{S}_{\tau,h_I}\mathbf{S}_{h_I,v} \\ \mathbf{S}_{v,h_R}\mathbf{S}_{h_R,\tau} + \mathbf{S}_{v,h_I}\mathbf{S}_{h_I,\tau}, \mathbf{S}_{v,h_R}\mathbf{S}_{h_R,v} + \mathbf{S}_{v,h_I}\mathbf{S}_{h_I,v} \end{bmatrix} \end{aligned} \tag{6.20}$$

with its elements:

$$\begin{aligned}\mathbf{H}_{0,1} &= \mathbf{S}_{\tau,v} - \frac{1}{\mathbf{S}_{h_R,h_R}}(\mathbf{S}_{\tau,h_R}\mathbf{S}_{h_R,v} + \mathbf{S}_{\tau,h_I}\mathbf{S}_{h_I,v}) \\ &= \frac{2}{\sigma^2}2\pi f_0 hh^H\mathbb{R}\{j\mathbf{w}^H\mathbf{q}\}- \\ &\frac{1}{\frac{2}{\sigma^2}\mathbf{u}^H\mathbf{u}}(\frac{2}{\sigma^2}2\pi f_0\mathbb{R}\{jh^H\mathbf{w}^H\mathbf{u}\}\frac{2}{\sigma^2}\mathbb{R}\{h\mathbf{u}^H\mathbf{q}\}- \\ &\frac{2}{\sigma^2}2\pi f_0\mathbb{R}\{h^H\mathbf{w}^H\mathbf{u}\}\frac{2}{\sigma^2}\mathbb{R}\{-jh\mathbf{u}^H\mathbf{q}\}) \\ &= \frac{2}{\sigma^2}2\pi f_0\{hh^H\mathbb{R}\{j\mathbf{w}^H\mathbf{q}\}- \\ &\frac{\mathbb{R}\{jh^H\mathbf{w}^H\mathbf{u}\}\mathbb{R}\{h\mathbf{u}^H\mathbf{q}\} - \mathbb{R}\{h^H\mathbf{w}^H\mathbf{u}\}\mathbb{R}\{-jh\mathbf{u}^H\mathbf{q}\}}{\mathbf{u}^H\mathbf{u}}\}\end{aligned} \tag{6.21}$$

$$\mathbf{H}_{1,0} = \mathbf{H}_{0,1}, \tag{6.22}$$

$$\mathbf{H}_{0,0} = \frac{2}{\sigma^2}(2\pi f_0 h^H)(2\pi f_0 h)\left[\frac{\mathbf{w}^H\mathbf{w}\mathbf{u}^H\mathbf{u} - \mathbf{w}^H\mathbf{u}\mathbf{u}^H\mathbf{w}}{\mathbf{u}^H\mathbf{u}}\right], \tag{6.23}$$

$$\mathbf{H}_{1,1} = \frac{2}{\sigma^2}hh^H\frac{\boldsymbol{q}^H\boldsymbol{q}\mathbf{u}^H\mathbf{u} - \boldsymbol{q}^H\boldsymbol{u}\boldsymbol{u}^H\boldsymbol{q}}{\mathbf{u}^H\mathbf{u}}. \tag{6.24}$$

Then we can obtain the closed-form expression for the joint CRLBs as [75]

$$CRLB_\tau = \frac{\mathbf{H}_{1,1}}{\mathbf{H}_{0,0}\mathbf{H}_{1,1} - \mathbf{H}_{0,1}\mathbf{H}_{0,1}}, \tag{6.25}$$

$$CRLB_v = \frac{\mathbf{H}_{0,0}}{\mathbf{H}_{0,0}\mathbf{H}_{1,1} - \mathbf{H}_{0,1}\mathbf{H}_{0,1}}. \tag{6.26}$$

6.4.4 Analysis on LoS Path CRLB

From (8.4) (6.13) (6.12) and (6.7), we can see that delay CRLB is a function of channel Doppler. However, interestingly, it does not vary with channel Doppler, which is proven next.

Note that $\mathbf{G}_v$ is a circular shift matrix. Each row is a circular shift of the first row and each column is a circular shift of the first column. Thus, we have $\mathbf{G}_v^H \mathbf{G}_v = \mathbf{I}$, where $\mathbf{I}$ is an identity matrix. Multiplying $\mathbf{G}_v^H$ to both sides of (6.9), we have

$$\mathbf{G}_v^H \mathbf{y}_f = h\mathbf{D}_\tau \mathbf{x}_f + \mathbf{G}_v^H \mathbf{z}. \tag{6.27}$$

From the equation above, we can see that by multiplying $\mathbf{G}^H$, we do not amplify the SNR, but the estimation problem becomes uncorrelated to channel Doppler. Thus, the delay CRLB becomes independent of Doppler. This implies that in the presence of a dominating LoS path, its delay estimation accuracy is not affected by the Doppler shift.

6.5 CRLB Minimization via Signal Optimization

In this section, we aim to minimize the CRLB by optimizing signal $\mathbf{x}_f$. Rewrite (6.6) as

$$\mathbf{y}_f = (\mathbf{x}_f^T \otimes \mathbf{I}) vec(\mathbf{H}_{fd}) + \mathbf{z}. \tag{6.28}$$

According to (6.10), the new form of the FIM matrix is given by

$$\mathbf{J}_{\tau_{l1},\tau_{l2}} = \frac{2}{\sigma^2}\mathbb{R}\{vec(h_{l1}\mathbf{G}_{v_{l1}}\mathbf{D}^{'}{}_{\tau_{l1}})^H (\mathbf{x}_f^*\mathbf{x}_f^T \otimes \mathbf{I})vec(h_{l2}\mathbf{G}_{v_{l2}}\mathbf{D}^{'}{}_{\tau_{l2}})\},$$

$$\mathbf{J}_{\tau_{l1},v_{l2}} = \frac{2}{\sigma^2}\mathbb{R}\{vec(h_{l1}\mathbf{G}_{v_{l1}}\mathbf{D}^{'}{}_{\tau_{l1}})^H (\mathbf{x}_f^*\mathbf{x}_f^T \otimes \mathbf{I})vec(h_{l2}\mathbf{G}^{'}{}_{v_{l2}}\mathbf{D}_{\tau_{l2}})\},$$

$$\mathbf{J}_{\tau_{l1},h_{R_{l2}}} = \frac{2}{\sigma^2}\mathbb{R}\{vec(h_{l1}\mathbf{G}_{v_{l1}}\mathbf{D}^{'}{}_{\tau_{l1}})^H (\mathbf{x}_f^*\mathbf{x}_f^T \otimes \mathbf{I})vec(\mathbf{G}_{v_{l2}}\mathbf{D}_{\tau_{l2}})\},$$

$$\mathbf{J}_{\tau_{l1},h_{I_{l2}}} = \frac{2}{\sigma^2}\mathbb{R}\{vec(h_{l1}\mathbf{G}_{v_{l1}}\mathbf{D}_{\tau_{l1}})^H (\mathbf{x}_f^*\mathbf{x}_f^T \otimes \mathbf{I})vec(j\mathbf{G}_{v_{l2}}\mathbf{D}_{\tau_{l2}})\},$$

$$\mathbf{J}_{v_{l1},\tau_{l2}} = \frac{2}{\sigma^2}\mathbb{R}\{vec(h_{l1}\mathbf{G}^{'}_{v_{l1}}\mathbf{D}_{\tau_{l1}})^H (\mathbf{x}_f^*\mathbf{x}_f^T \otimes \mathbf{I})vec(h_{l2}\mathbf{G}_{v_{l2}}\mathbf{D}^{'}{}_{\tau_{l2}})\},$$

$$\mathbf{J}_{v_{l1},v_{l2}} = \frac{2}{\sigma^2}\mathbb{R}\{vec(h_{l1}\mathbf{G}^{'}{}_{v_{l1}}\mathbf{D}_{\tau_{l1}})^H (\mathbf{x}_f^*\mathbf{x}_f^T \otimes \mathbf{I})vec(h_{l2}\mathbf{G}^{'}{}_{v_{l2}}\mathbf{D}_{\tau_{l2}})\},$$

$$\mathbf{J}_{v_{l1},v_{l2}} = \frac{2}{\sigma^2}\mathbb{R}\{vec(h_{l1}\mathbf{G}^{'}{}_{v_{l1}}\mathbf{D}_{\tau_{l1}})^H (\mathbf{x}_f^*\mathbf{x}_f^T \otimes \mathbf{I})vec(h_{l2}\mathbf{G}^{'}{}_{v_{l2}}\mathbf{D}_{\tau_{l2}})\},$$

$$\mathbf{J}_{v_{l1},h_{R_{l2}}} = \frac{2}{\sigma^2}\mathbb{R}\{vec(h_{l1}\mathbf{G}^{'}{}_{v_{l1}}\mathbf{D}_{\tau_{l1}})^H (\mathbf{x}_f^*\mathbf{x}_f^T \otimes \mathbf{I})vec(\mathbf{G}_{v_{l2}}\mathbf{D}_{\tau_{l2}})\},$$

$$\mathbf{J}_{v_{l1},h_{I_{l2}}} = \frac{2}{\sigma^2}\mathbb{R}\{vec(h_{l1}\mathbf{G}^{'}{}_{v_{l1}}\mathbf{D}_{\tau_{l1}})^H (\mathbf{x}_f^*\mathbf{x}_f^T \otimes \mathbf{I})vec(j\mathbf{G}_{v_{l2}}\mathbf{D}_{\tau_{l2}})\},$$

$$\mathbf{J}_{h_{R_{l1}},h_{R_{l2}}} = \frac{2}{\sigma^2}\mathbb{R}\{vec(\mathbf{G}_{v_{l1}}\mathbf{D}_{\tau_{l1}})^H (\mathbf{x}_f^*\mathbf{x}_f^T \otimes \mathbf{I})vec(\mathbf{G}_{v_{l2}}\mathbf{D}_{\tau_{l2}})\},$$

$$\mathbf{J}_{h_{R_{l1}},h_{I_{l2}}} = \frac{2}{\sigma^2}\mathbb{R}\{vec(\mathbf{G}_{v_{l1}}\mathbf{D}_{\tau_{l1}})^H (\mathbf{x}_f^*\mathbf{x}_f^T \otimes \mathbf{I})vec(j\mathbf{G}_{v_{l2}}\mathbf{D}_{\tau_{l2}})\},$$

$$\mathbf{J}_{h_{I_{l1}},h_{I_{l2}}} = \frac{2}{\sigma^2}\mathbb{R}\{vec(j\mathbf{G}_{v_{l1}}\mathbf{D}_{\tau_{l1}})^H (\mathbf{x}_f^*\mathbf{x}_f^T \otimes \mathbf{I})vec(j\mathbf{G}_{v_{l2}}\mathbf{D}_{\tau_{l2}})\}.$$

$$\mathbf{J}_{\tau_{l2},\tau_{l1}} = \frac{2}{\sigma^2}\mathbb{R}\{vec(h_{l1}\mathbf{G}_{v_{l1}}\mathbf{D}^{'}{}_{\tau_{l1}})^H (\mathbf{x}_f^*\mathbf{x}_f^T \otimes \mathbf{I})vec(h_{l2}\mathbf{G}_{v_{l2}}\mathbf{D}^{'}{}_{\tau_{l2}})\},$$

$$\mathbf{J}_{v_{l2},\tau_{l1}} = \frac{2}{\sigma^2}\mathbb{R}\{vec(h_{l1}\mathbf{G}_{v_{l1}}\mathbf{D}^{'}{}_{\tau_{l1}})^H (\mathbf{x}_f^*\mathbf{x}_f^T \otimes \mathbf{I})vec(h_{l2}\mathbf{G}^{'}{}_{v_{l2}}\mathbf{D}_{\tau_{l2}})\},$$

$$\mathbf{J}_{h_{R_{l2}},\tau_{l1}} = \frac{2}{\sigma^2}\mathbb{R}\{vec(h_{l1}\mathbf{G}_{v_{l1}}\mathbf{D}^{'}{}_{\tau_{l1}})^H (\mathbf{x}_f^*\mathbf{x}_f^T \otimes \mathbf{I})vec(\mathbf{G}_{v_{l2}}\mathbf{D}_{\tau_{l2}})\},$$

$$\mathbf{J}_{h_{I_{l2}},\tau_{l1}} = \frac{2}{\sigma^2}\mathbb{R}\{vec(h_{l1}\mathbf{G}_{v_{l1}}\mathbf{D}_{\tau_{l1}})^H (\mathbf{x}_f^*\mathbf{x}_f^T \otimes \mathbf{I})vec(j\mathbf{G}_{v_{l2}}\mathbf{D}_{\tau_{l2}})\},$$

$$\mathbf{J}_{\tau_{l2},v_{l1}} = \frac{2}{\sigma^2}\mathbb{R}\{vec(h_{l1}\mathbf{G}^{'}_{v_{l1}}\mathbf{D}_{\tau_{l1}})^H (\mathbf{x}_f^*\mathbf{x}_f^T \otimes \mathbf{I})vec(h_{l2}\mathbf{G}_{v_{l2}}\mathbf{D}^{'}{}_{\tau_{l2}})\},$$

$$\mathbf{J}_{v_{l2},v_{l1}} = \frac{2}{\sigma^2}\mathbb{R}\{vec(h_{l1}\mathbf{G}^{'}{}_{v_{l1}}\mathbf{D}_{\tau_{l1}})^H (\mathbf{x}_f^*\mathbf{x}_f^T \otimes \mathbf{I})vec(h_{l2}\mathbf{G}^{'}{}_{v_{l2}}\mathbf{D}_{\tau_{l2}})\},$$

$$\mathbf{J}_{v_{l2},v_{l1}} = \frac{2}{\sigma^2}\mathbb{R}\{vec(h_{l1}\mathbf{G}^{'}{}_{v_{l1}}\mathbf{D}_{\tau_{l1}})^H (\mathbf{x}_f^*\mathbf{x}_f^T \otimes \mathbf{I})vec(h_{l2}\mathbf{G}^{'}{}_{v_{l2}}\mathbf{D}_{\tau_{l2}})\},$$

$$\mathbf{J}_{h_{R_{l2}},v_{l1}} = \frac{2}{\sigma^2}\mathbb{R}\{vec(h_{l1}\mathbf{G}^{'}{}_{v_{l1}}\mathbf{D}_{\tau_{l1}})^H (\mathbf{x}_f^*\mathbf{x}_f^T \otimes \mathbf{I})vec(\mathbf{G}_{v_{l2}}\mathbf{D}_{\tau_{l2}})\},$$

$$\mathbf{J}_{h_{I_{l2}},v_{l1}} = \frac{2}{\sigma^2}\mathbb{R}\{vec(h_{l1}\mathbf{G}^{'}{}_{v_{l1}}\mathbf{D}_{\tau_{l1}})^H (\mathbf{x}_f^*\mathbf{x}_f^T \otimes \mathbf{I})vec(j\mathbf{G}_{v_{l2}}\mathbf{D}_{\tau_{l2}})\},$$

$$\mathbf{J}_{h_{R_{l2}},h_{R_{l1}}} = \frac{2}{\sigma^2}\mathbb{R}\{vec(\mathbf{G}_{v_{l1}}\mathbf{D}_{\tau_{l1}})^H (\mathbf{x}_f^*\mathbf{x}_f^T \otimes \mathbf{I})vec(\mathbf{G}_{v_{l2}}\mathbf{D}_{\tau_{l2}})\},$$

$$\mathbf{J}_{h_{I_{l2}},h_{R_{l1}}} = \frac{2}{\sigma^2}\mathbb{R}\{vec(\mathbf{G}_{v_{l1}}\mathbf{D}_{\tau_{l1}})^H (\mathbf{x}_f^*\mathbf{x}_f^T \otimes \mathbf{I})vec(j\mathbf{G}_{v_{l2}}\mathbf{D}_{\tau_{l2}})\},$$

$$\mathbf{J}_{h_{I_{l2}},h_{I_{l1}}} = \frac{2}{\sigma^2}\mathbb{R}\{vec(j\mathbf{G}_{v_{l1}}\mathbf{D}_{\tau_{l1}})^H (\mathbf{x}_f^*\mathbf{x}_f^T \otimes \mathbf{I})vec(j\mathbf{G}_{v_{l2}}\mathbf{D}_{\tau_{l2}})\}.$$

Similar to [79], My goal is to reduce the greatest CRLB matrix eigenvalue. Maximising the FIM's smallest eigenvalue is equal to minimising the greatest eigenvalue of the CRLB matrix. This optimization problem can be formulated as the following SDP problem

$$\begin{aligned} &\min_{\mathbf{Q}} \; -t \\ &s.t.\ \mathbf{J} \succeq t\mathbf{I},\ \mathbf{Q} \succeq 0,\ Tr(\mathbf{Q}) \leqslant P, \end{aligned} \tag{6.29}$$

where $\mathbf{Q} = \mathbf{x}_f^* \mathbf{x}_f^T$ and t is an auxiliary variable.

It is not always possible to transform $\mathbf{Q}$ into $\mathbf{x}_f^* \mathbf{x}_f^T$ after resolving $\mathbf{Q}$. Here, we adopt an approximate approach which assigns the eigenvector corresponding to the maximum eigenvalue of $\mathbf{Q}$ to $\mathbf{x}_f$.

6.6 Simulation Results

In this section, we investigate the impact of channel parameters and the number of pilots on the CRLB in time-varying channels and compare our optimized signal design with others, considering one OFDM symbol with known training pilots. The pilots are uniformly distributed over subcarriers, with zeros at other subcarriers. The simulation parameters are provided in Table I, unless otherwise stated.

6.6.1 LoS Path Channels

As shown in Figure 6.1, though the LoS-path delay CRLB is a function of Doppler, the delay CRLB is not affected by the channel's Doppler values. This simulation result align with the theoretical derivation results in Section 6.4.4. This suggests that in a LoS dominating scenario, there is no need to optimize the preamble design for delay sensing.

Table 6.1: Simulation Parameters

Number of subcarriers, N	32
Number of pilots, L_p	8
Channel SNR, SNR	30 dB
Bandwidth, B	1
Sampling period, T_0	1
Number of subpath, L	2
Total transmission power, P	1

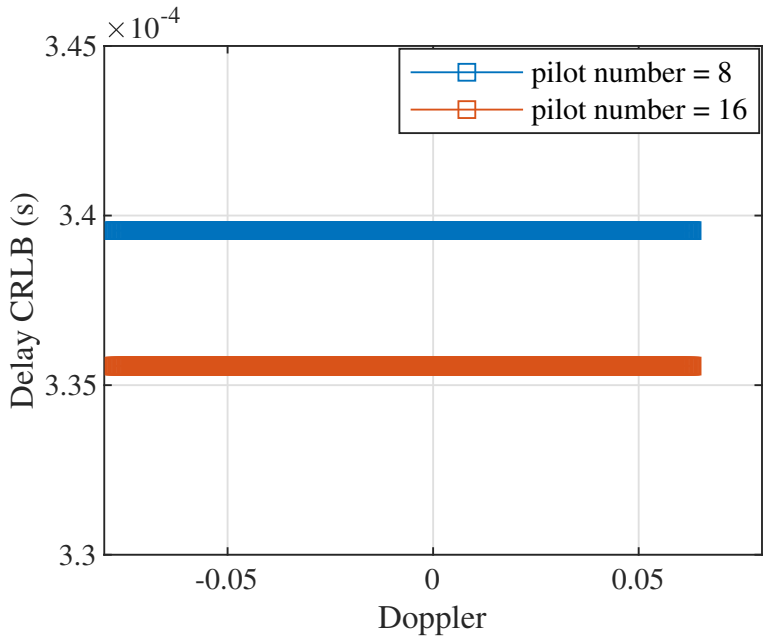

Figure 6.1: LoS path CRLB in time-varying channels.

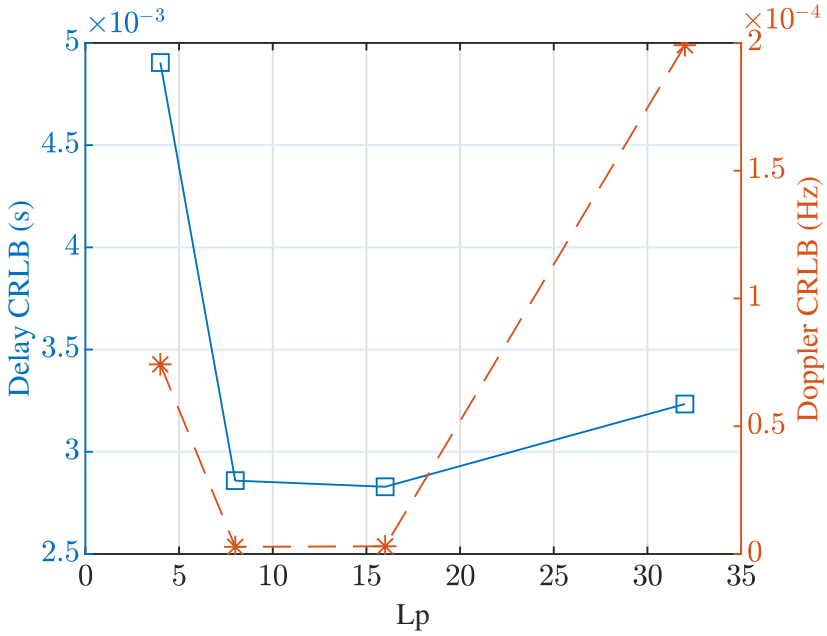

Figure 6.2: CRLB with different pilot number in time-varying channels,N=32.

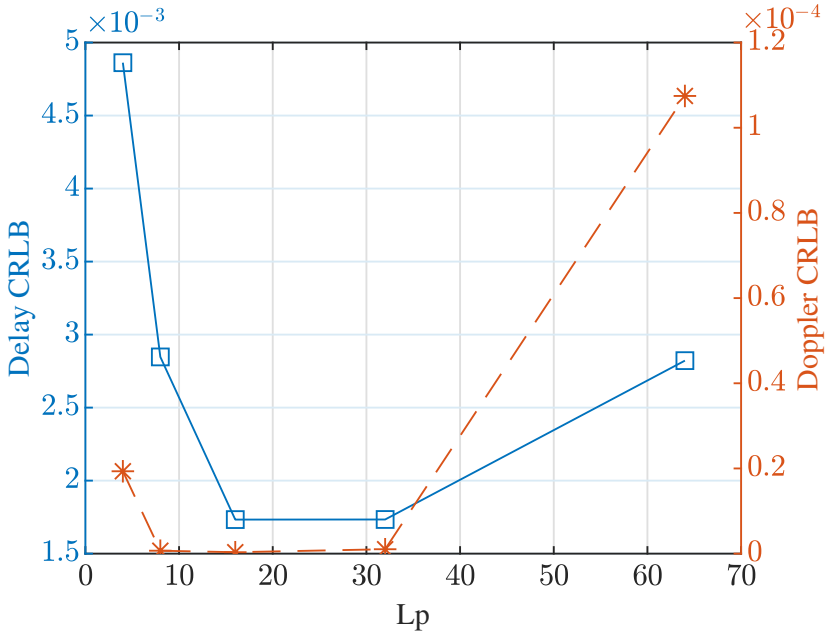

Figure 6.3: CRLB with different pilot number in time-varying channels,N=64.

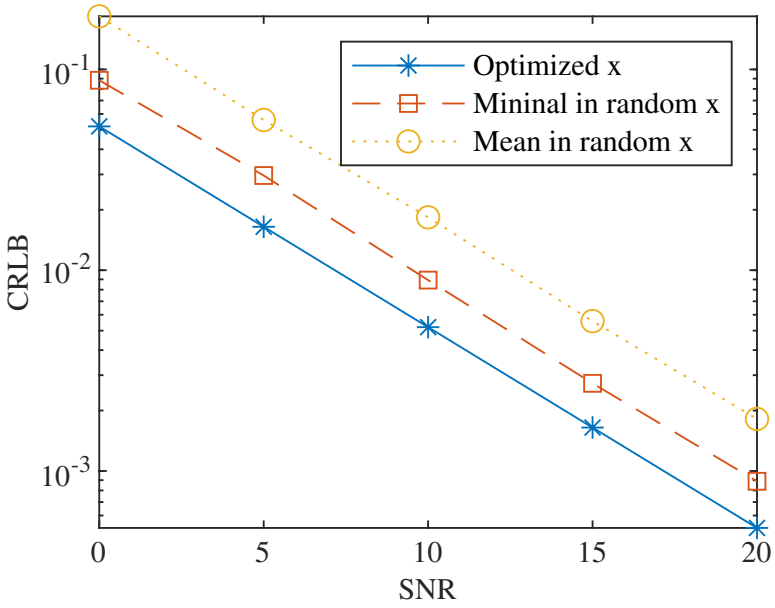

Figure 6.4: CRLB optimization in time-varying channels.

6.6.2 Multipath Channels

Figure 6.3 illustrates how the multipath delay CRLB and Doppler CRLB vary with the number of pilots. The cyclic prefix is assumed to be sufficiently long. In these simulations, two paths are considered. It can be observed that both delay CRLB and Doppler CRLB decrease initially with the increase of pilot number, due to improved sensing accuracy. However, beyond a certain threshold, Inter-Carrier Interference (ICI) caused by Doppler becomes dominant, resulting in a higher CRLB as the number of pilots increases.

Figure 6.4 demonstrates the performance of our optimization method. Only the delay and Doppler CRLBs are considered here. The mean and mininal CRLBs in 100 realizations of randomly generated signals are used as two baselines for comparison. It can be observed from the figure that CRLB decreases with increased SNR, and the CRLBs achieved by our optimized signals are always lower than the other two

baselines.

6.7 Conclusions

This chapter investigates the performance bounds of the ISAC system in time-varying channels. The study introduces time-varying channel models and derives the delay and Doppler CRLB as the sensing performance bound in such channels. CRLB minimization has been conducted by optimizing the transmission signal. The simulation results reveal how parameters affect the CRLB. It can also be seen from the results that our optimized signals achieve lower CRLBs than the benchmarks. These findings have significant implications for the design and optimization of ISAC systems in time-varying channels.

Chapter 7

Conclusions and Future Work

7.1 Concluding Remarks

In Chapter 4, a pioneering concept termed the mixed-stage OTFS system is introduced. This innovative system allows a single OTFS frame to accommodate multiple delay-Doppler grids. This approach offers users the adaptability to adjust grid sizes based on varying channel conditions, resulting in amplified system performance.

We first delve into the impact of delay-Doppler grid size on communication performance. Our simulation demonstrates that optimizing the delay-Doppler grid size in accordance with specific channel conditions has the potential to enhance overall system performance. Consequently, the mixed-stage OTFS system is presented, outlining the mechanisms for integrating data symbols of different delay-Doppler grid sizes into a unified OTFS frame. Our simulations underscore the mixed-stage OTFS system's superiority over traditional OTFS due to its inherent flexibility.

In Chapter 5, a frequency-domain sensing framework is proposed for a general OFDM ISAC system operating in time-varying channels. We initially offer an

enhanced closed-form expression for received signals over time-varying channels. Subsequently, we develop intra-block and inter-block sensing framework, with an exemplified periodogram sensing algorithm and pilot design. By combining intra-block and inter-block sensing, this framework exhibits potential for sensing large Doppler frequencies with high resolution. Simulation results validate the proposed framework, laying a robust foundation for frequency-domain sensing in OFDM ISAC systems.

Chapter 6 investigates the performance bounds of ISAC system in time-varying channels. The study derives the delay and Doppler Cramér-Rao Lower Bound (CRLB) as the sensing performance bounds in such channels. We conduct CRLB optimization by designing the preamble signal. Simulation outcomes illustrate the impact of parameters on the CRLB and indicate that our optimized signals achieve lower CRLBs compared to benchmarks.

7.2 Future Work

Future work in ISAC systems for time-varying channels involves several key areas of focus. Firstly, there is a need to develop advanced signal processing techniques that can adaptively handle rapidly changing channel conditions in real-time. This includes dynamic channel estimation and adaptive modulation and coding.

Secondly, researchers need to design algorithms for dynamic resource allocation, such as bandwidth and transmit power, to maximize ISAC system performance in time-varying channels. Balancing the trade-offs between communication and sensing objectives based on current channel conditions is crucial.

Integration with emerging 5G and beyond-5G networks is also essential. Leveraging capabilities like massive MIMO and millimeter-wave communication can improve

ISAC system performance.

Finally, conducting extensive experimental validations and field trials is critical. This will help assess ISAC system performance in real-world time-varying channel environments and validate proposed algorithms and techniques.

Specifically, for the research in this thesis, we list some of the possible future work below:

Chapter 4 holds potential for further enhancement. Currently, the pilot scheme employed to address high Doppler effects relies on zero guarding symbols, proving efficient in managing ICI. However, this scheme significantly compromises spectral efficiency. Investigating the design of pilots tailored specifically for time-varying channels is a valuable avenue for further exploration. Additionally, the existing basic 2D-FFT estimation algorithm exhibits lower accuracy. Exploring and implementing more sophisticated channel estimation methods would significantly improve performance. Considering that OFDM remains the dominant wireless communication system, ensuring the adaptability of these pilot schemes or estimation algorithms to OFDM systems is imperative. Current practices separate intra-block and inter-block sensing; future work can focus on advanced techniques that fuse these processes seamlessly.

In Chapter 5, while establishing the LoS CRLB is significant, deriving an explicit expression for the multi-path CRLB needs further study. Although complex, attaining an explicit multi-path CRLB expression would enable further theoretical analysis in this domain.

Regarding Chapter 6, the existing framework of mixed-stage OTFS exclusively caters to the downlink of a multiple access system. Extending this framework to facilitate its use in both the uplink and downlink necessitates additional research. Ensuring

bidirectional functionality would greatly enhance the practical applicability of the mixed-stage OTFS system.

Chapter 8

Appendix

8.1 Proof of Theorem 1 in Chapter 6

Based on the results in Section III, the FIM in the LoS scenario can be written as

$$\mathbf{O} = \begin{bmatrix} \mathbf{O}_{0,0} & \mathbf{O}_{0,1} & \mathbf{O}_{0,2} \\ \mathbf{O}_{1,0} & \mathbf{O}_{1,1} & \mathbf{O}_{1,2} \\ \mathbf{O}_{2,0} & \mathbf{O}_{1,2}^T & \mathbf{O}_{2,2} \end{bmatrix}, \tag{8.1}$$

with the elements of FIM

$$\mathbf{O}_{0,0} = \frac{2}{\sigma^2}(2\pi f_0 h^H)(2\pi f_0 h)\mathbf{w}^H\mathbf{w},$$

$$\mathbf{O}_{0,1} = \frac{2}{\sigma^2}2\pi f_0 \mathbb{R}\{j h^H \mathbf{w}^H \mathbf{u}\},$$

$$\mathbf{O}_{0,2} = -\frac{2}{\sigma^2}2\pi f_0 \mathbb{R}\{h^H \mathbf{w}^H \mathbf{u}\},$$

$$\mathbf{O}_{1,2} = 0$$

$$\mathbf{O}_{1,1} = \frac{2}{\sigma^2}\mathbf{u}^H\mathbf{u},$$

$$\mathbf{O}_{2,2} = \frac{2}{\sigma^2}\mathbf{u}^H\mathbf{u}.$$

$$\mathbf{O}_{1,0} = \frac{2}{\sigma^2}2\pi f_0\mathbb{R}\{jh^H\mathbf{w}^H\mathbf{u}\},$$

$$\mathbf{O}_{2,0} = -\frac{2}{\sigma^2}2\pi f_0\mathbb{R}\{h^H\mathbf{w}^H\mathbf{u}\},$$

$$\mathbf{O}_{2,1} = 0$$

The first diagonal entry of $\mathbf{O}^{-1}$ is $[\mathbf{O}^{-1}]_{0,0}$. Based on the entries of $\mathbf{O}$ obtained above, we calculate $[\mathbf{O}^{-1}]_{0,0}$ as [75],

$$\left[\mathbf{O}^{-1}\right]_{0,0} = B^{-1}, \tag{8.2}$$

$$\begin{aligned} B \triangleq \mathbf{O}_{0,0} - [\mathbf{O}_{0,1}\mathbf{O}_{0,2}]\begin{bmatrix} \mathbf{O}_{1,1} & \mathbf{O}_{1,2} \\ \mathbf{O}_{2,1} & \mathbf{O}_{2,2} \end{bmatrix}^{-1}\begin{bmatrix} \mathbf{O}_{1,0} \\ \mathbf{O}_{2,0} \end{bmatrix} \\ = \mathbf{O}_{0,0} - \frac{(\mathbf{O}_{0,1}\mathbf{O}_{1,0} + \mathbf{O}_{0,2}\mathbf{O}_{2,0})}{\mathbf{O}_{1,1}} \\ = \frac{2}{\sigma^2}(2\pi f_0 h^H)(2\pi f_0 h)[\frac{\mathbf{w}^H\mathbf{w}\mathbf{u}^H\mathbf{u} - \mathbf{w}^H\mathbf{u}\mathbf{u}^H\mathbf{w}}{\mathbf{u}^H\mathbf{u}}]. \end{aligned} \tag{8.3}$$

$$\begin{aligned} CRLB_\tau &= \left[\mathbf{O}^{-1}\right]_{0,0} \\ &= \frac{1}{\frac{2}{\sigma^2}(2\pi f_0 h^H)(2\pi f_0 h)}\frac{\mathbf{u}^H\mathbf{u}}{\mathbf{w}^H\mathbf{w}\mathbf{u}^H\mathbf{u} - \mathbf{w}^H\mathbf{u}\mathbf{u}^H\mathbf{w}}. \end{aligned} \tag{8.4}$$

8.2 Proof of Theorem 2 in Chapter 6

Similar to Section IV-A, we calculate the FIM and get the Doppler CRLB as

$$Q = \begin{bmatrix} Q_{0,0} & Q_{0,1} & Q_{0,2} \\ Q_{1,0} & Q_{1,1} & Q_{1,2} \\ Q_{2,0} & Q_{2,1} & Q_{2,2} \end{bmatrix}$$

We calculate elements of FIM as follows

$$Q_{0,0} = \frac{2}{\sigma^2} h h^H \boldsymbol{q}^H \boldsymbol{q}$$

$$Q_{0,1} = \frac{2}{\sigma^2} \mathbb{R}\{h^H \boldsymbol{q}^H \boldsymbol{u}\}$$

$$Q_{0,2} = \frac{2}{\sigma^2} \mathbb{R}\{j h^H \boldsymbol{q}^H \boldsymbol{u}\}$$

$$Q_{1,2} = 0$$

$$Q_{2,1} = 0$$

$$Q_{1,1} = \frac{2}{\sigma^2} \mathbf{u}^H \mathbf{u}$$

$$Q_{2,2} = \frac{2}{\sigma^2} \mathbf{u}^H \mathbf{u}$$

$$Q_{1,0} = \frac{2}{\sigma^2} \mathbb{R}\{h^H \boldsymbol{q}^H \boldsymbol{u}\}$$

$$Q_{2,0} = \frac{2}{\sigma^2}\mathbb{R}\{jh^H \boldsymbol{q}^H \boldsymbol{u}\}$$

According to [75],

$$\left[Q^{-1}\right]_{0,0} = H^{-1} \tag{8.5}$$

$$\begin{aligned} H &\triangleq Q_{0,0} - [Q_{0,1}Q_{0,2}]\begin{bmatrix} Q_{1,1} & Q_{1,2} \\ Q_{2,1} & Q_{2,2} \end{bmatrix}^{-1}\begin{bmatrix} Q_{1,0} \\ Q_{2,0} \end{bmatrix} \\ &= Q_{0,0} - \frac{(Q_{0,1}Q_{1,0} + Q_{0,2}Q_{2,0})}{Q_{1,1}} \\ &= \frac{2}{\sigma^2} hh^H \frac{\boldsymbol{q}^H \boldsymbol{q}\mathbf{u}^H\mathbf{u} - \boldsymbol{q}^H \boldsymbol{u}\boldsymbol{u}^H \boldsymbol{q}}{\mathbf{u}^H\mathbf{u}} \end{aligned}$$

$$CRLB_v = \frac{2}{\sigma^2} hh^H \frac{\boldsymbol{q}^H \boldsymbol{q}\mathbf{u}^H\mathbf{u} - \boldsymbol{q}^H \boldsymbol{u}\boldsymbol{u}^H \boldsymbol{q}}{\mathbf{u}^H\mathbf{u}}. \tag{8.6}$$

Bibliography

[1] L. Gaudio, M. Kobayashi, G. Caire, and G. Colavolpe, "On the effectiveness of OTFS for joint radar parameter estimation and communication," *IEEE Trans. Wireless Commun.*, vol. 19, no. 9, pp. 5951–5965, 2020. DOI: 10.1109/TWC.2020.2998583.

[2] W. Yuan, Z. Wei, S. Li, J. Yuan, and D. W. K. Ng, "Integrated sensing and communication-assisted orthogonal time frequency space transmission for vehicular networks," *IEEE Journal of Selected Topics in Signal Processing*, vol. 15, no. 6, pp. 1515–1528, 2021. DOI: 10.1109/JSTSP.2021.3117404.

[3] H. Godrich, A. M. Haimovich, and R. S. Blum, "Cramer Rao bound on target localization estimation in MIMO radar systems," in *2008 42nd Annual Conference on Information Sciences and Systems*, 2008, pp. 134–139.

[4] R. Niu, R. S. Blum, P. K. Varshney, and A. L. Drozd, "Target localization and tracking in noncoherent multiple-input multiple-output radar systems," *IEEE Transactions on Aerospace and Electronic Systems*, vol. 48, no. 2, pp. 1466–1489, 2012.

[5] P. Raviteja, K. T. Phan, and Y. Hong, "Embedded pilot-aided channel estimation for OTFS in delay-doppler channels," *IEEE Trans. Vehicular Tech.*, vol. 68, no. 5, pp. 4906–4917, 2019. DOI: 10.1109/TVT.2019.2906357.

[6] W. Shen, L. Dai, J. An, P. Fan, and R. W. Heath, "Channel estimation for orthogonal time frequency space (OTFS) massive MIMO," *IEEE Trans. Signal Process.*, vol. 67, no. 16, pp. 4204–4217, 2019. DOI: 10.1109/TSP.2019.2919411.

[7] H. Qu, G. Liu, L. Zhang, M. A. Imran, and S. Wen, "Low-dimensional subspace estimation of continuous-doppler-spread channel in OTFS systems," *IEEE Trans. Commun.*, vol. 69, no. 7, pp. 4717–4731, 2021. DOI: 10.1109/TCOMM.2021.3072744.

[8] H. Zhang, X. Huang, and J. A. Zhang, "Adaptive transmission with frequency-domain precoding and linear equalization over fast fading channels," *IEEE Trans. Wireless Commun.*, vol. 20, no. 11, pp. 7420–7430, 2021. DOI: 10.1109/TWC.2021.3083652.

[9] J. Hao, J. Wang, and C. Pan, "Low complexity ici mitigation for mimo-ofdm in time-varying channels," *IEEE Transactions on Broadcasting*, vol. 62, no. 3, pp. 727–735, 2016. DOI: 10.1109/TBC.2016.2550763.

[10] Y. M. Khattabi and S. A. Alkhawaldeh, "Performance analysis of spatial modulation under rapidly time-varying rayleigh fading channels," *IEEE Access*, vol. 7, pp. 110 594–110 604, 2019. DOI: 10.1109/ACCESS.2019.2934000.

[11] Y. Sun, J. A. Zhang, K. Wu, and R. P. Liu, "Frequency-domain sensing in time-varying channels," *IEEE Wireless Communications Letters*, vol. 12, no. 1, pp. 16–20, 2022.

[12] W. Li and J. C. Preisig, "Estimation of rapidly time-varying sparse channels," *IEEE Journal of Oceanic Engineering*, vol. 32, no. 4, pp. 927–939, 2007. DOI: 10.1109/JOE.2007.906409.

[13] K. J. Kim and R. Iltis, "Joint detection and channel estimation algorithms for qs-cdma signals over time-varying channels," *IEEE Transactions on Com-*

munications, vol. 50, no. 5, pp. 845–855, 2002. DOI: 10.1109/TCOMM.2002.1006565.

[14] H.-N. Lee and G. Pottie, "Fast adaptive equalization/diversity combining for time-varying dispersive channels," *IEEE Transactions on Communications*, vol. 46, no. 9, pp. 1146–1162, 1998. DOI: 10.1109/26.718557.

[15] X. Ma, H. Ye, and Y. Li, "Learning assisted estimation for time- varying channels," in *2018 15th International Symposium on Wireless Communication Systems (ISWCS)*, 2018, pp. 1–5. DOI: 10.1109/ISWCS.2018.8491068.

[16] D. Schafhuber and G. Matz, "Mmse and adaptive prediction of time-varying channels for ofdm systems," *IEEE Transactions on Wireless Communications*, vol. 4, no. 2, pp. 593–602, 2005. DOI: 10.1109/TWC.2004.843055.

[17] Z. Tang, R. C. Cannizzaro, G. Leus, and P. Banelli, "Pilot-assisted time-varying channel estimation for ofdm systems," *IEEE Transactions on Signal Processing*, vol. 55, no. 5, pp. 2226–2238, 2007. DOI: 10.1109/TSP.2007.893198.

[18] J.-C. Lin, "Least-squares channel estimation for mobile ofdm communication on time-varying frequency-selective fading channels," *IEEE Transactions on Vehicular Technology*, vol. 57, no. 6, pp. 3538–3550, 2008. DOI: 10.1109/TVT.2008.919611.

[19] D. Hu, X. Wang, and L. He, "A new sparse channel estimation and tracking method for time-varying ofdm systems," *IEEE Transactions on Vehicular Technology*, vol. 62, no. 9, pp. 4648–4653, 2013. DOI: 10.1109/TVT.2013.2266282.

[20] M. Başaran, H. Şenol, S. Erküçük, and H. A. Çırpan, "Channel estimation for tds-ofdm systems in rapidly time-varying mobile channels," *IEEE Transactions on Wireless Communications*, vol. 17, no. 12, pp. 8123–8135, 2018. DOI: 10.1109/TWC.2018.2874228.

[21] Y. Liu, Z. Tan, H. Wang, S. Xu, and K. S. Kwak, "Channel estimation for macrocellular ofdm uplinks in time-varying channels," *IEEE Transactions on Vehicular Technology*, vol. 61, no. 4, pp. 1709–1718, 2012. DOI: 10.1109/TVT.2012.2187939.

[22] Q. Qin, L. Gui, B. Gong, and S. Luo, "Sparse channel estimation for massive mimo-ofdm systems over time-varying channels," *IEEE Access*, vol. 6, pp. 33 740–33 751, 2018. DOI: 10.1109/ACCESS.2018.2843783.

[23] Y. Acar, H. Doğan, and E. Panayırcı, "On channel estimation for spatial modulated systems over time-varying channels," *Digital Signal Processing*, vol. 37, pp. 43–52, 2015, ISSN: 1051-2004. DOI: https://doi.org/10.1016/j.dsp.2014.11.004. [Online]. Available: https://www.sciencedirect.com/science/article/pii/S1051200414003212.

[24] Y. Liao, Y. Hua, and Y. Cai, "Deep learning based channel estimation algorithm for fast time-varying mimo-ofdm systems," *IEEE Communications Letters*, vol. 24, no. 3, pp. 572–576, 2020. DOI: 10.1109/LCOMM.2019.2960242.

[25] Q. Qin, L. Gui, P. Cheng, and B. Gong, "Time-varying channel estimation for millimeter wave multiuser mimo systems," *IEEE Transactions on Vehicular Technology*, vol. 67, no. 10, pp. 9435–9448, 2018. DOI: 10.1109/TVT.2018.2854735.

[26] M. Sun, X. Wang, C. Zhao, *et al.*, "Adaptive sensing schedule for dynamic spectrum sharing in time-varying channel," *IEEE Transactions on Vehicular Technology*, vol. 67, no. 6, pp. 5520–5524, 2018. DOI: 10.1109/TVT.2018.2797318.

[27] L. Shen, Y. Zakharov, B. Henson, N. Morozs, and P. D. Mitchell, "Adaptive filtering for full-duplex uwa systems with time-varying self-interference channel," *IEEE Access*, vol. 8, pp. 187 590–187 604, 2020. DOI: 10.1109/ACCESS.2020.3031010.

[28] Z. Tang and G. Leus, "Low-complexity equalization of time-varying channels with precoding," *IEEE Transactions on Signal Processing*, vol. 54, no. 9, pp. 3642–3648, 2006. DOI: 10.1109/TSP.2006.879261.

[29] L. Li, Y. Liang, P. Fan, and Y. Guan, "Low complexity detection algorithms for otfs under rapidly time-varying channel," in *2019 IEEE 89th Vehicular Technology Conference (VTC2019-Spring)*, 2019, pp. 1–5. DOI: 10.1109/VTCSpring.2019.8746420.

[30] C. Dumard and T. Zemen, "Low-complexity mimo multiuser receiver: A joint antenna detection scheme for time-varying channels," *IEEE Transactions on Signal Processing*, vol. 56, no. 7, pp. 2931–2940, 2008. DOI: 10.1109/TSP.2007.916133.

[31] A.-Y. Lu, Y.-F. Chen, and S.-M. Tseng, "Reduced complexity hybrid beamforming for time-varying channels in millimeter wave mimo systems," *Wireless Personal Communications*, vol. 124, no. 3, pp. 2391–2410, 2022.

[32] W.-C. Pao, Y.-F. Chen, and M.-G. Tsai, "An adaptive allocation scheme in multiuser ofdm systems with time-varying channels," *IEEE Transactions on Wireless Communications*, vol. 13, no. 2, pp. 669–679, 2014. DOI: 10.1109/TW.2013.123013.121981.

[33] Y. Guo, Q. Yang, and K. S. Kwak, "Quality-oriented rate control and resource allocation in time-varying ofdma networks," *IEEE Transactions on Vehicular Technology*, vol. 66, no. 3, pp. 2324–2338, 2017. DOI: 10.1109/TVT.2016.2575920.

[34] G. Giancola, L. De Nardis, M.-G. Di Benedetto, and E. Dubuis, "Dynamic resource allocation in time-varying ultra wide band channels," in *2004 IEEE International Conference on Communications (IEEE Cat. No.04CH37577)*, vol. 6, 2004, 3581–3585 Vol.6. DOI: 10.1109/ICC.2004.1313211.

[35] S. Kittipiyakul and T. Javidi, "Resource allocation in ofdma with time-varying channel and bursty arrivals," *IEEE Communications Letters*, vol. 11, no. 9, pp. 708–710, 2007. DOI: 10.1109/LCOMM.2007.070672.

[36] S. Li, S. Lin, L. Cai, W. Li, and G. Zhu, "Joint resource allocation and computation offloading with time-varying fading channel in vehicular edge computing," *IEEE Transactions on Vehicular Technology*, vol. 69, no. 3, pp. 3384–3398, 2020. DOI: 10.1109/TVT.2020.2967882.

[37] M. Neely, E. Modiano, and C. Rohrs, "Power allocation and routing in multibeam satellites with time-varying channels," *IEEE/ACM Transactions on Networking*, vol. 11, no. 1, pp. 138–152, 2003. DOI: 10.1109/TNET.2002.808401.

[38] S. Dominic and L. Jacob, "Distributed resource allocation for d2d communications underlaying cellular networks in time-varying environment," *IEEE Communications Letters*, vol. 22, no. 2, pp. 388–391, 2018. DOI: 10.1109/LCOMM.2017.2771778.

[39] F. Qu and L. Yang, "On the estimation of doubly-selective fading channels," *IEEE Transactions on Wireless Communications*, vol. 9, no. 4, pp. 1261–1265, 2010. DOI: 10.1109/TWC.2010.04.080631.

[40] C. Pirak, Z. J. Wang, K. J. R. Liu, and S. Jitapunkul, "Adaptive channel estimation using pilot-embedded data-bearing approach for mimo-ofdm systems," *IEEE Transactions on Signal Processing*, vol. 54, no. 12, pp. 4706–4716, 2006. DOI: 10.1109/TSP.2006.881265.

[41] N. Sun and J. Wu, "Maximizing spectral efficiency for high mobility systems with imperfect channel state information," *IEEE Transactions on Wireless Communications*, vol. 13, no. 3, pp. 1462–1470, 2014. DOI: 10.1109/TWC.2014.012314.130772.

[42] A. P. Kannu and P. Schniter, "Design and analysis of mmse pilot-aided cyclic-prefixed block transmissions for doubly selective channels," *IEEE Transactions*

on Signal Processing, vol. 56, no. 3, pp. 1148–1160, 2008. DOI: 10.1109/TSP.2007.908969.

[43] T. Cui, C. Tellambura, and Y. Wu, "Low-complexity pilot-aided channel estimation for ofdm systems over doubly-selective channels," in *IEEE International Conference on Communications, 2005. ICC 2005. 2005*, vol. 3, 2005, 1980–1984 Vol. 3. DOI: 10.1109/ICC.2005.1494685.

[44] J. K. Tugnait, S. He, and H. Kim, "Doubly selective channel estimation using exponential basis models and subblock tracking," *IEEE Transactions on Signal Processing*, vol. 58, no. 3, pp. 1275–1289, 2010. DOI: 10.1109/TSP.2009.2036047.

[45] X. Hou, S. Li, C. Yin, and G. Yue, "Two-dimensional recursive least square adaptive channel estimation for ofdm systems," in *Proceedings. 2005 International Conference on Wireless Communications, Networking and Mobile Computing, 2005.*, vol. 1, 2005, pp. 232–236. DOI: 10.1109/WCNM.2005.1544024.

[46] L. Rugini, P. Banelli, and G. Leus, "Chapter 7 - OFDM communications over time-varying channels," in *Wireless Communications Over Rapidly Time-Varying Channels*, F. Hlawatsch and G. Matz, Eds., Oxford: Academic Press, 2011, pp. 285–336, ISBN: 978-0-12-374483-8. DOI: https://doi.org/10.1016/B978-0-12-374483-8.00007-8.

[47] C.-Y. Hsu and W.-R. Wu, "Low-complexity ici mitigation methods for high-mobility siso/mimo-ofdm systems," *IEEE Transactions on Vehicular Technology*, vol. 58, no. 6, pp. 2755–2768, 2009. DOI: 10.1109/TVT.2008.2011275.

[48] Z. Dong, P. Fan, and X. Lei, "Mobility adaptation in ofdm systems over rapidly time-varying fading channels," in *2014 IEEE International Conference on Communication Systems*, 2014, pp. 318–322. DOI: 10.1109/ICCS.2014.7024817.

[49] Z. Wei, W. Yuan, S. Li, *et al.*, "Orthogonal time-frequency space modulation: A promising next-generation waveform," *IEEE Wireless Commun.*, vol. 28, no. 4, pp. 136–144, 2021. DOI: 10.1109/MWC.001.2000408.

[50] P. Raviteja, K. T. Phan, Y. Hong, and E. Viterbo, "Interference cancellation and iterative detection for orthogonal time frequency space modulation," *IEEE Transactions on Wireless Communications*, vol. 17, no. 10, pp. 6501–6515, 2018. DOI: 10.1109/TWC.2018.2860011.

[51] T. Bouchoucha, S. Ahmed, T. Al-Naffouri, and M.-S. Alouini, "Dft-based closed-form covariance matrix and direct waveforms design for mimo radar to achieve desired beampatterns," *IEEE Transactions on Signal Processing*, vol. 65, no. 8, pp. 2104–2113, 2017. DOI: 10.1109/TSP.2017.2656840.

[52] R. Schmidt, "Multiple emitter location and signal parameter estimation," *IEEE Transactions on Antennas and Propagation*, vol. 34, no. 3, pp. 276–280, 1986. DOI: 10.1109/TAP.1986.1143830.

[53] R. Zhu, J. Wen, and X. Xiong, "Forward-looking imaging algorithm for airborne radar based on beam-space multiple signal classification," in *2020 IEEE 20th International Conference on Communication Technology (ICCT)*, 2020, pp. 1276–1280. DOI: 10.1109/ICCT50939.2020.9295943.

[54] X. Ren, Y. Qin, and L. Tian, "Three-dimensional imaging algorithm for tomography sar based on multiple signal classification," in *2014 IEEE International Conference on Signal Processing, Communications and Computing (ICSPCC)*, 2014, pp. 120–123. DOI: 10.1109/ICSPCC.2014.6986165.

[55] Z. Lu, L. Zhang, J. Zhang, and J. Zhang, "Parallel optimization of broadband underwater acoustic signal music algorithm on gpu platform," in *2017 4th International Conference on Systems and Informatics (ICSAI)*, 2017, pp. 704–708. DOI: 10.1109/ICSAI.2017.8248377.

[56] Y.-q. Li, Q. Xie, N. Wang, X. Xiang, and F.-c. Lu, "Simulation of pd location in power transformer based on root multiple signal classification method," in *2009 IEEE 9th International Conference on the Properties and Applications of Dielectric Materials*, 2009, pp. 553–556. DOI: 10.1109/ICPADM.2009.5252369.

[57] A. M. Elbir, "Deepmusic: Multiple signal classification via deep learning," *IEEE Sensors Letters*, vol. 4, no. 4, pp. 1–4, 2020. DOI: 10.1109/LSENS.2020.2980384.

[58] E. Zhao, F. Zhang, D. Zhang, and S. Pan, "Three-dimensional multiple signal classification (3d-music) for super-resolution fmcw radar detection," in *2019 IEEE MTT-S International Wireless Symposium (IWS)*, 2019, pp. 1–3. DOI: 10.1109/IEEE-IWS.2019.8804015.

[59] K. Almidfa, G. Tsoulos, and A. Nix, "Performance analysis of esprit, tls-esprit and unitary-esprit algorithms for doa estimation in a w-cdma mobile system," in *First International Conference on 3G Mobile Communication Technologies*, 2000, pp. 200–203. DOI: 10.1049/cp:20000042.

[60] B. Jo and J.-W. Choi, "Sine-based eb-esprit for source localization," in *2018 IEEE 10th Sensor Array and Multichannel Signal Processing Workshop (SAM)*, 2018, pp. 326–330. DOI: 10.1109/SAM.2018.8448668.

[61] Y. Taoliu, Z. Wei, and Z. Xiufen, "A solution of rotation invariance based esprit(sri-esprit) method approach to direction-of-arrival estimation," in *The 2012 International Workshop on Microwave and Millimeter Wave Circuits and System Technology*, 2012, pp. 1–4. DOI: 10.1109/MMWCST.2012.6238171.

[62] P. Das, A. Bhattacharjee, and S. Pathak, "Performance analysis of tls-esprit and qr tls- esprit algorithm for direction of arrival estimation," in *2015 International Conference on Communications and Signal Processing (ICCSP)*, 2015, pp. 1395–1398. DOI: 10.1109/ICCSP.2015.7322739.

[63] S. S. Das, V. Rangamgari, S. Tiwari, and S. C. Mondal, "Time domain channel estimation and equalization of cp-otfs under multiple fractional dopplers and residual synchronization errors," *IEEE Access*, vol. 9, pp. 10 561–10 576, 2021. DOI: 10.1109/ACCESS.2020.3046487.

[64] R. Hadani, S. Rakib, M. Tsatsanis, *et al.*, "Orthogonal time frequency space modulation," in *2017 IEEE Wireless Communications and Networking Conference (WCNC)*, 2017, pp. 1–6. DOI: 10.1109/WCNC.2017.7925924.

[65] A. Farhang, A. RezazadehReyhani, L. E. Doyle, and B. Farhang-Boroujeny, "Low complexity modem structure for ofdm-based orthogonal time frequency space modulation," *IEEE Wireless Communications Letters*, vol. 7, no. 3, pp. 344–347, 2018. DOI: 10.1109/LWC.2017.2776942.

[66] W. Yuan, Z. Wei, J. Yuan, and D. W. K. Ng, "A simple variational bayes detector for orthogonal time frequency space (otfs) modulation," *IEEE Transactions on Vehicular Technology*, vol. 69, no. 7, pp. 7976–7980, 2020. DOI: 10.1109/TVT.2020.2991443.

[67] Y. Yang and R. S. Blum, "Mimo radar waveform design based on mutual information and minimum mean-square error estimation," *IEEE Transactions on Aerospace and Electronic Systems*, vol. 43, no. 1, pp. 330–343, 2007. DOI: 10.1109/TAES.2007.357137.

[68] T. Tian, T. Zhang, L. Kong, G. Cui, and Y. Wang, "Mutual information based partial band coexistence for joint radar and communication system," in *2019 IEEE Radar Conference (RadarConf)*, Apr. 2019, pp. 1–5. DOI: 10.1109/RADAR.2019.8835671.

[69] Z. Zhu, S. Kay, and R. S. Raghavan, "Information-theoretic optimal radar waveform design," *IEEE Signal Process. Lett.*, vol. 24, no. 3, pp. 274–278, Mar. 2017, ISSN: 1070-9908. DOI: 10.1109/LSP.2017.2655879.

[70] J. A. Zhang, M. L. Rahman, K. Wu, *et al.*, "Enabling joint communication and radar sensing in mobile networks - a survey," *IEEE Commun. Surv. Tut.*, vol. 24, no. 1, pp. 306–345, 2022. DOI: 10.1109/COMST.2021.3122519.

[71] L. Gaudio, M. Kobayashi, G. Caire, and G. Colavolpe, "On the effectiveness of otfs for joint radar parameter estimation and communication," *IEEE Transactions on Wireless Communications*, vol. 19, no. 9, pp. 5951–5965, 2020. DOI: 10.1109/TWC.2020.2998583.

[72] J. A. Zhang, L. Luo, and X. Huang, "Multicarrier systems based on multistage layered ifft structure," *IEEE Signal Processing Letters*, vol. 20, no. 7, pp. 665–668, 2013. DOI: 10.1109/LSP.2013.2262937.

[73] J. A. Zhang, F. Liu, C. Masouros, *et al.*, "An overview of signal processing techniques for joint communication and radar sensing," *IEEE J. Sel. Topics in Signal Process.*, pp. 1–20, 2021. DOI: 10.1109/JSTSP.2021.3113120.

[74] B. Xiong, Z. Zhang, J. Zhang, H. Jiang, J. Dang, and L. Wu, "Novel multi-mobility v2x channel model in the presence of randomly moving clusters," *IEEE Trans. on Wireless Commun.*, vol. 20, no. 5, pp. 3180–3195, 2021.

[75] M. F. Keskin, V. Koivunen, and H. Wymeersch, "Limited feedforward waveform design for ofdm dual-functional radar-communications," *IEEE Transactions on Signal Processing*, vol. 69, pp. 2955–2970, 2021.

[76] P. Stoica and A. Nehorai, "Performance study of conditional and unconditional direction-of-arrival estimation," *IEEE Transactions on Acoustics, Speech, and Signal Processing*, vol. 38, no. 10, pp. 1783–1795, 1990. DOI: 10.1109/29.60109.

[77] P. Stoica, E. Larsson, and A. Gershman, "The stochastic crb for array processing: A textbook derivation," *IEEE Signal Processing Letters*, vol. 8, no. 5, pp. 148–150, 2001. DOI: 10.1109/97.917699.

[78] A. Kaewpukdee and P. Uthansakul, "Characteristic of line-of-sight in infrastructure-to-vehicle visible light communication using mimo technique," *Computers, Materials and Continua*, vol. 74, pp. 1025–1048, Sep. 2022. DOI: 10.32604/cmc.2023.032569.

[79] Z. Ni, J. A. Zhang, K. Yang, X. Huang, and T. A. Tsiftsis, "Multi-metric waveform optimization for multiple-input single-output joint communication and radar sensing," *IEEE Transactions on Communications*, vol. 70, no. 2, pp. 1276–1289, 2021.